1989

Studies In Asymmetric Catalysis

Fan-chou Xu

NOTICE

The quality of this microform is heavily dependent upon the quality of the original thesis submitted for microfilming. Every effort has been made to ensure the highest quality of reproduction possible.

If pages are missing, contact the university which granted the degree.

Some pages may have indistinct print especially if the original pages were typed with a poor typewriter ribbon or if the university sent us an inferior photocopy.

Reproduction in full or in part of this microform is governed by the Canadian Copyright Act, R.S.C. 1970, c. C-30, and subsequent amendments.

AVIS

La qualité de cette microforme dépend grandement de la qualité de la thèse soumise au microfilmage. Nous avons tout fait pour assurer une qualité supérieure de reproduction.

S'il manque des pages, veuillez communiquer avec l'université qui a conféré le grade.

La qualité d'impression de certaines pages peut laisser à désirer, surtout si les pages originales ont été dactylographiées à l'aide d'un ruban usé ou si l'université nous a fait parvenir une photocopie de qualité inférieure.

La reproduction, même partielle, de cette microforme est soumise à la Loi canadienne sur le droit d'auteur, SRC 1970, c. C-30, et ses amendements subséquents.

STUDIES IN ASYMMETRIC CATALYSIS

by

Fan-Chou Xu

Department of Chemistry

Submitted in partial fulfilment

of the requirements for the degree of

Doctor of Philosophy

Faculty of Graduate Studies

The University of Western Ontario

London, Ontario

November, 1988.

ISBN 0-315-49344-5

ABSTRACT

Studies of the homogeneous, asymmetric hydrosilylation of prochiral ketones using chiral Rh catalysts of the amphos, P-N, and diamphos, P-N-N, chelate ligands in both solution and the solid state are described. Initially, the complexes [Rh(I)Cl(*R*-amphos)PPh_3] and [Rh(III)Cl_3-(*R*-diamphos)] were prepared and structurally characterized using X-ray crystallographic techniques. These studies provided a basis for relating the catalyst shape to the optical yield.

The stability of the [Rh(I)Cl(*R*-amphos)PPh_3] catalyst in solution and the formation of its oxidative addition products, as well as the labilities of species actually present in the solution during a hydrosilylation reaction, were studied using spectroscopic techniques, including ^1H and ^{31}P NMR, Visible, Infra Red, and Mass spectroscopy. The results obtained allowed the elucidation of a mechanistic scheme for homogeneous, asymmetric hydrosilylation. In a certain favourable case, an oxidative addition product $RhHCl(SiCl_3)(PPh_3)_2$ was isolated and characterized by a single crystal X-ray diffraction study. A new and bulky α-naphthylphenyldihydrosilane was synthesized and used as the silane reagent with the catalysts [Rh(*R*-amphos)NBD]ClO_4, [RhCl(*R*-amphos)(PPh_3)] and [RhCl(*S*-amphos)(PPh_3)]. Using a ratio of catalyst to substrate of either 1:490 or 1:100, turnover numbers of 407

and 460 cycles were measured over a period of roughly 3 days. The silyl ether products were converted to the alcohols and α-NpPhSi*HMe by hydrolysis after addition of the appropriate Grignard reagent. Very high chemical yields, from 80% to 95%, fairly high optical yields of the alcohol, up to 57%, and relatively low optical yields of (-)-α-NpPhMeSi*H were obtained. Only the (*S*)-configuration of the silane, (-)-α-NpPhMeSi*H, was observed with both *R* and *S*-amphos ligands. The results obtained with the bulky silane have improved upon the optical yields previously achieved for the hydrosilylation of prochiral ketones with Ph_2SiH_2 and $PhMe_2SiH$.

The results described in this thesis provide a clear basis for the improvement of the optical yields in the asymmetric hydrosilylation of prochiral ketones catalyzed by chiral Rh-(P-N) complexes.

ACKNOWLEDGEMENTS

At this time I wish to thank Dr. Nicholas C. Payne for the encouragement and guidance he has given me, and especially for his great patience and support during the course of this research.

I am grateful for the assistance offered to me by the many members of the faculty, staff and students in this department.

Finally, I wish to thank the University of Western Ontario for financial support.

TABLE OF CONTENTS

LIST OF TABLES

LIST OF FIGURES

LIST OF APPENDIX

ABBREVIATIONS AND NOMENCLATURE

The following abbreviations appear throughout this work. They are listed in order of appearance

ABBREVIATION	NAME
Me	Methyl
Pr	Propyl
Ph	Phenyl
L-DOPA	Dihydroxyphenylalanine
DIOP	2,3-o-isopropylidene-2,3-dihydroxy-1,4-bis(diphenylphosphino)butane
DIPAMP	1,2-bis(o-anisylphenylphosphino)ethane
PROPHOS	1,2-bis(diphenylphosphino)propane
CHIRAPHOS	2,3-bis(diphenylphosphino)butane
BPPM	N-butoxycarbonyl-4-diphenylphosphino-2-(diphenylphosphinomethyl)pyrrolidine
BPPFA	N,N-dimethyl-1-[1',2-bis(diphenylphosphino-ferrocenyl]ethylamine
R-(+)-BMPPt	Dichlorobis[*R*-(+)-benzylmethylphenylphosphine] di-μ-chlorodiplatinum(II)
R-(-)-MPPPt	Dichlorobis[*R*-(-)-methyl-n-propyl-phenyl-phosphine]di-μ-chlorodiplatinum(II)
R-(+)-BMP	*R*-(+)-benzylmethylphenylphosphine
α-Np	α-naphthyl
Et	Ethyl
COD	1,5-cyclooctadiene
NBD	Norbornadiene, bicyclo[2,2,1]hepta-2,5-diene
diphos	1,2-bis(diphenylphosphino)ethane
Py	pyridine
amphos (P-N)	N,N-dimethyl-1-(o-(diphenylphosphino)phenyl)-ethylamine

amars	N,N-dimethyl-1-(o-(diphenylarsino)phenyl) ethylamine
dicyphos	N,N-dimethyl-1-(o-(dicyclohexylphosphino) phenyl)ethylamine
Bu	butyl
dibutphos	N,N-dimethyl-1-(o-(di-tert-butylphosphino)-phenyl)ethylamine
NCS	thiocyanate
EAC	ethyl-(Z)-α-acetamidocinnamate
diamphos (P–N–N)	N-methyl-(N',N'-dimethyl)-1-(o-(diphenyl-phosphino)phenyl)ethyldiaminoethane
Cy	cyclohexyl
ca.	approximately
(*S*)-BMPP	(*S*)-benzylmethylphenylphosphine
M.P.	melting point
B.P.	boiling point
optical yield	percentage of major enantiomer minus percentage of minor enantiomer in a product mixture
e.e.	enantiomeric excess, same as optical yield
$[\alpha]_D^{20}$	Specific rotation of a Na D line source (λ=589 nm) by an optically active solution at 20°C
NMR	Nuclear Magnetic Resonance
U.V.	Ultraviolet-Visible
I.R.	Infra Red
TLC	Thin Layer Chromatography

CHAPTER 1

INTRODUCTION

1.1 Preamble

Many naturally occurring organic compounds, such as amino acids and carbohydrates, display optical activity, with only one of the enantiomers showing physiological activity. For example, L-glutamic acid markedly enhances the taste of food, whereas D-glutamic acid does not. Proteins are composed of sequential combinations of L-amino acids only. By contrast, in a laboratory synthesis of a molecule with one chiral centre, a 1:1 mixture of the two enantiomers will be obtained in the absence of an asymmetric environment. One aim of current research in inorganic chemistry is the design and synthesis of chiral transition metal complexes which will catalyse the stereoselective formation of chiral products with an efficiency approaching that of natural systems.

1.2 Enantioselective Catalysis

The term, asymmetric synthesis, describes a reaction in which an achiral unit in an ensemble of substrate molecules, which must have either enantiotopic or diastereotopic groups or faces, is converted by a reactant into a chiral unit in such a manner that the stereoisomeric products are produced in unequal amounts. The stereoisomeric products may be enantiomeric or diastereomeric, and they will be chiral and nonracemic. This is to say, an asymmetric synthesis is a process which converts a prochiral unit into a chiral unit in

such a way that unequal amounts of stereoisomeric products result. For the purpose of this definition, "reactant" includes not only the usual chemical reagents but also solvents, catalysts, and physical forces such as a circularly polarized light. In attempting such syntheses, either in a research laboratory or on an industrial scale, the cost and availability of the asymmetric environment is a major consideration. For a reaction performed in an optically active solvent, large quantities of the solvent are needed. For a reaction using an optically active auxiliary, which can be a chiral substituent either in the precursor or the reactant, a stoichiometric amount of chiral information is sufficient. If the chiral information is made part of an optically active catalyst, a minimum amount is required, because the catalyst re-enters each catalytic cycle with its optical activity. This concept is called enantioselective catalysis, and its application leads to a multiplication of the chiral information contained in the catalyst. Thus, in principle, with a small quantity of an optically active catalyst it should be possible to make large quantities of optically active products [1-5]. This is an attractive prospect for both research and industry.

The elegant and economic concept of enantiosepecific catalysis is used by the enzymes in man, animals, and plants to produce all the optically active substances needed for life [6]. However, enzymes perform these spectacularly fast and stereospecific reactions only with their natural

substrates. Even for molecules closely related to the natural substrates, a remarkable drop in enzymatic turnover and stereoselectivity is usually observed. In this situation, it is necessary to develop man-made enantioselective catalysts which not only could be used to prepare natural optically active substances but also optically active products not occurring in nature

In 1968, Horner et al [7] and Knowles et al [8] independently found that prochiral olefins could be hydrogenated enantioselectively with Rh complexes of the Wilkinson type, containing optically active phosphines PMePrPh, chiral at the phosphorus atom. However, with these unidentate phosphine ligands only poor optical inductions were achieved, and these complexes did not form a practical prochiral synthetic route.

A milestone in the development of enantioselective catalysis was Kagan's synthesis of the diphosphine DIOP, starting from tartaric acid [9,10]. The bidentate coordination of the ligand DIOP reduces the number of possible conformations open to two unidentate ligands, therefore favouring high optical inductions [11]. Furthermore, the two phenyl rings at the phosphorus atom turned out to be good chirality transmitters from the ligand backbone. When prochiral substrates are converted into optically active products with Rh complexes of DIOP, eg. hydrogenation of Z-α-acetamidocinnamic acid to give N-acetylphenylalanine, an enantiomer ratio of 90.5/9.5 was achieved [12].

This finding stimulated worldwide research into the synthesis of optically active diphosphines [13-18]. From a variety of new ligands, five are depicted along with DIOP in Figure 1.1.1. DIPAMP was the basis of the first commercial application of the concept of enantioselective catalysis [19]. As its Rh complex, it formed a crucial step in the synthesis of the drug, L-DOPA, for Parkinson's disease, which is produced in the Monsanto amino acid process by hydrogenation of the corresponding dehydroamino acid. PROPHOS [20], prepared from lactic acid, has one asymmetric center in the chelate backbone, whereas CHIRAPHOS [21] has two. BPPM [22] is a derivative of the amino acid proline and BPPFA [23] is a ferrocene derivative.

Most of the early work in the field of enantioselective catalysis has centered around the hydrogenation of prochiral olefins, especially the amino acid precursors. But the concept is increasingly applied to other reactions due to the great demand for optically active products.

A variety of transition metal complexes with chiral tertiary phosphine ligands have proved effective for the catalytic asymmetric hydrosilylation of prochiral ketones (Figure 1.1.2). These reactions permit the preparation of chiral alcohols. Kumada found that both dichlorobis[*R*-(+)-benzylmethylphenylphosphine]-di-μ-chlorodiplatinum(II), [*R*-(+)-BMPPt], and dichlorobis[*R*-(-)-methyl-n-propylphenylphosphine]di-μ-chlorodiplatinum(II), [*R*-(-)-MPPPt] were effective asymmetric hydrosilylation catalysts for alkyl aryl

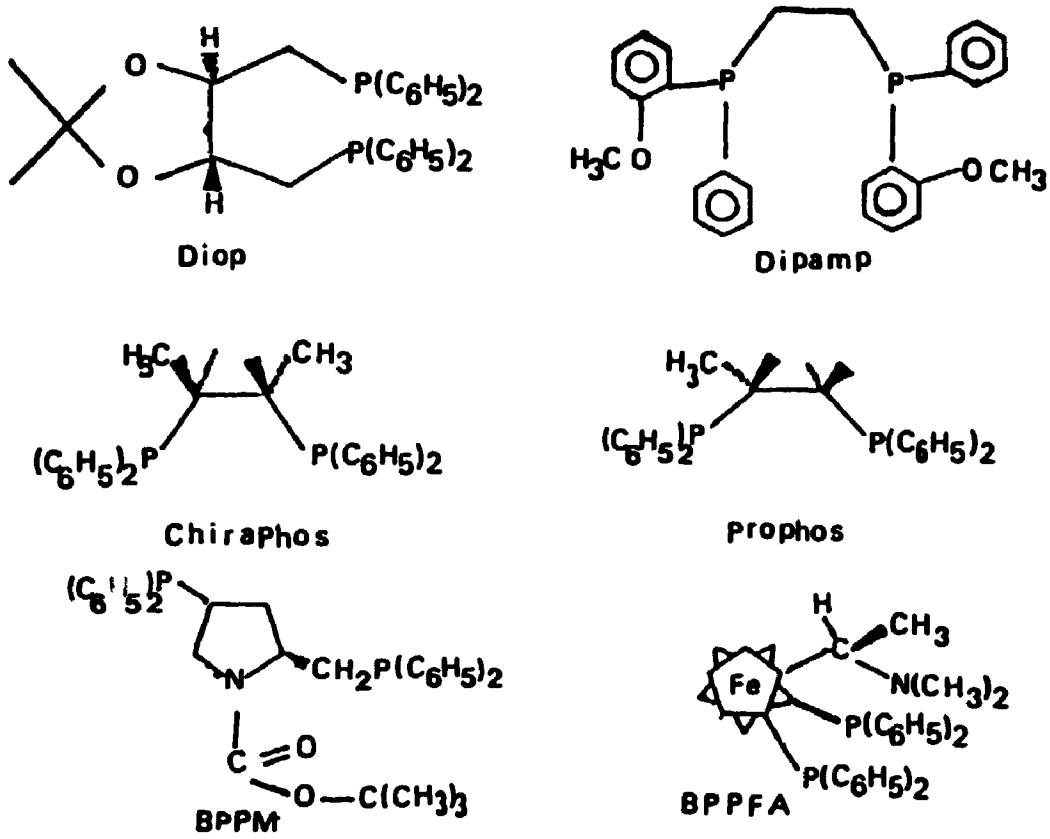

Figure 1.1.1 Prominent optically active diphosphine.

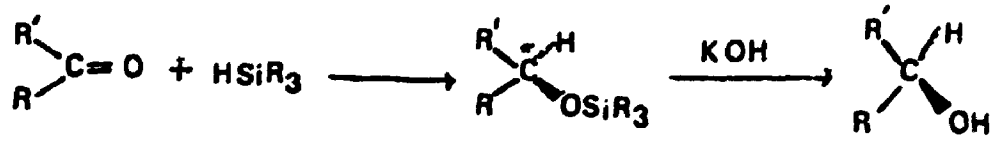

Figure 1.1.2 Asymmetric hydrosilylation of a prochiral ketone and subsequent hydrolysis to yield a chiral alcohol.

ketones. However, the optical yields of the product alcohols were relatively low [24,25]. A chiral cationic rhodium complex prepared from optically active [*R*-(+)-benzylmethylphenylphosphine], *R*-(+)-BMP, is effective for the asymmetric hydrosilylation of prochiral ketones with dialkyl or trialkylsilanes [26]. The extent of the asymmetric induction, as well as the configuration of the predominant alcohol produced, are dependent not only on the structure of the prochiral ketone, but also on the particular silane used.

Hydrosilylation of acetophenone with α-naphthylphenylsilane catalyzed by a (-)-DIOP rhodium complex leads to asymmetric induction at both the carbon and silicon atom of the silyl ether product. Reaction of this silyl ether with ethyl Grignard yields: (-)-1-NpPhEtSiH (32%e.e.) and (+)-PhCHOHME (55%e.e.) [27]. The DIOP-rhodium(I) complex had high optical yields for dihydrosilanes [47].

Both soluble chiral DIOP rhodium complexes and the analogous polymer-bound chiral DIOP rhodium complexes (Figure 1.1.3) yield similar results in catalytic asymmetric hydrosilylation reactions of prochiral ketones [28,29].

Hydrosilylation of acetophenone with diphenylsilane catalyzed using the in-situ system $[Rh(COD)CL]_2$ / pyridine thiazolidine (1:13) (Figure 1.1.4) by Brunner [30] gave the highest optical yields, 98% (catalyst:substrate=1:140)

Stephan and Payne achieved selectivities of up to 72% with a Rh(I)-amphos catalyst (Figure 1.1.5) by using $(C_6H_5)_2SiH_2$ [31]

Mckay and Payne developed another two ligands which were

dicyphos (Figure 1.1.6) and dibutphos (Figure 1.1.7) [32]. The rhodium(I) complexes with those two ligands produced adequate chemical yields but low optical yields in hydrosilylations of prochiral ketones, which was ascribed to the existence of two conformers with opposite phenyl ring arrangments which could lead to optically inactive products [32].

However, our understanding of the mechanism of such processes has not kept up with the rapid experimental development of new ligands, and today asymmetric catalysis is still largely empirical. Therefore the investigation of mechanisms and relative intermediates for the enantioselective catalysis has attracted our attention, since understanding of both will greatly assist in the design of new catalysts.

1.3 Mechanisms of Enantioselective Catalysis

1.Mechanism of olefin hydrogenation

Reactions involving transition metal complexes consist of elementary processes, most of which, such as oxidative-addition, reductive elimination, insertion, deinsertion, and external attack on coordinated ligands, proceed under mild reaction conditions. In order to discuss mechanisms of enantioselective catalysis, we first review the well-known mechanism of olefin hydrogenation by a transition metal complex. Two possible cycles are shown in Figure 1.1.8 [33].

In cycle A, H_2 first oxidatively adds to a coordinatively unsaturated species LnM in step (a), and complexation of an olefin in step (b) gives the dihydrido-olefin complex [M].

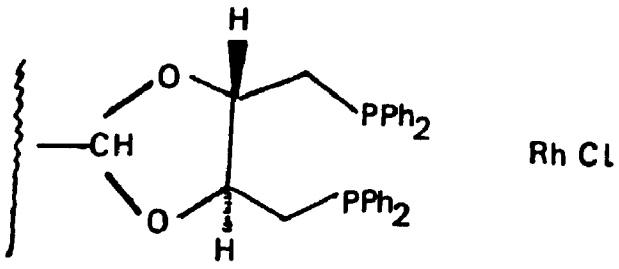

Figure 1.1.3 The polymer-bound chiral DIOP rhodium complex.

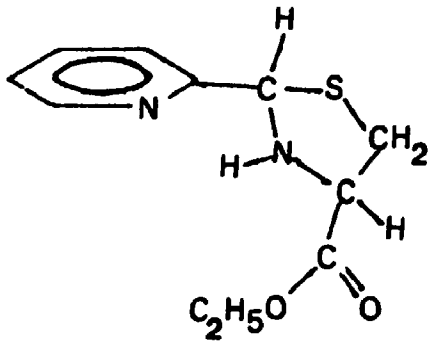

Figure 1.1.4 The Structure of pyridine thiazolidine ligand.

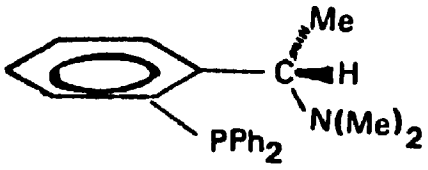

Figure 1.1.5 The structure of [N,N-dimethyl-1-(o-(diphenyl -phosphino)phenyl)ethylamine,amphos,.

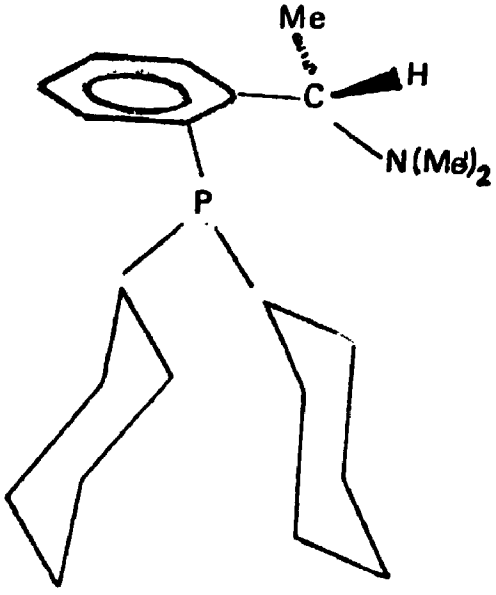

Figure 1.1.6 The structure of dicyphos

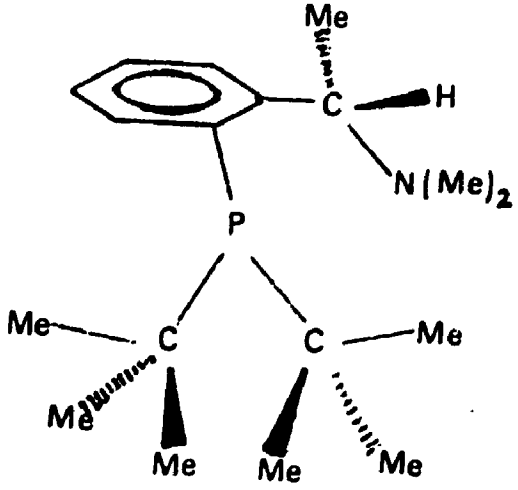

Figure 1.1.7 The structure of dibutphos.

The ensuing olefin insertion into one of the two M-H bonds [step (e)] gives a hydrido-alkyl complex that, on reductive elimination in step (f), liberates the alkane with regeneration of the coordinatively unsaturated complex LnM. This reacts further with H_2 to drive the catalytic cycle A in an anticlockwise direction. Figure 1.1.8 also illustrates cycle B, involving initial olefin complexation [step (c)] to LnM. Molecular hydrogen oxidatively adds to the olefin complex in step (d) to give the dihydrido-olefin species [M], which undergoes olefin insertion and reduction elimination of alkane. This regenerates LnM and thus drives the catalytic cycle B in a clockwise direction.

2. Mechanism of asymmetric hydrogenation.

The mechanism for homogeneous asymmetric hydrogenation using Rh-diphosphine complexes follows the same sequence of steps as in Figure 1.1.8. The mechanism differs in that the chiral catalyst provides an asymmetric environment which affects the coordination of the prochiral substrate species. In general, the unidentate chiral phosphines used in earlier work gave low and variable optical yields. The bidentate ditertiary phosphines are more rigidly coordinated to the metal and result in a greater constraint on the coordinated substrate. The nature of the substrate also affects the stero-selectivity. Figure 1.1.9 illustrates coordination of (Z)α-acetamidocinnamate with a rhodium complex containing a chiral bidentate diphosphine ligand (P-*P) [34,35].

On coordination of the olefin, asymmetry is induced at the

α-carbon atom of the olefin so that two diastereomers (A & B) are formed. The major diastereomer can be isolated, and its X-ray structure has been determined. The minor diastereomer could not be detected spectroscopically, so it must be present in amounts of less than 5%. In the former, the rhodium atom is bound to the si face, producing the minor diastereomer, and, in the latter, to the re face, producing the major diastereomer.

It was found that the predominant product of hydrogenation with the rhodium complex containing (S,S)-chiraphos was the *R* isomer with over 95% enantiomeric excess, and that it was produced from the minor diastereomer [50]. [The enantiomeric excess is a currently used measure of optical yield and is defined as the quantity $(X_R-X_S)/(X_R+X_S)*100$, where X_R and X_S are the relative quantities of *R* and *S* enantiomers. e.g. if 98% of one isomer and 2% of the other are produced, the enantiomeric excess (e.e) is 96% [18]].

Halpern [98] explained that, despite its smaller concentration, the minor diastereomer is hydrogenated more rapidly, since the activation energy $\Delta G^{\neq}_{mino}$ for H_2 addition to the minor diastereomer is significantly smaller than that for the major diastereomer. The minor diastereomer is the sterically favored diastereomer of the H_2 oxidative-addition adduct by examination of space filling (CPK) model [35], while the major diastereomer of the asymmetric induction arises from the stereoselectivity in the initial binding step rather than from the relative rates of hydrogenation of the

diastereomeric complexes [86a,94]. These results are schematically illustrated in Figure 1.2.0 [33]. Thus the important of kinetic studies in conjunction with structural studies is obvious, in order to understand the mechanism of the enantioselectivity.

3. Mechanism of asymmetric hydrosilylation of prochiral ketones

The addition of a compound containing an Si-H bond to olefins, acetylenes, aldehydes, and ketones is called hydrosilylation [36]. The mechanism of hydrosilylation probably resembles that of hydrogenation, and a possible scheme is shown in Figure 1.2.1 [29,46].

In this mechanism, an oxidative-addition of R_3SiH to a low-valent transition metal complex with cleavage of the Si-H bond has a precedent (step a). The prochiral ketone subsequently coordinates to the resulting the silylhydridometal complex, giving a silylhydridoalkyl(aryl)oxo metal complex (step b). Insertion of the coordinated prochiral ketone group into the M-SiR_3 bond (step c) gives the diastereomeric α-silyloxyalkyl or α-silyloxyaryl hydridometal intermediates that reductively eliminate chiral silyl ether products (step e) [33,46]

1.4 Study of Intermediates of Enantioselective Catalysis.

1.Wilkinson catalyst's intermediates

The homogeneous hydrogenation catalytic cycle by Wilkinson's complex depends entirely on the formation, concentration, and fate of the three-coordinate intermediate Rh(I)Cl-$(PPh_3)_2$ [36,86a,94]. It has been proposed by Tolman that

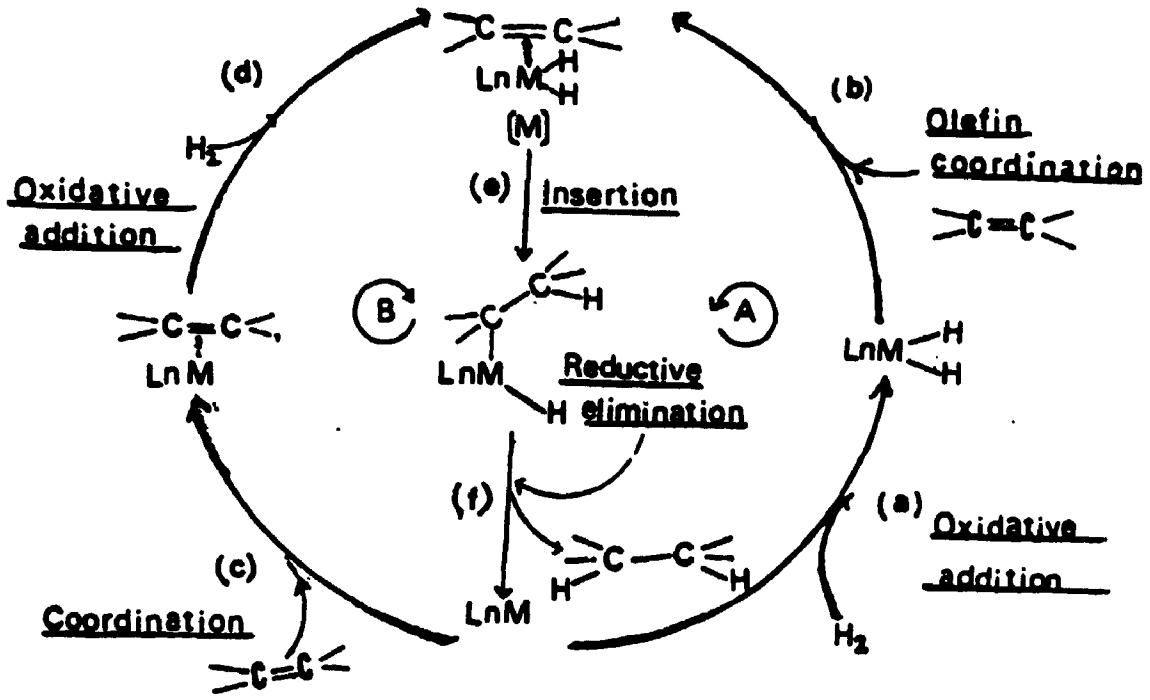

Figure 1.1.8 Two possible catalytic cycles in olefine hydrogenation with a transition metal complex catalyst.

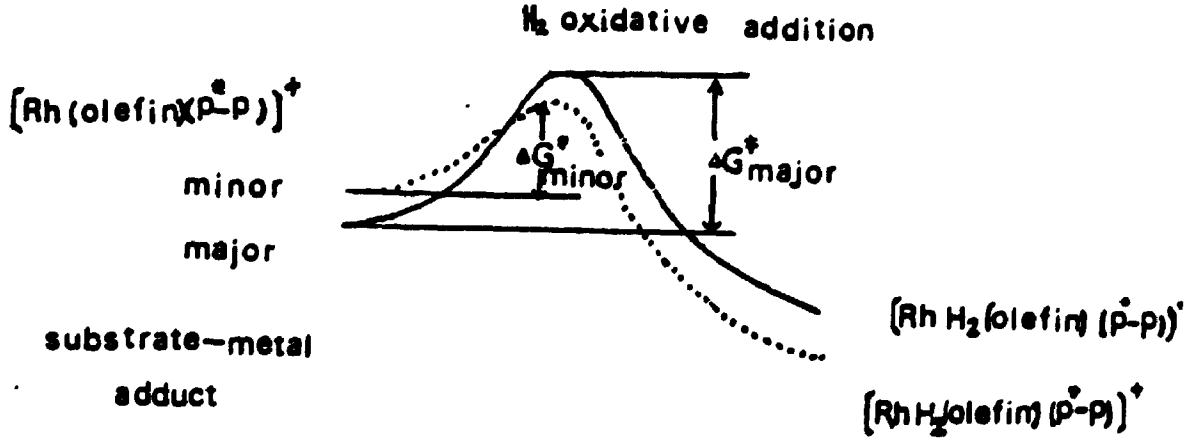

Figure 1.2.0 Schematic representation of control of asymmetric hydrogenation by a chiral rhodium catalyst.

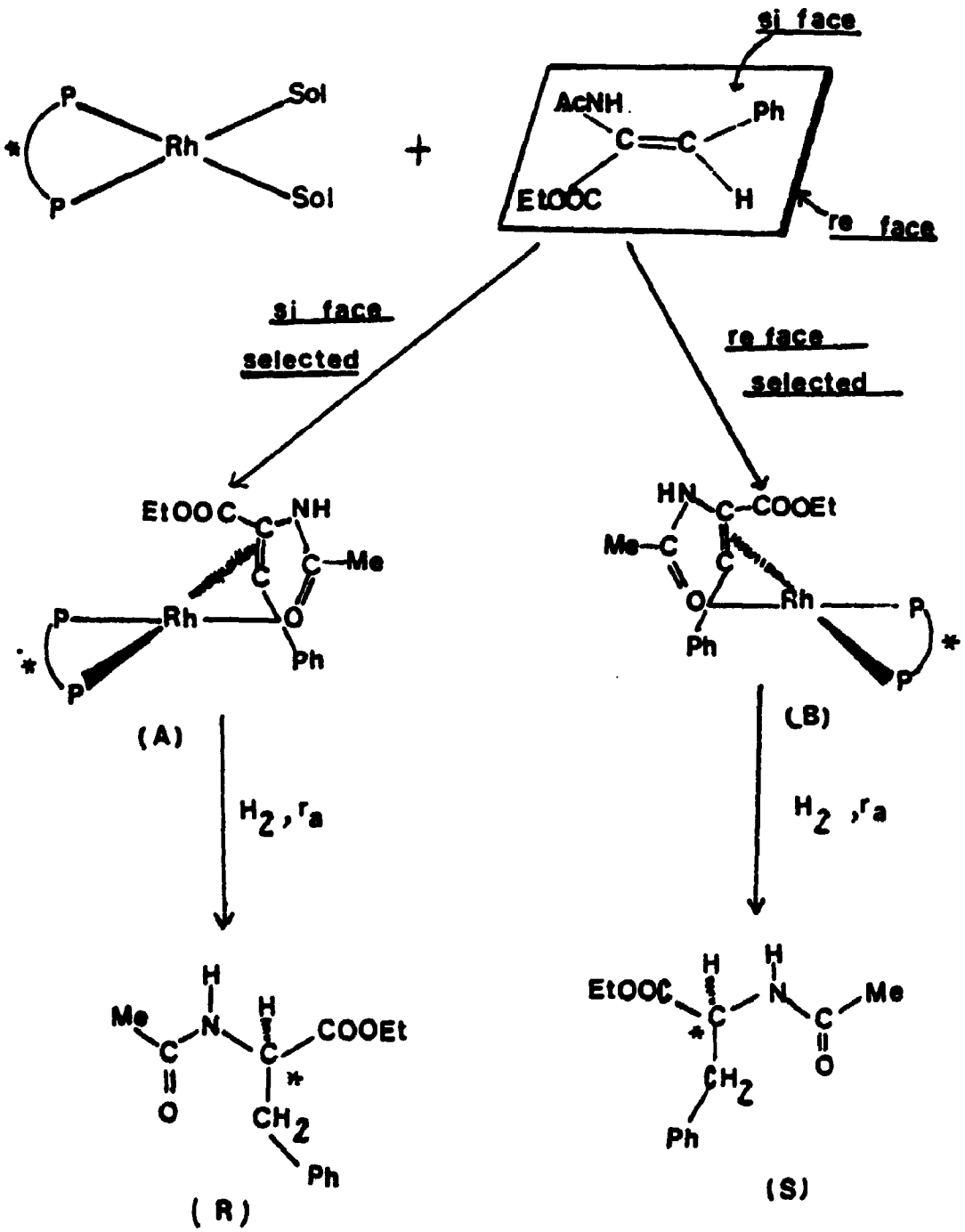

Figure 1.1.9 Two pathways in asymmetric hydrogenation of (Z)-α-acetamidocinnamate (EAC) catalyzed by a rhodium complex having a chiral bidentate ligand.

this species must be solvated, since the unsolvated compound violates the 16-electron rule [37,38]. Violation of this rule, however, is positively advantageous for catalytic intermediates. The 16-electron rule applies to stable, isolable species, and as Halpern points out [39], the least desirable properties of such intermediates are stability and isolability. It is difficult to prove or disprove whether $Rh(I)Cl(PPh_3)_2$ is solvated. A solvated species is proposed in one mechanistic scheme, and a solvent concentration term is incorporated in the kinetic equation [40].

The inhibiting effect of added triphenylphosphine, and experiments performed at tertiary phosphine-rhodium ratios of 2 [41] both indicated that the most active species in the catalytic cycle is the complex $Rh(III)(H)Cl(H)(PPh_3)_2$ rather than the corresponding tris(triphenylphosphine) complex. Halpern points out that both the tris- and bis(triphenylphosphino)dihydrido complexes participate in the catalytic process, but the reaction rate of the former is much slower than the latter [39].

The addition of alkene to form an octahedral dihydrido alkene complex requires the alkene to be cis to at least one hydrido ligand. Originally it was believed [42] that the alkene added to a site cis to two mutally cis hydrido ligands. The most recent view, in accordance with trans effect considerations, is that the complex formed has the geometry shown in Figure 1.2.2; that is, the alkene is added trans to one hydrido ligand and inevitably cis to the second [43].

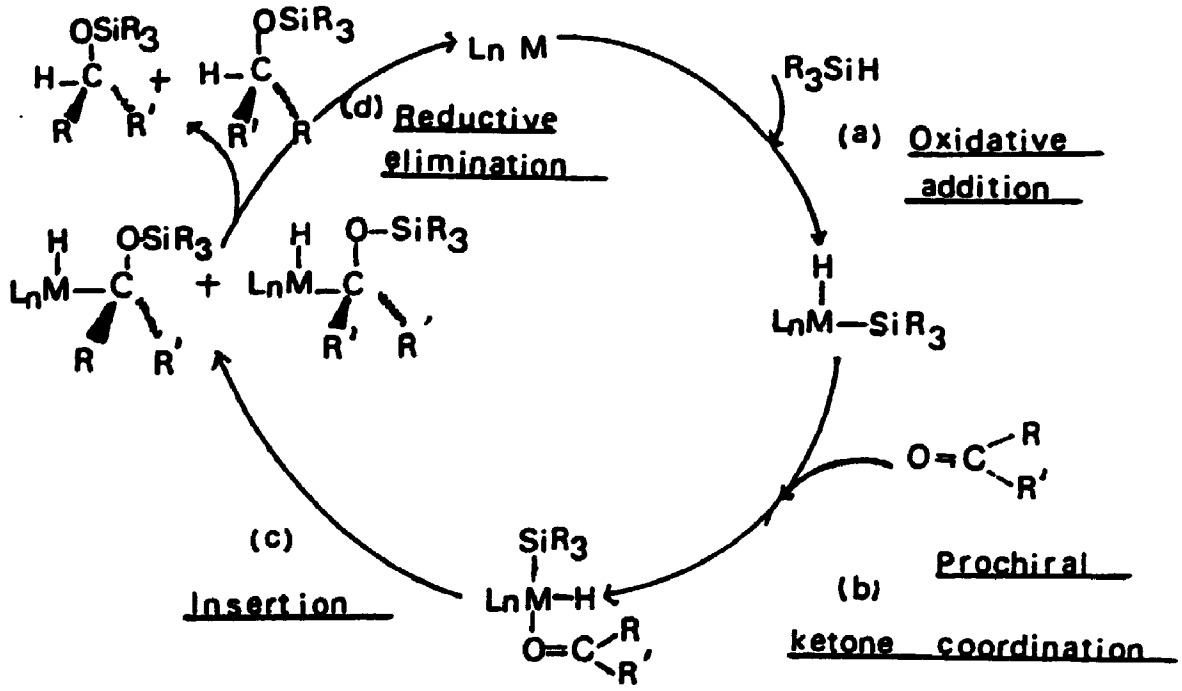

Figure 1.2.1 Mechanism of prochiral ketone hydrosilylation (ligands are omitted).

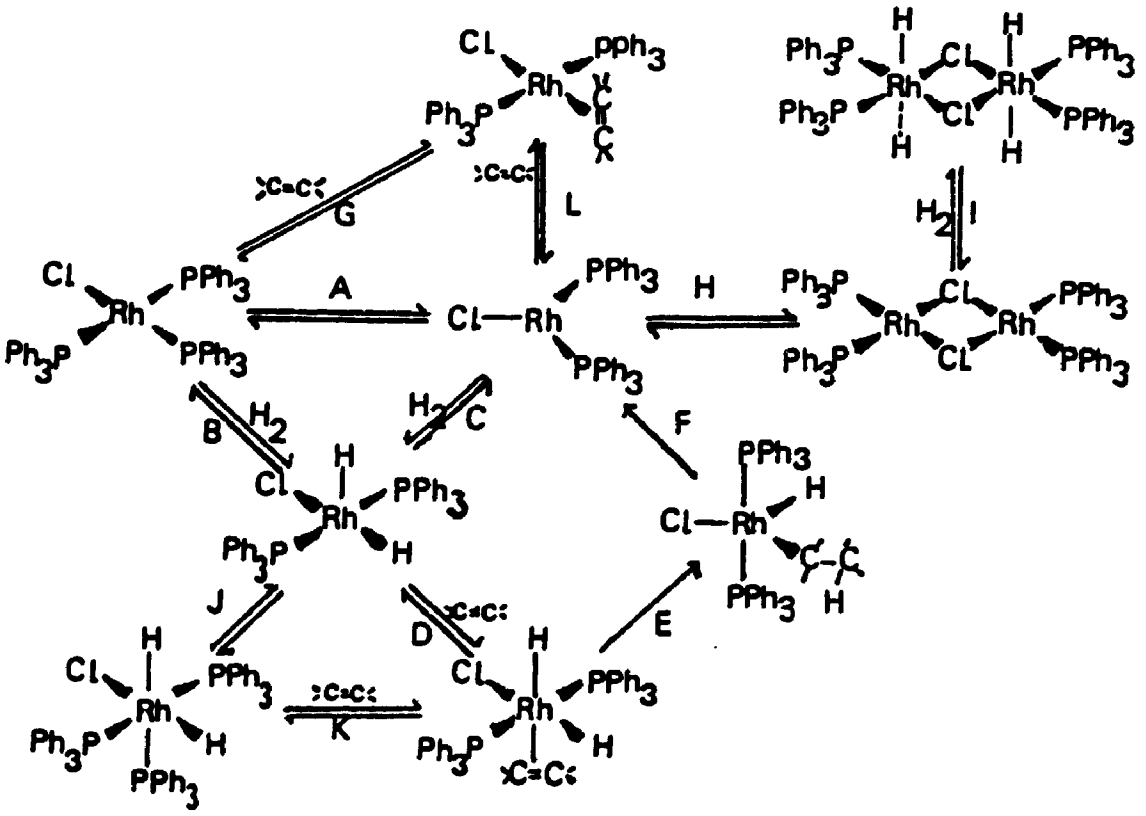

Figure 1.2.2 The intermediates of Wilkinson catalyst.

Figure 1.2.2 shows all possible intermediates of a Wilkinson-type catalyst [36].

The oxidative addition of hydrosilanes to chloro-tris-(triphenylphosphine)rhodium(I) (Wilkinson catalyst) forms the five-coordinate species $Rh(III)HCl(SiR_3)(PPh_3)_2$. Despite the widespread use of the $Rh(III)HCl(SiR_3)(PPh_3)_2$ complex in catalytic hydrosilylation, comparatively few complexes have been isolated and characterized [36]. The complexes are usually solvated [44]. It has been shown by X-ray crystallography that the solvent of crystallization in $Rh(III)HCl(SiCl_3)(PPh_3)_2.XSiHCl_3$ is not associated with the rhodium. The complex is approximately trigonal bipyramidal, with phosphine ligands in axial positions. However, an ortho hydrogen of one triphenylphosphine ligand molecule is sufficiently close to the metal to raise the coordination number arguably to six; the angle ∠PRhP is only 162° (Figure 1.2.3) [45].

2. The α-silyloxyalkylrhodium complex intermediates.

Asymmetric hydrosilylation reactions are catalyzed by a rhodium(I) complex with optically active phosphine ligands, e.g. $[P^*(CH_3)(Ph)(CH_2C_6H_5)]$ ligand. A mechanism of the induction of asymmetry was proposed by Ojima et al [48]. He thought that the configuration of the α-silyloxyalkyl rhodium complex (Figure 1.2.4) intermediate was very important, and depended upon the relative bulkiness of the substituents of ketones, those of the chiral phosphine and of the silyloxy groups. With a silyloxy group bulkier than either of the

substituents of the ketone, i.e., ≡SiO > L > S, stereochemical considerations, using a Dreiding model of the intermediate, led them to the conclusion that the silyloxy group should occupy the quasi-apical position, which is the least hindered site and lies between the methyl and the benzyl group of the chiral phosphines. It follows, that the substituent L lies between the methyl and phenyl groups, and the substituent S lies between the benzyl and phenyl groups. The arrangement is shown as C_1 in Figure 1.2.5 in which (*S*)-BMPP is employed as a ligand. In a similar manner, when the order of bulkiness is L > ≡SiO > S, the most stable arrangement is C_2, and when L > S > ≡SiO, the most stable arrangement is C_3. As can be seen from Figure 1.2.5, the alcohol derived from C_1 has the same configuration as that derived from C_3, whereas the alcohol derived from C_2 has an opposite configuration, given the priority sequence proposed by Cahn, Ingold and Prelog [49] of the substituents on the carbon atom.

Kumada also points out [51] that, because of the formation of a pair of diastereomeric α-silyloxyalkyl rhodium intermediates, the predominant configuration and the extent of enantiomeric excess of the product already would have been determined. It is, therefore, reasonable to suppose that the steric demands of not only the chiral phosphine ligand, but also of the substituents on the silicon atom bound to the rhodium catalyst, exhibit a significant effect on the selection of enantiotopic faces of a prochiral ketone.

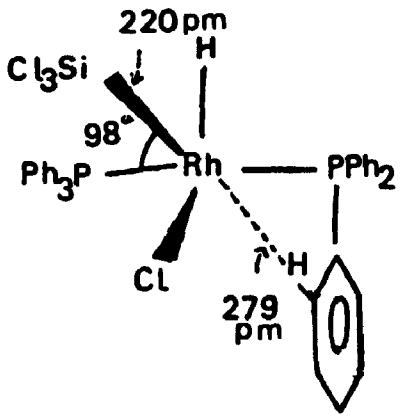

Figure 1.2.3 The structure of silyhydrido rhodium complex [RhHCl(SiCl)$_2$(PPh)$_2$].

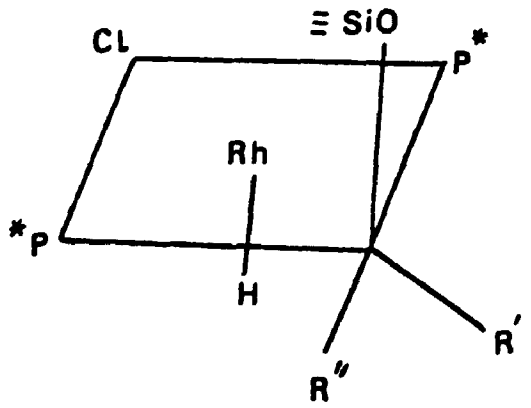

Figure 1.2.4 The square-pyramidal structure of the α-Silyloxyalkyl rhodium complex.

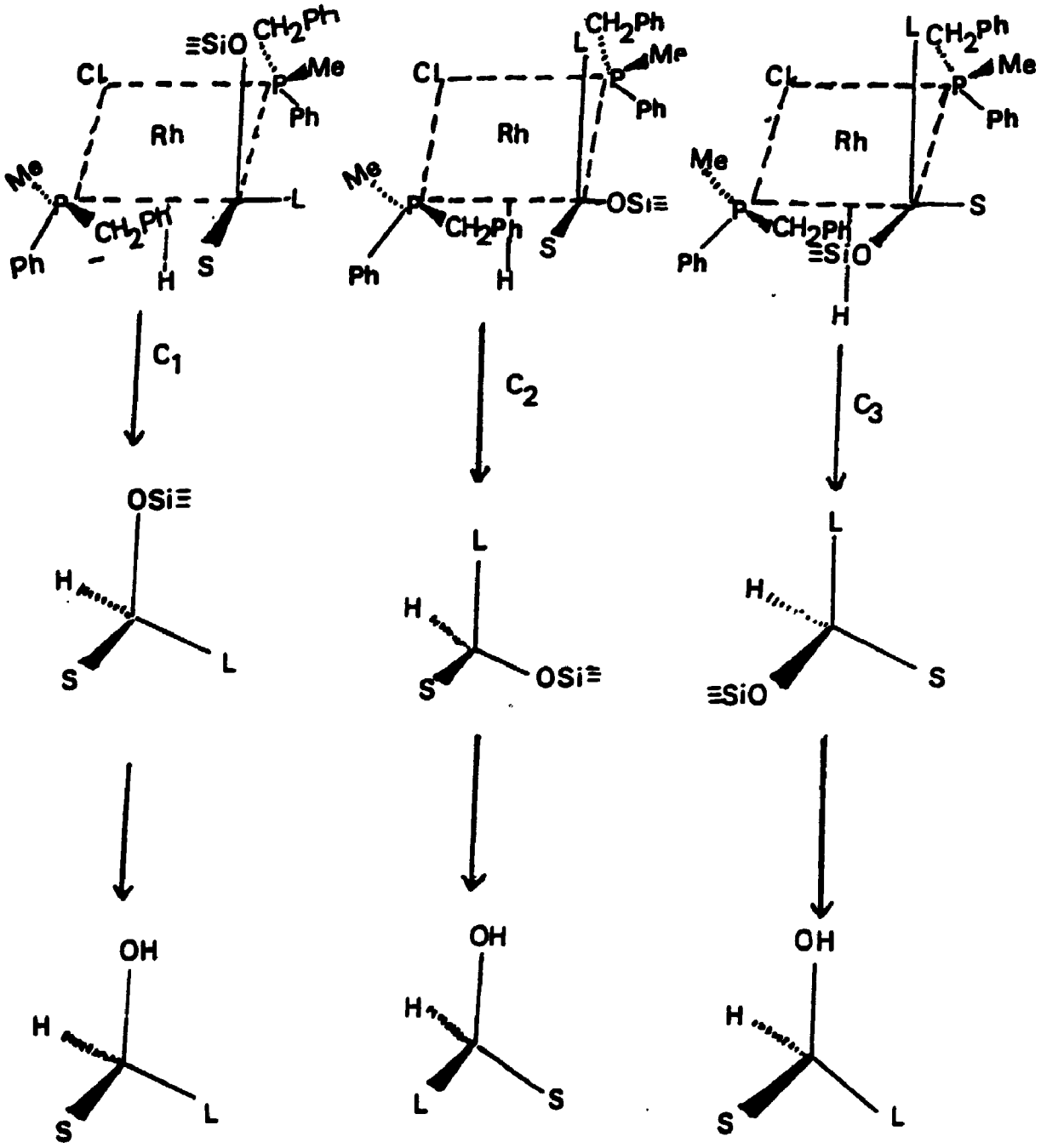

Figure 1.2.5 The configuration of the intermediates.

1.5 Scope of the Thesis

Our interest in the enantioselective catalysis field is focussed on the study of the intermediates formed from the rhodium amphos complex [31,32] during homogeneous, asymmetric hydrosilylation reactions, in order to understand the mechanism of optical discrimination in this system.

Most of the work described in this thesis involves the synthesis and study of the geometry and stability of derivatives of the neutral Rh(I)Cℓ(*R*-amphos)(PPh_3) complex, (Figure 1.1.5 shows the amphos ligand), and the features of its oxidative addition products formed by reaction with the silane $HSiCℓ_3$ both in solution and in the solid state.

Spectroscopic techniques including ^1H & ^{31}P NMR, Visible, Infra Red, and Mass spectroscopies were used to monitor the formation of the oxidative addition products - perhaps the catalytic intermediates in asymmetric hydrosilylation reactions - since these techniques provide information not only about the composition, but also about the configuration and labilities of species actually present in solution. These studies have resulted in the elucidation of a mechanistic scheme for homogeneous, asymmetric hydrosilylation.

X-ray crystallographic techniques were employed to determine three single crystal structures: the first was the neutral Rh(I)Cℓ(*R*-amphos)(PPh_3) complex; secondly, in a certain favorable case, one of the oxidative addition

adducts in the reaction of Rh(I)Cl(*S*-amphos)(PPh_3) with $HSiCl_3$, chlorohydridotrichlorosilylbis(triphenylphosphine) rhodium(III), was isolated and characterized; the third was a Rh complex containing the diaminophosphine ligand (the ligand was made by Ian Mckay - an earlier member of our research group). These structural studies have helped us to better our understanding of the features which give rise to the asymmetric environment presented by a catalyst to a substrate molecule.

Another project described herein is a study of the optical yields of hydrosilylation of prochiral ketones with α-naphthylphenyldihydrosilane, catalyzed by neutral and cationic Rh(I)-amphos complexes. This particular silane was prepared and the optical yields of both alcohol and MeSiH(Ph)(α-Naphthyl) were determined. This project extends the study of asymmetric hydrosilylation to the use of very bulky silane as a reagent. It has helped us to understand that the extent of the asymmetric induction, as well as the configuration of the predominant alcohol produced, are dependent not only on the structure of the chiral phosphine ligand and those of the prochiral ketones, but also on the nature of the particular silane used.

CHAPTER 2

Synthesis, ^{1}H & ^{31}P NMR, and X-ray Crystal Structure of Chloro-[(*R*)-N,N-dimethyl-1-(o-(diphenylphosphino)phenyl)-ethylamine](triphenylphosphine)rhodium(I).

2.1 Introduction

The oxidative-addition of a hydrosilane $HSiR_3$ to chiral Rh-aminophosphine complexes has aroused our interest and the study of the resulting intermediate species has been expected to further our understanding of the mechanism of asymmetric, homogeneous hydrosilylation of prochiral ketones using such complexes as catalysts. In earlier studies of these systems, the structures of three chiral complexes of rhodium containing a norbornadiene (NBD) ligand, and either an aminoarsine [31] or an aminophosphine [32] ligand were determined, and the structure of a dichloropalladium aminophosphine complex was reported [52,53]. Two geometrical isomers were found for the Rh-aminophosphine species in solution [54], since the substrate ketone (or a solvent molecule) can coordinate in a position either cis or trans to the phosphine group (Figure 2.1.1). It was therefore of interest to examine which site would be preferentially occupied by a bulky ligand, and to discover whether the trans-influence or steric bulk would determine the product.

Reaction of triphenylphosphine with the complex [RhCl(amphos)S] gave only a cis isomer, $Rh(I)Cl(Ph_3P)$-

[(*R*)-o-((C$_6$H$_5$)$_2$PC$_6$H$_4$CHCH$_3$N(CH$_3$)$_2$], which was isolated from solution. In this chapter, the results of synthesis, ^{1}H & ^{31}P NMR and single crystal X-ray structure determination of Rh(I)Cl(R-amphos)(Ph$_3$P) are reported. As this is the first of the three structural determinations presented in this thesis, the experimental procedures are described in more detail than in later chapters.

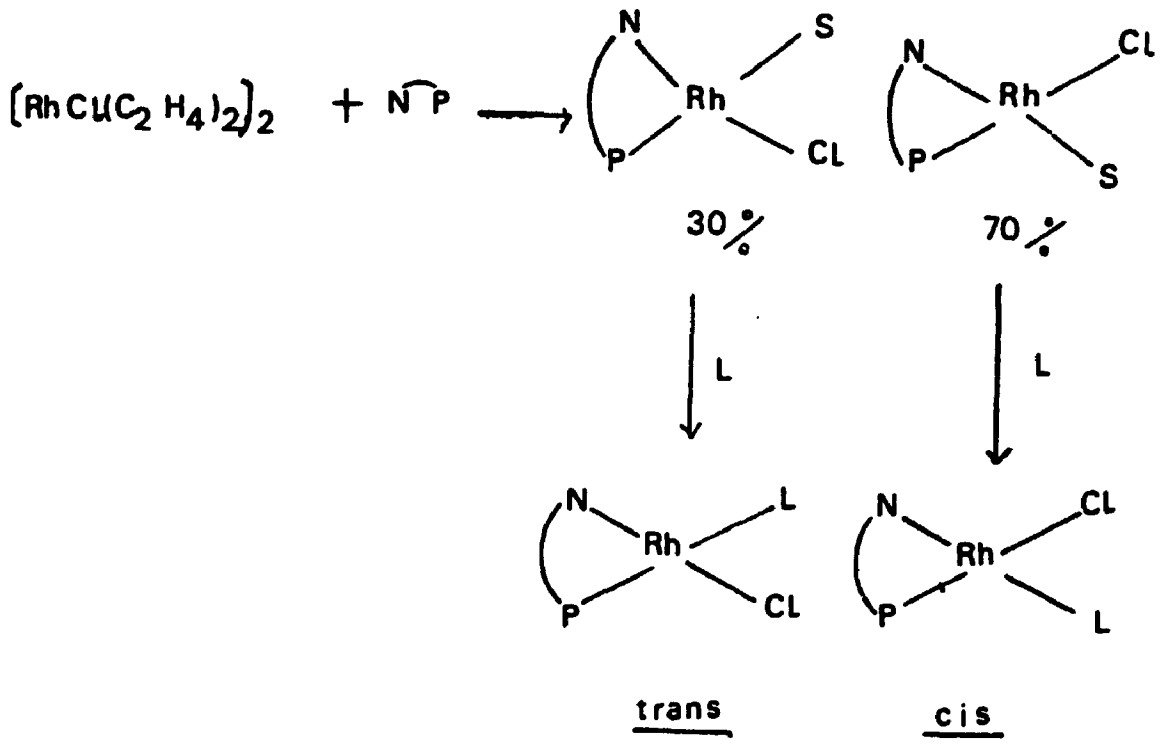

Figure 2.1.1 Geometric isomerism for the complexes [RhCl(amphos)S] and [RhCl(amphos)L], where S is a solvent, L is the ligand.

2.2 Synthesis, ^{1}H & ^{31}P NMR of Rh(I)Cl(*R*-amphos)(PPh$_3$) Complex.

1. Synthetic procedure.

(*R*)-N,N-dimethyl-1-(o-(diphenylphosphino)phenyl)ethylamine,

(*R*-amphos), as prepared previously [31], 85mg (0.256 mmole) and triphenylphosphine, 67 mg (0.256 mmole) were added to a solution of $[(C_2H_4)_2RhCl]_2$ ('Cramer's compound'), as prepared previously [55]), 50 mg (0.128 mmole) in dry degassed CH_2Cl_2 (15 mL) under an argon atmosphere. Schlenk-tube techniques were used throughout. After gas evolution (C_2H_4) ceased (30 minutes), stirring was continued for another three hours. The red solution was filtered under argon into a Schlenk-tube, removing unreacted starting material. The solvent was evaporated and a red gel remained. Dry, degassed acetone, 15 mL, was added and the mixture was concentrated until red hexagonal crystals, m.p. 126° (dec.), formed. Elemental analysis: found: C 65.02, H 5.65, N 1.96 % ; calc. C 65.45, H 5.32, N 1.91 %.

2. ^1H & ^{31}P NMR spectroscopy.

^1H NMR data for amphos, the free ligand, the cation of the salt [Rh(*R*-amphos)NBD]ClO_4, the complex (A) [RhCl(*R*-amphos)-(PPh_3)], and a third species, are summarized in Table 2.2.1. ^{31}P NMR data for the complex (A) and the third species are summarized in Table 2.2.2. All ^{31}P & ^1H NMR spectra were recorded on Varian XL-300 and XL-200 spectrometers respectively.

The ^{31}P NMR spectrum of [RhCl(*R*-amphos)(PPh_3)], complex (A), in dilute solution in CD_2Cl_2 consists of two doublets of doublets, Figure 2.2.4. One is centered at 25.3 ppm, which represents the P atom of the amphos ligand coupled to the Rh atom and cis coupled to the PPh_3 ligand; another is centered

at 19.2 ppm, and is the P atom of the PPh_3 ligand coupled to the Rh atom and cis coupled to the amphos ligand. In spectra of freshly prepared solutions, there was no sign of dissociation of the PPh_3 ligand; however, on standing, a peak at 26.79(s) ppm appeared which is attributed to triphenylphosphine oxide.

In the ^1H NMR spectrum of (A) in dilute solution in CD_2Cl_2, the N-methyl protons form a doublet centered at 3.30 ppm, with a small (4 Hz) coupling which could be attributed to either a 3-bond coupling to Rh, or to a 4-bond coupling through rhodium to the P atom of PPh_3 trans to the N atom. Some extra peaks in the N-methyl proton region occur at 3.24(s) and 1.98(s) ppm as very weak signals; the intensity ratio between the 3.30 ppm signal and those extra peaks is approximately 10:1. The C-methyl protons form a doublet centered at 1.48 ppm, accompanied by a very weak doublet at 1.34 ppm.

Surprisingly, we were unable to recrystallize the complex from either CH_2Cl_2 or $CHCl_3$. The ^{31}P NMR spectrum of a concentrated solution of (A) in $CDCl_3$ is shown in Figure 2.2.5, the ^1H NMR spectrum of a more concentrated solution in CD_2Cl_2 is shown in Figure 2.2.3. Both spectra show extra peaks at the higher concentration. In Figure 2.2.5, there are extra signals in the form of two doublets of doublets of comparable intensity, shifted slightly up field. This spectrum is best explained by postulating some dissociation of the Rh-N bond [56b] to form complex (B). The chemical shift of the P atom of the amphos ligand in which the N atom is not

bonded to the Rh metal in (B) is more up field than that of the P atom of the amphos ligand in (A), and the signal due to the PPh_3 ligand in (B) is more up field too, because the P atom of the PPh_3 ligand is trans to the solvent instead of a N atom. The same explanation applies to the observed coupling.

This dissociation is also seen in the ^1H NMR, Figure 2.2.3. The intensity ratio between the N-methyl protons centered at 3.30 ppm and the extra peaks at 1.98(s) and 3.24(s) ppm is now 3:1. The intensity of the doublet at 1.34(d) ppm is also greater. There was no sign of a signal at 2.84(s) ppm attributable to an amphos·HCℓ ligand [32].

A close inspection of the resonance centered at 24.39 ppm, Figure 2.2.5, shows an anomalous four lines shape in which the outside two lines are more intense than the two inside lines. Furthermore, the intensity ratio between the extra signals centered at 24.39 ppm and the extra signals centered at 18.80 ppm is only approximately 1:1. The overlap in the spectrum prevents an accurate measurement, but the ratio may be as high as 1.3:1. In concentrated solution, a signal due to either free PPh_3 at -20 ppm, or triphenylphosphine oxide at +26 ppm, is always found. We assume that additional species may also be present in the solution.

The greatest contribution to the extra signals is from complex (B). Two geometrical isomers are unlikely to be present [60], because the ^{31}P NMR spectra for (A) and (B) showed the P atom on amphos of (B) to be 0.91 ppm upfield of that of (A), but the P atom of PPh_3 of complex (B) was only

0.40 ppm upfield of that of (A). Dissociation of Rh-N bond is easier because the PPh_3 ligand is a π-bonding ligand, which has a " trans-influence" in weakening the bond trans to it.

A possible reaction scheme is shown in Figure 2.2.2 [57,58]

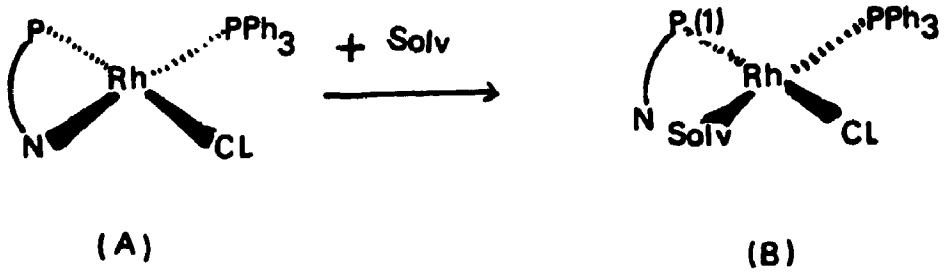

(A) (B)

Figure 2.2.2 Dissociation of the square planar $RhCl(PPh_3)$-(*R*-amphos) complex.

Table 2.2.1 ^1H NMR data and assignment for ligand and complexes.

Assignment	Chemical shift (ppm)				Coupling constant (Hz)			
	Ligand[b]	Cation[a]	Complex (A)[a]	(B)[a]	Ligand	Cation	Complex (A)	(B)
Phenylaromatic (m)	6.9-7.6	7.2-7.5	6.5-7.9	6.5-7.9				
1H (d of q) methine	4.16	3.62	4.94	4.94	$J(HC-CH_3)$ = 6.0 $J(PC=CCH)$ = 6.0	$J(HC-CH_3)$ = 9.0 $J(PC=CCH)$ = 2.0	$J(HC-CH_3)$ = 7.0 $J(PC=CCH)$ = 2.0	$J(HC-CH_3)$ = 7.0 $J(PC=CCH)$ = 2.0
6H N-methyl	2.04(s)	2.62(d)	3.30(d)	3.24(s) 1.98(s)		$J(CH_3-N-CH_3)$= 8.0	$J(PPh_3-N-CH_3)$= 4.0	
3H chiral centre - methyl	1.20(d)	1.72(d)	1.48(d)	1.34(d) 1.48(d)	$J(HC-CH_3)$ = 6.0	$J(HC-CH_3)$ = 9.0	$J(HC-CH_3)$ = 7.0	$J(HC-CH_3)$ = 7.0

a. in $CDCl_3$ at room temptr.; b. in CD_2Cl_2 at room temptr.

Table 2.2.2 ^{31}P NMR spectra data and assignment for complexes

Compound	Assignment	Chemical Shift (ppm) a	Coupling Constant (Hz)
[Rh(R-amphos)(PPh_3)Cl]	P in amphos	25.3 (d of d)	J(Rh- P)=151.0
	P' in PPh_3	19.2 (d of d)	J(Rh-P')=125.0
			J(P'-P)=22.9
Complex (A)			
[Rh(R-amphos)Cl]$_2$(PPh_3)	P(1) in amphos(free	24.39(d of d)	J(Rh-P")=151.0
Complex (B)	lone pair in N)		
	P' in PPh_3	18.80 (d of d)	J(Rh-P')=125.0
+free PPh_3	free PPh_3	-20.0 (s)	J(P"-P')=22.9

a in $CDCl_3$ at room temptr

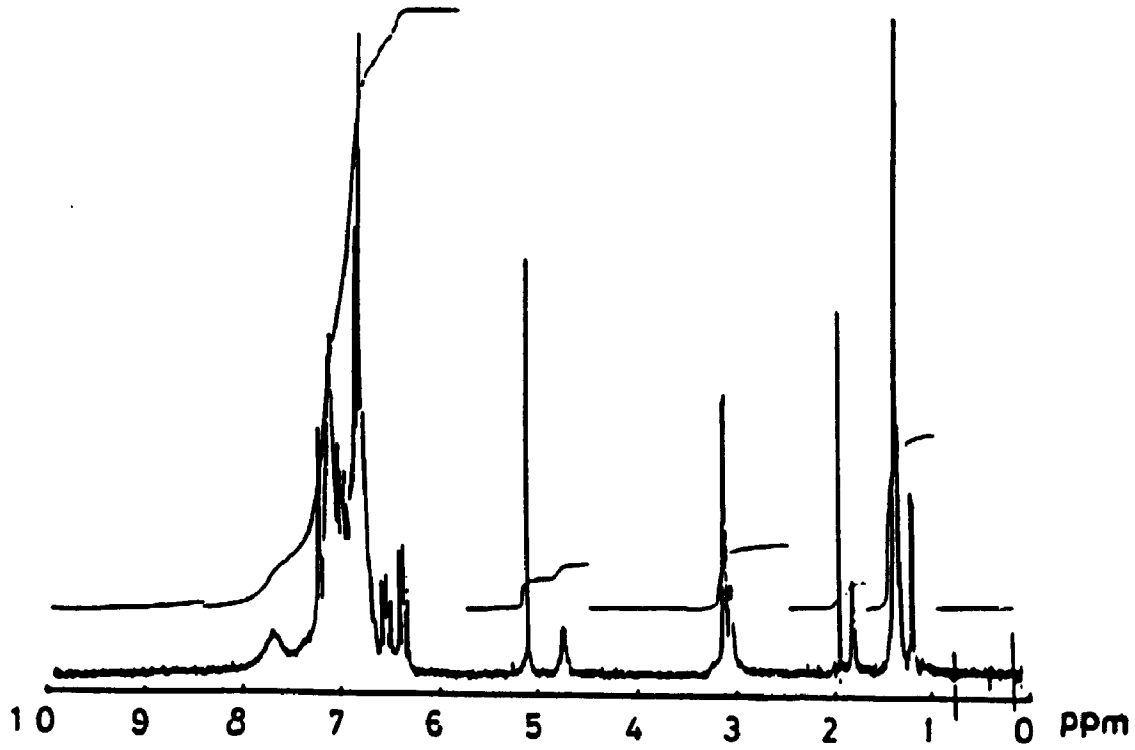

Figure 2.2.3 ^{1}H NMR spectrum of Rh-amphos complex in concentrated solution in CD_2Cl_2.

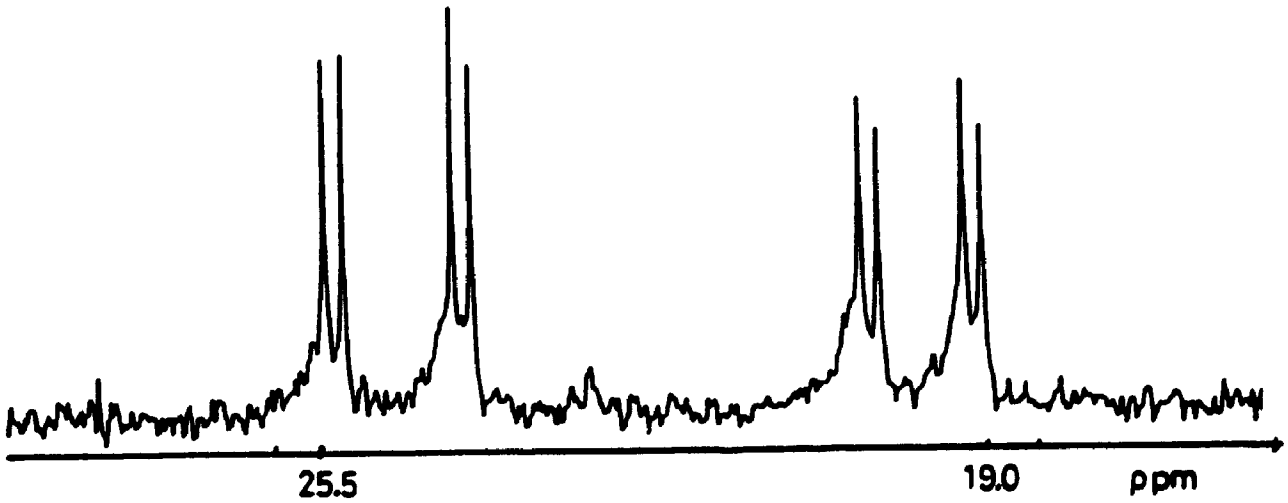

Figure 2.2.4 ^{31}P NMR spectrum of Rh-amphos complex in diluted solution in CD_2Cl_2.

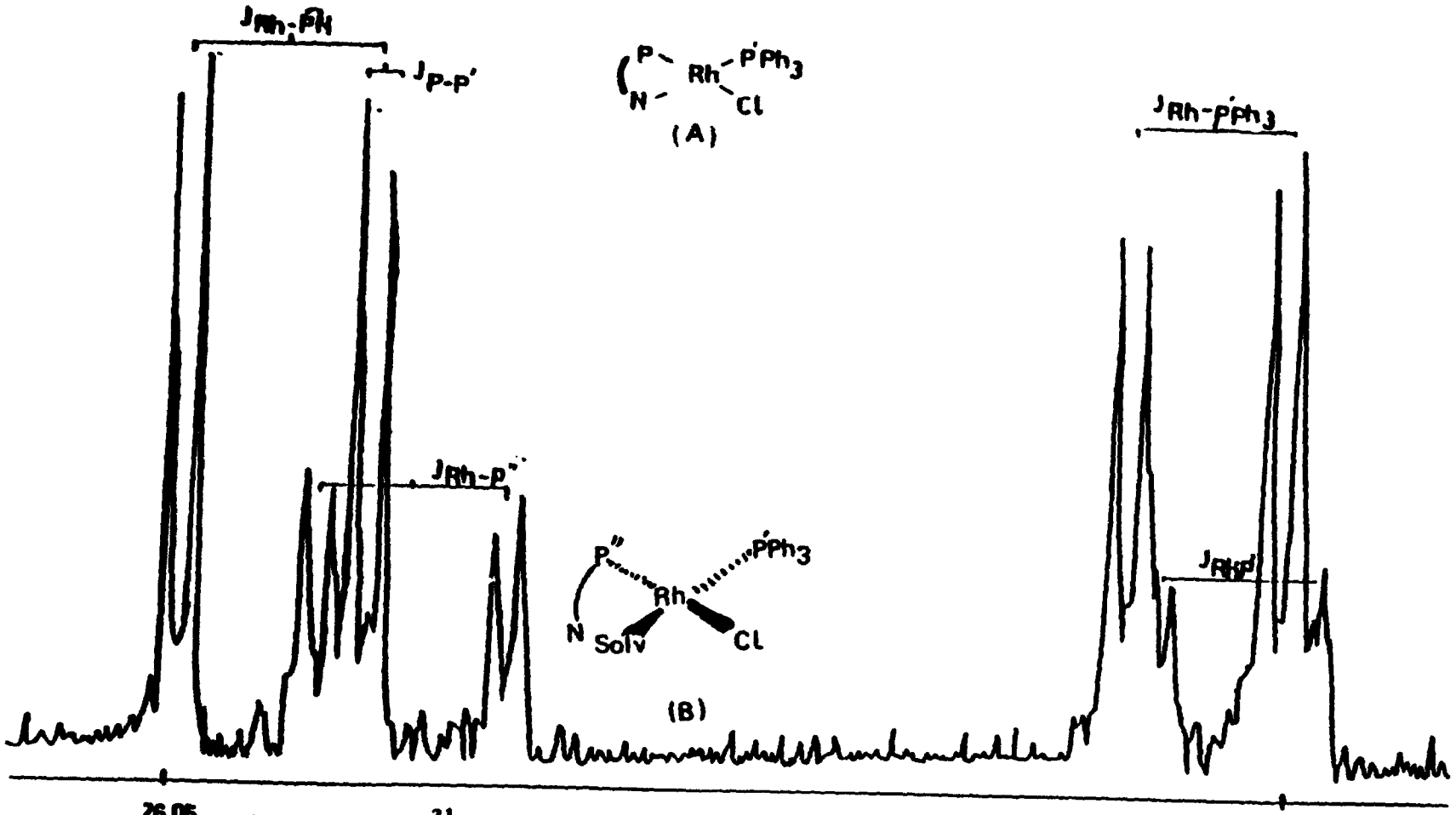

FIGURE 2.2.5 ^{31}P NMR Spectrum of Rh-amphos Complex in Concentrated Solution in $CDCl_3$.

2.3. A Single Crystal X-ray Diffraction Study of Rh(I)Cl-(*R*-amphos)(PPh_3)

1. Photographic examination.

A crystal is a complex, though orderly, arrangement of atoms. All atoms in the path of an X-ray beam scatter X-rays simultaneously. In general, the scattered waves interfere with and destroy one another, but in certain specific directions, they combine to form new wavefronts. This cooperative scattering is known as diffraction. The directions of possible diffraction depend on the size and shape of the unit cell. Certain classes of diffraction are systematically extinguished by lattice centering and by the presence of space-group symmetry elements. The intensities of the diffracted waves depend on the kind and arrangement of atoms in the crystal structure. Thus a study of the geometry of diffraction from a crystal yields the unit cell dimensions. An analysis of the missing spots gives the unit symmetry (space group) of the structure. The intensities are needed to work out the arrangement of atoms.

A photographic examination employing Weissenberg and Precession techniques can be used to provide the unit cell constants, and the symmetry of the crystal lattice, and together with the density, to provide the number of formula units per cell. The theoretical background for these techniques is presented in many texts (i.e. [61]) and will not be described here.

The red, hexagonal crystals of Rh(I)Cl(*R*-amphos)(PPh_3) were examined using binocular and polarizing microscopes to find one suitable for photographic study. The crystal chosen was transparent, with proper size and uniform, well-formed external faces. When examined with plane-polarized light, a single crystal in which the lattice is not isotropic should appear uniformly dark once every 90° turn and be bright once in every 90° turn. Crystals which are made up of two or more fragments with different orientations will often reveal themselves by displaying both dark and light regions at one time, and should be discarded at this stage. The crystal chosen was mounted such that the long dimension was roughly coincident with the rotational axis of the goniometer head. It was along this dimension that the crystal extinguished plane-polarized light.

The crystal was transferred to a Stoe Weissenberg camera, with which Cu Kα radiation (λ = 1.5418 Å) was used throughout the photography. X-rays were used to align the crystal more accurately about a direct axis; these setting photographs showed a mirror plane perpendicular to the rotation axis, implying lattice symmetry higher than triclinic. Zero, first and second level Weissenberg photographs were recorded. They showed the hk0, hk1 and hk2 classes of reflections and revealed mm symmetry, suggesting the orthorhombic system. The same crystal was transferred to a Buerger precession camera without remounting. The precession technique involves rotation of the crystal about a reciprocal axis, so that c^*

replaces the direct axis, c, as the rotation axis. In this case, the direct axis and the reciprocal axis of rotation were coincident Setting photgraphs were taken to align more accurately thc crystal about the reciprocal axis, and 0kℓ, 1kℓ, 2kℓ, h0ℓ, h1ℓ, and h2ℓ reciprocal lattice levels were taken. The symmetry of the photographs corresponded to the Laue group mmm, confirming that the crystal belonged to the orthorhombic system with systematic absences, h odd for h00, k odd for 0k0, and ℓ odd for 00ℓ. The known chiral nature of the complex is consistent with the unambiguous assignment of the space group $P2_12_12_1$, D^4_2, No.19. From the photographs, the following preliminary unit cell constants were calculated.

a = 17.27 Å $\quad\quad$ $\alpha = \beta = \gamma = 90°$

b = 18.99 Å $\quad\quad$ cell volume = 3480 Å^3

c = 10.66 Å

The density, 1.403 g/cm^3, was determined by flotation in a mixture of dichloromethane and hexanes. These data indicate Z = 4, for which the calculated density is 1.400 g/cm^3. No crystallgraphic symmetry is imposed upon the molecular species.

2. Data collection

A second crystal was chosen, having approximate dimensions 0.33 x 0.24 x 0.19 mm^3, and a similar morphology to that selected for the photographic examination. An optical goniometry study on a Huber two-circle optical goniometer revealed twelve faces, to be identified as {100}, {010}, and {111}. After data collection, the crystal faces were accurately measured by a microscope fitted with a filar

eyepiece in preparation for an absorption correction.

Intensity data were collected on an Enraf-Nonius CAD-4F diffractometer, using Mo Kα radiation (λ = 0.71069 Å), monochromatized by graphite. (The 0,0,2 graphite plane acts as the reflection plane for monochromator.) The crystal, mounted in a random orientation, was centred optically at the view position (θ =12 and -73°) to obtain the correct height. A Polaroid rotation photograph at Kappa = 0 found a strong reflection which was suitable for use with the ALIGN routine [99] to improve the crystal centering. Once the crystal was centered, the peak was checked by plotting an ω-scan with a wide open counter. The peak was single. 15 to 20 low and high angle, strong reflections located from the Polaroid photograph were located and centered using the routines, PHOTO and SETANG, in order to get preliminary cell constants and an orientation matrix. The reflections were all indexed using the routine, INDEX. The reflection (1,0,2) was used to align the crystal such that its center of gravity was coincident with the center of the X-ray beam.

24 strong, high angle reflections, selected from the photographs, were used to further improve the orientation matrix and cell constants. A quick sampling data collection for the 25° to 30° shell was performed in order to get even higher angle data and a good orientation matrix. ω-scans for the (1,0,2), (2,0,0), (0,2,0) and (0,0,6) reflections confirmed that the crystal was single and suitable for data collection. The average peak width at base was 0.21° and at

half-height was 0.14°. Cell constants and an orientation matrix were refined based on the setting angles at +θ and -θ of 24 carefully centred reflections with 30°<2θ<38° at 293K. Satisfactory standard deviations were achieved on all dimensions. The crystal is acentric (space group $P2_12_12_1$). Only 1/8 of the total reflections were collected, and so Friedel pairs were not included. 5767 observations ($0 \leq h \leq 22$, $0 \leq k \leq 24$, $0 \leq l \leq 13$ by routine TH) were collected using a θ - 2θ scan (moving crystal - moving detector method) up to a maximum 2θ of 60° (routine DATCOL); ($\sin\theta/\lambda = 0.70354$ $Å^{-1}$). Variable scan rates within a maximum per datum of 75 sec. and 0.80° of scan width, were used in order to optimize counting statistics. Later, 35 reflections which had asymmetric backgrounds were collected again by using scans of width 1.40°.

Background measurements were recorded at 25% extensions of the scan range. For extremely strong reflections, a Zr foil attenuator with an accurately known transmission factor was inserted between crystal and counter to protect the counter from overloading. Rates in excess of 102,400 counts, when recorded, were automatically attenuated [99].

Standard reflections, (1,0,2), (2,0,0), (0,2,0) and (0,0,6) were recorded every 10600 sec. of X-ray exposure time (average decay 0.5%, no correction applied). An orientation check, using three reflections which were (12,5,0), (0,16,4), (0,2,8), was done at 200 reflection intervals throughout data collection to look for movement of the crystal and for

instrument instability. Deviation of the observed position of the reflection from the calculated position by an amount equal to or greater than 0.02° resulted in recentering and recalculation of the orientation matrix before data collection resumed. During the data collection, four reorientations were required. Crystal data and experimental conditions are summarized in Table 2.3.1. At the conclusion of data collection, ω-scans were recorded again for the standard reflections; peak widths at half-height were 0.11°, 0.14°, 0.15°, 0.14° respectively. These values, average 0.14°, were unchanged, and indicated that the crystal stayed single and of good quality during the data collection.

3.Data reduction.

Data reduction and structure solution refinement were done using the Enraf-Nonius Structure Determination Package Version 3.0, 1986, running on a DEC-PDP 11/23+ computer [63]. The programme, BEGIN, performed the correction for background, monochromator polarization, and Lorentz and crystal polarization effects.

The structure factor modulus, $|F(h,k,\ell)|$, is related to the experimentally observed intensities, $I(h,k,\ell)$, by

$$|F_{(hk\ell)}| = (K \times I_{(hk\ell)} / LP)^{\frac{1}{2}} \times A \times D$$

Here, LP is the Lorentz-polarization correction factor. Lorentz and polarization effects are both functions of 2θ. The term K depends on crystal size, beam intensity and background. The term A refers to absorption of the X-ray beam. The final term D is a measure of reflection decay in

Table 2.3.1 Summary of crystal data and experimental conditions

compound	$C_{40}H_{39}ClNP_2Rh$
mol. wt.	734.07
unit cell dimens.	a = 17.238(6) Å
	b = 18.876(7) Å
	c = 10.643(4) Å
	$\alpha = \beta = \gamma = 90°$
cell volume.	3467(1) Å^3
Z	4
density obsd.	1.403(1) g/cm^3
calcd.	1.400 g/cm^3
space group	$P2_12_12_1$ (D_2^4, No.19)
abs. coefficient	MoKα 6.105 cm^{-1}
radiation	MoKα, λ = 0.71069 Å
temperature	18°C
crystal-counter distance	205 mm
receiving aperture horiz.;vert.	6.00+0.35*tanθ; 4.0mm
scan range	0.80+0.35*tanθ
background	at 25% scan extensions
scan type	θ-2θ
data collected	+h,+k,+l for $0 < 2\theta < 60°$,
	$0 \leq h \leq 22$, $0 \leq k \leq 24$,
	$0 \leq l \leq 13$.
standard reflections	(102),(200),(020),(006).
crystal faces	{100}, {010}, {111}.
absorption grid	12 x 8 x 20
transmission factors	max. 0.998 min.0.868

the X-ray beam.

The corrections for background are needed because of white radiation in the X-ray beam, and are made by assuming a linear relation between the two background counts recorded at the limits of the scan. The Lorentz correction is necessary because the different reciprocal lattice points, h,k,ℓ, take different times to pass through the sphere of reflection. Polarization effects arise from the fact that the efficiency of reflection of $I_{\parallel}$ (one vector parallel to the reflecting plane) will be represented to a greater extent in the reflected beam than in $I_{\perp}$ (another vector at right angles to $I_{\parallel}$). While the incident X-ray beam was unpolarized, the diffracted beam is partially polarized (assuming the incident beam has not been monochromatized). An incident X-ray beam from a graphite crystal monochromator has a vertical partial polarization, and then the appropriate correction must be made, since it will affect the subsequent reflections from the crystal under study.

Standard deviations were estimated based on counting statistics, where

$$[\sigma(F_{obs}^2)]^2=[\ S^2\ (C + B\ R^2) + (P\ (F_{obs}^2)^2]\ /\ L_P^2$$

and F_{obs}^2 = |I| = magnitude of the reflections intensity

S^2 = the scan rate squared.

C = the total integrated peak count.

B = the total background count.

R^2 = the ratio (squared) of scan time to background counting time.

P = an experimental instability factor introduced to downweight intense reflections, first chosen as 0.04.

LP = Lorentz polarization factor.

Of the 5769 reflections processed, 3645 reflections has intensities greater than $3\sigma(I)$, and 32 systematic absence reflections were rejected.

In preparation for an absorption correction, Program CRYSTAL was used, in conjection with the Huber optical goniometer, to assign indices to the crystal faces. Perpendicular distances from an origin to the crystal faces were measured with a filar microscope eyepiece. A perspective view of the crystal, produced by the program ORTEP, is presented in Figure 2.3.1.

A program, ABSCOR, was then used to apply to a Gaussian absorption correction. If an incident X-ray beam of intensity I_o falls on an absorbing material, then at a depth t the intensity will be given by $I_t = I_o \exp(-\mu t)$, where μ is the linear absorption coefficient of the material. Hence the data were corrected for these differential absorption effects. A Gaussian grid of dimensions 12 x 8 x 20 was used for the calculation. Transmission factors for the crystal ranged from 0.868 to 0.998. At the completion of data reduction, there were 3604 unique reflections available for the solution and refinement of the structure.

4. Structure solution and refinement.

The intensities of the diffracted rays that are measured when data are collected during a structure determination do

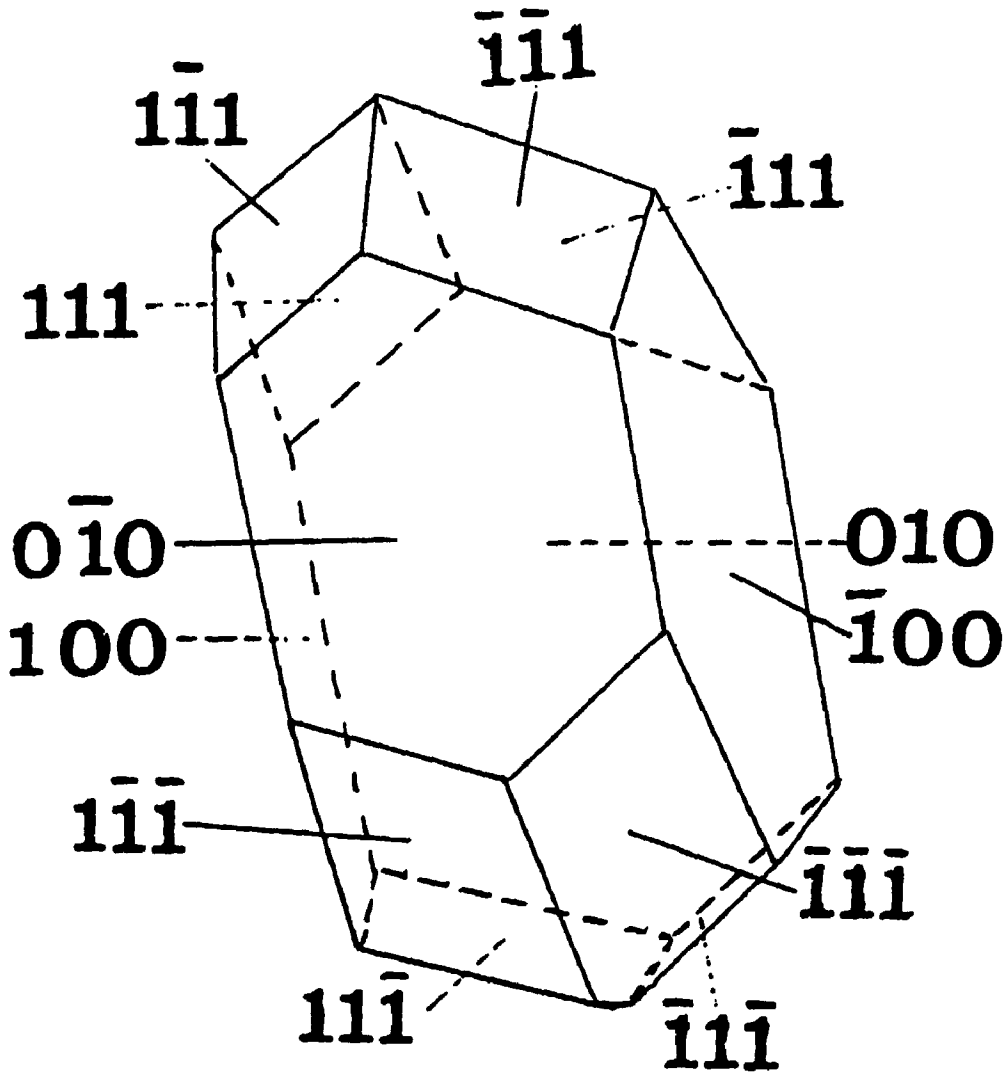

Figure 2.3.1 A drawing of the data crystal. Dotted edges are hidden from view.

not provide all the information that is needed to solve the structure. The structure amplitude |F|, $[|F_{hk\ell}| \sim (I)^{\frac{1}{2}}]$ is readily obtained, but the phase associated with it is not known. If both the magnitude and the phase of the structure factor were known for all the hkℓ reflections, then an electron density map of the unit cell could be obtained from a Fourier synthesis. In an attempt to overcome this phase problem, Patterson used the squares of the structure amplitudes, $|F|^2$, as Fourier coefficients. Peaks in a Patterson systhesis correspond to interatomic vectors in real space. Peak heights are roughly proportional to the product of the atomic numbers of the atoms giving rise to the peaks. The Patterson function is centrosymmetric, as every peak on the vector map will be related to a similar peak by a centre of symmetry. If a Patterson synthesis is calculated for a crystal containing a heavy atom, then maxima on the vector map which represent heavy atom - heavy atom vectors will appear as much larger peaks than any of the others.

A 3-dimensional Patterson synthesis was used to determine the positional parameters of the Rh, P and Cℓ atoms (program FOUR). A series of least-squares refinements and difference Fourier syntheses were then used to locate the remaining 40 carbon atoms and one nitrogen atom. The structure was refined by full-matrix least-squares techniques on F, minimizing the function $\Sigma\, \omega\, (|F_o| - |F_c|)^2$, where the weight ω is defined as $4F_o^2 / [\, \sigma^2\, (F_o^2)]$, and F_o and F_c are the observed and calculated structure amplitudes. (program

LSFM). Scattering factors for all atoms were those of Cromer and Waber [64]. The real and imaginary components of anomalous dispersion were those of Cromer and Waber [64], and were included for all atoms.

Non-hydrogen atoms were first refined as isotropic spheres. In subsequent refinement cycles, begining with the heavy atoms and progressing to lighter atoms, isotropic spheres were replaced by anisotropic thermal ellipsoids in order to improve the description of the thermal vibration of the atoms. This model converged at residuals of $R_1 = 0.050$ and $R_2 = 0.065$ prior to H atom location, where

$$R_1 = [\Sigma \, ||F_o| - |F_c||]/[\Sigma \, |F_o|]$$

$$R_2 = [\, (\Sigma \, \omega \, (|F_o| - |F_c|)^2) \, / \, (\Sigma \, \omega \, (F_o)^2) \,]^{\frac{1}{2}}$$

All 39 H atoms were located in a difference Fourier synthesis, using only data with $\sin\theta/\lambda < 0.35$. Peak weights ranged from 0.50(7) to 0.35(5) $e\text{Å}^{-3}$. Methyl hydrogen atoms were fitted by a least-squares procedure (program HYDRO). The H atoms were included in idealized positions (sp^2 hybridization, C-H 0.90 Å; sp^3 hybridization, C-H 0.95 Å), with isotropic thermal parameters fixed at 110% of the isotropic values of the atoms to which they were bonded. As the refinement progressed, all 39 H atom parameters were recalculated in the structure factor calculations but were not refined. Refinement progressed until no shifts greater than 10^{-4}Å were observed for the atomic positional parameters and all shifts were less than $10^{-2}\sigma$. In the final five cycles, 3604 unique reflections with $I > 3\sigma(I)$ were used to refine 256

variables. Convergence was achieved at residuals of R_1 = 0.0408 and R_2 = =0.0496 and the error in an observation of unit weight was 1.36 electrons (P = 0.04) [100].

The absolute configuation, *R*, was known from the ligand synthesis and could be confirmed by a Rogers' ETA value calculation. The ETA value was set to 1; convergence of 45 non-hydrogen atoms was achieved at R_1 = 0.0408 and R_2 = 0.0496, and the error in an observation of unit weight was 1.36 electrons (P = 0.04). When three cycles of refinement were performed on the inverted hand of the model (i.e. ETA = -1) under the same conditions, agreement factors of R_1 = 0.0432 and R_2 = 0.0524 were obtained, poorer than those observed for the *R* model. No attempt was made to compare Friedel pairs, since there had not been recorded.

A total difference Fourier synthesis showed that the two highest peaks, were at fractional coordinates (-0.0332, 0.000, -0.0293) and (-0.0488, -0.0488, 0.0546) with electron density $\Delta\rho$ = 0.487 $e\text{Å}^{-3}$ at a distance of 0.895(3) Å from the Rh atom, $\Delta\rho$ = 0.465 $e\text{Å}^{-3}$ at a distance of 0.736(9) Å from the Rh atom. These were considered to be of no chemical significance. A statistical analysis of R_1 and R_2 in terms of data collection order, F_o, $\lambda^{-1}\sin\theta$, and classes of indices showed no unusual trends, indicating a satisfactory weighting scheme and no significant secondary extinction.

Final positional and U(equivalent) thermal parameters are given in Table 2.3.2 for the non-hydrogen atoms. Anisotropic thermal parameters, H atom parameters, root-mean-square

amplitudes of vibration, selected torsional angles and mean plane calculations are given in Tables 2.3.3, 2.3.4, 2.3.5, 2.3.6, and 2.3.7 respectively. Structure factor amplitudes are listed in Appendix 1.

2.4 Structure Description.

The lack of significant residual electron density in the final difference Fourier synthesis confirms that the model chosen is appropriate. A stereoview of the whole molecule showing the atom numbering scheme, and a perspective view of the molecule with the triphenylphosphine ligand removed are given in Figures 2.4.1 and 2.4.2. Atoms are drawn as 40% probability thermal ellipsoids. Selected intramolecular distances and angles are given in Tables 2.4.1 and 2.4.2.

The crystals are built up from discrete molecules, for which the shortest intermolecular distances are 2.37 Å, HC(64)....HC(53) at (X, Y, Z-1); 2.44 Å, HC(56)....HC(25) at (X-1, Y, Z); and 2.48 Å, H2C(1)....HC(54) at (X, Y, Z-1). The shortest metal - metal distance is 8.34 Å, Rh....Rh at (X, 1+Y, Z-1).

What is often required from the results of an X-ray diffraction study is a decision whether a bond length or angle in a structure differs significantly from some other dimension in the same or a different structure. We can specify the probability that two measurements of a quantity will agree within certain limits if only random errors are present. We have made use of the statistical quantity λ, where

Table 2.3.2 Non-hydrogen Atomic Positional ($\times 10^4$) and Thermal ($\times 10^3$) Parameters.

Atom	X	Y	Z	U or Ueq($Å^2$)
Rh	4326.7(2)	5315.3(2)	-3.7(5)	28.94(7)
Cl	3872.3(11)	6508.4(8)	-365(2)	51.4(4)
P(1)	4563.5(7)	4172.3(6)	21(2)	30.5(3)
P(2)	5363.5(9)	5630.3(8)	-1150(2)	32.0(3)
N	3299(3)	5187(3)	1278(4)	35(1)
C(1)	3253(5)	5803(4)	2146(6)	56(2)
C(2)	2589(4)	5212(4)	479(7)	49(2)
C(3)	3257(4)	4524(3)	2083(5)	39(2)
C(4)	3932(4)	4502(4)	3042(6)	51(2)
C(11)	4826(3)	3782(3)	-1480(6)	33(1)
C(12)	5364(4)	3230(4)	-1641(7)	49(2)
C(13)	5483(4)	2936(4)	-2807(8)	62(2)
C(14)	5098(5)	3193(4)	-3844(8)	67(2)
C(15)	4584(5)	3750(4)	-3712(8)	66(2)
C(16)	4436(4)	4038(3)	-2528(7)	45(2)
C(21)	3683(3)	3646(3)	372(6)	37(1)
C(22)	3529(4)	3031(3)	-306(6)	48(2)
C(23)	2888(4)	2611(3)	-31(11)	66(2)
C(24)	2403(4)	2814(4)	949(9)	67(2)
C(25)	2537(4)	3426(4)	1593(8)	55(2)
C(26)	3171(3)	3859(3)	1305(6)	38(1)
C(31)	5260(3)	3791(3)	1144(6)	35(1)
C(32)	5229(4)	3092(4)	1527(7)	51(2)
C(33)	5741(5)	2842(5)	2425(8)	72(2)

Table 2.3.2 continued

Atom	X	Y	Z	U or Ueq(Å^2)
C(34)	6298(6)	3254(5)	2888(9)	83(3)
C(35)	6352(6)	3944(5)	2537(10)	87(3)
C(36)	5818(4)	4222(4)	1662(8)	59(2)
C(41)	5848(4)	6408(3)	-426(6)	43(1)
C(42)	6336(5)	6851(5)	-1101(9)	73(2)
C(43)	6769(5)	7389(5)	-447(9)	81(3)
C(44)	6671(5)	7453(4)	827(9)	72(2)
C(45)	6178(5)	7040(5)	1434(9)	73(2)
C(46)	5757(4)	6525(4)	843(7)	58(2)
C(51)	5174(3)	5877(3)	-2796(6)	36(1)
C(52)	5769(4)	6040(4)	-3647(7)	56(2)
C(53)	5603(4)	6208(4)	-4877(8)	63(2)
C(54)	4856(4)	6242(4)	-5280(7)	61(2)
C(55)	4265(4)	6077(4)	-4468(7)	53(2)
C(56)	4421(4)	5907(3)	-3229(6)	44(2)
C(61)	6240(4)	5067(3)	-1376(6)	40(1)
C(62)	6824(4)	5086(4)	-508(7)	55(2)
C(63)	7498(5)	4672(5)	-654(9)	74(2)
C(64)	7544(5)	4233(5)	-1700(9)	74(2)
C(65)	6981(4)	4220(4)	-2581(7)	57(2)
C(66)	6309(4)	4630(4)	-2421(7)	49(2)

Anisotropically refined atoms are given in the form of the isotropic equivalent thermal parameter defined as:
$(1/6\pi^2)[a^2*B(1,1)+b^2*B(2,2)+c^2*B(3,3)+ab(\cos\gamma)*B(1,2)+ac(\cos\beta)*B(1,3)+bc(\cos\alpha)*B(2,3)]$

Table 2.3.3 Anisotropic Thermal Parameters ($\times 10^2$)

Name	U(1,1)	U(2,2)	U(3,3)	U(1,2)	U(1,3)	U(2,3)
Rh	32.3(1)	26.7(1)	27.8(1)	3.2(2)	1.9(3)	1.2(3)
Cl	58.9(9)	35.4(6)	60(1)	11.4(7)	16.1(8)	10.3(7)
P(1)	33.0(5)	28.6(5)	29.8(6)	2.2(5)	0(1)	0.6(9)
P(2)	30.0(6)	31.6(7)	34.4(7)	2.8(6)	1.8(7)	1.9(7)
N	40(2)	38(2)	28(2)	6(2)	5(2)	4(2)
C(1)	82(5)	52(4)	34(3)	9(4)	13(4)	-0(3)
C(2)	41(3)	62(4)	44(3)	5(3)	-2(3)	5(3)
C(3)	42(3)	49(3)	25(3)	1(3)	8(3)	6(3)
C(4)	57(4)	58(4)	39(3)	7(3)	-6(3)	3(3)
C(21)	37(3)	31(3)	41(3)	-3(2)	-7(2)	5(2)
C(22)	52(3)	38(3)	55(5)	-8(3)	-8(3)	-3(3)
C(23)	61(4)	45(3)	91(5)	-16(3)	-9(6)	-2(5)
C(24)	48(4)	50(4)	102(6)	-15(3)	4(4)	4(5)
C(25)	41(3)	51(4)	72(5)	1(3)	2(4)	5(4)
C(26)	36(3)	35(3)	42(3)	6(3)	-0(3)	14(3)

The form of the anisotropic thermal parameter is: $\exp[-2\pi^2(h^2a^2U(1,1) + k^2b^2U(2,2) + l^2c^2U(3,3) + 2hkabU(1,2) + 2hlacU(1,3) + 2klbcU(2,3))]$ where a, b, and c are reciprocal lattice constants.

Table 2.3.4 Hydrogen Atomic Positional ($\times 10^4$) and Thermal ($\times 10^3$) Parameters

Atom	X	Y	Z	U(Å^2)
HC(3)	2795	4545	2568	43
HC(12)	5634	3068	-976	53
HC(13)	5819	2572	-2891	68
HC(14)	5178	2998	-4604	74
HC(15)	4343	3929	-4393	72
HC(16)	4091	4394	-2447	50
HC(22)	3848	2902	-934	54
HC(23)	2787	2216	-472	72
HC(24)	1995	2539	1154	73
HC(25)	2211	3554	2213	60
HC(32)	4871	2798	1190	56
HC(33)	5698	2391	2695	80
HC(34)	6642	3076	3438	91
HC(35)	6726	4223	2861	95
HC(36)	5839	4682	1448	66
HC(42)	6379	6801	-1940	81
HC(43)	7096	7679	-865	88
HC(44)	6945	7778	1260	79
HC(45)	6120	7100	2266	81
HC(46)	5418	6262	1283	64
HC(52)	6265	6035	-3383	61
HC(53)	5993	6296	-5415	69
HC(54)	4748	6369	-6076	67
HC(55)	3772	6078	-4745	58
HC(56)	4024	5815	-2701	49
HC(62)	6779	5372	161	61

Table 2.3.4 continued

Atom	X	Y	Z	U(Å²)
HC(63)	7885	4691	-90	82
HC(64)	7960	3948	-1788	82
HC(65)	7038	3950	-3268	63
HC(66)	5923	4610	-2991	54
H1C(1)	2800	5762	2649	68
H2C(1)	3699	5808	2669	68
H3C(1)	3231	6227	1669	68
H1C(2)	2581	4808	-55	62
H2C(2)	2143	5210	1001	62
H3C(2)	2597	5631	-13	62
H1C(4)	4457	4413	2842	64
H2C(4)	3894	4763	3798	64
H3C(4)	3666	4057	3144	64

H1C(1), H2C(1), H3C(1) are bonded to C(1); H1C(2), H2C(2), H3C(2) are bonded to C(2); H1C(4), H2C(4), H3C(4) are bonded to C(4).

Table 2.3.5 Root-Mean-Square Amplitudes of Thermal Vibration (Å)

Atom	Min.	Int'med.	Max.
Rh	0.159	0.165	0.186
Cl	0.174	0.208	0.284
P(1)	0.166	0.173	0.184
P(2)	0.167	0.177	0.191
N	0.160	0.182	0.218
C(1)	0.174	0.224	0.295
C(2)	0.194	0.212	0.253
C(3)	0.145	0.210	0.226
C(4)	0.189	0.231	0.256
C(21)	0.172	0.179	0.219
C(22)	0.179	0.224	0.249
C(23)	0.185	0.263	0.307
C(24)	0.183	0.253	0.320
C(25)	0.203	0.223	0.270
C(26)	0.150	0.192	0.232

Table 2.3.6 Selected Torsion Angles in Degrees

Atom 1	Atom 2	Atom 3	Atom 4	Angle
N	Rh	P(1)	C(21)	25.13(24)
P(1)	Rh	N	C(1)	143.70(37)
P(1)	Rh	N	C(2)	-100.88(36)
P(1)	Rh	N	C(3)	21.14(37)
Rh	P(1)	C(21)	C(22)	137.28(45)
Rh	P(1)	C(21)	C(26)	-42.68(53)
Rh	N	C(3)	C(4)	64.36(54)
Rh	N	C(3)	C(26)	-65.08(54)
C(1)	N	C(3)	C(4)	-59.52(62)
C(1)	N	C(3)	C(26)	171.05(50)
C(2)	N	C(3)	C(4)	-173.93(50)
C(2)	N	C(3)	C(26)	56.64(60)
N	C(3)	C(26)	C(21)	57.06(76)
N	C(3)	C(26)	C(25)	-124.89(59)
C(4)	C(3)	C(26)	C(21)	-70.57(76)
C(4)	C(3)	C(26)	C(25)	107.48(66)
P(1)	C(21)	C(22)	C(23)	177.50(58)
C(26)	C(21)	C(22)	C(23)	-2.54(98)
P(1)	C(21)	C(26)	C(3)	1.76(83)
P(1)	C(21)	C(26)	C(25)	-176.24(50)
C(22)	C(21)	C(26)	C(3)	-178.20(56)
C(22)	C(21)	C(26)	C(25)	3.80(90)
C(21)	C(22)	C(23)	C(24)	-0.65(115)
C(22)	C(23)	C(24)	C(25)	2.57(125)
C(23)	C(24)	C(25)	C(26)	-1.29(121)
C(24)	C(25)	C(26)	C(3)	179.88(67)
C(24)	C(25)	C(26)	C(21)	-1.95(104)

TABLE 2.3.7 Results of Least-Squares Plane Calculations

The equation of the plane is of the form $Ax + By + Cz - D = 0$

where A,B,C & D are constants and x,y & z are orthogonalized coordinates

Plane No	A	B	C	D	Atom	x	y	z	Distance	Esd
1	-0 5948	-0 1224	-0 7945	-5 6646						
					----------Atoms In Plane----------					
					RH	7 4643	10 0367	-0 0039	0 000	0 000
					N	5 6914	9 7946	1 3605	0 000	0 005
					P(1)	7 8727	7 8783	0.0227	0 000	0 002
					----------Other Atoms----------					
					C(1)	5 6127	10.9567	2 2845	-0 830	0 007
					C(2)	4 4671	9 8410	0.5102	1 398	0 007
					C(3)	5 6182	8 5423	2.2173	-0 484	0.006
					C(4)	6 7834	8.5017	3 2390	-1 984	0 007
					C(21)	6.3531	6 8853	0.3957	0 729	0.006
					C(22)	6 0873	5 7226	-0.3261	1 603	0 007
					C(23)	4 9820	4 9304	-0.0330	2 124	0 010
					C(24)	4 1460	5.3133	1 0106	1 746	0 009
					C(25)	4 3764	6 4694	1.6963	0 922	0 008
					C(26)	5 4704	7 2863	1 3092	0 416	0.006
2	-0 5374	-0 2203	-0 8140	-6 1655						
					----------Atoms In Plane----------					
					RH	7.4643	10.0367	-0.0039	-0.054	0.000
					P(1)	7.8727	7.8783	0 0227	0.180	0 002
					P(2)	9 2528	10.6315	-1.2242	-0.153	0.002
					N	5 6914	9.7946	1.3605	-0.159	0 005
					CL	6.6793	12 2895	-0.3884	0.185	0 002
					Chi Squared =	44913				
3	-0 5377	-0 2197	-0 8140	-6 1476						
					----------Atoms In Plane----------					
					P(1)	7 8727	7 8783	0.0227	0 165	0 002
					P(2)	9 2528	10.6315	-1 2242	-0 166	0 002
					N	5 6914	9.7946	1 3605	-0.172	0 005
					CL	6 6793	12.2895	-0 3884	0.173	0 002
					Chi Squared =	31576				
					----------Other Atoms----------					
					RH	7 4643	10.0367	-0.0039	-0.067	0 000

TABLE 2.3.7
continued

4	0.7350	0 6602	-0 1549	11.0841	----------Atoms In Plane----------					
					C(11)	8 3258	7 1423	-1 5762	-0 006	0 006
					C(12)	9 2539	6 1000	-1.7473	0 015	0 007
					C(13)	9 4596	5 5435	-2 9891	-0 009	0 008
					C(14)	8 7943	6 0292	-4 0930	-0 006	0 008
					C(15)	7 9082	7 0815	-3 9517	0 015	0 008
					C(16)	7 6525	7 6248	-2 6913	-0 009	0.006
					Chi Squared =	13				
					----------Other Atoms----------					
					P(1)	7.8727	7 8783	0 0227	-0 100	0 001
5	-0 5810	0 5134	-0 6579	-0.2055	----------Atoms In Plane----------					
					C(21)	6 3531	6 8853	0 3957	-0 020	0 006
					C(22)	6 0873	5 7226	-0 3261	0 004	0 007
					C(23)	4 9820	4 9304	-0 0330	0 014	0 009
					C(24)	4 1460	5 3133	1 0106	-0 016	0 008
					C(25)	4 3764	6 4694	1 6963	0 000	0 007
					C(26)	5 4704	7 2863	1 3892	0 018	0 006
					Chi Squared =	28				
					----------Other Atoms----------					
					P(1)	7 8727	7 8783	0 0227	-0 102	0 002
6	0 6224	-0 2594	-0 7384	2 0866	----------Atoms In Plane----------					
					C(31)	9 0743	7 1580	1 2177	0 005	0 006
					C(32)	9 0200	5 8393	1 6258	0 012	0 007
					C(33)	9 9039	5 3660	2 5816	-0 021	0 009
					C(34)	10 8651	6 1445	3 0747	0 011	0 010
					C(35)	10 9579	7 4472	2 7016	0 007	0 010
					C(36)	10 0370	7 9731	1 7690	-0 014	0 008
					Chi Squared =	15				
					----------Other Atoms----------					
					P(1)	7 8727	7 8783	0 0227	-0 047	0 002
7	-0 7421	0 6499	-0 1640	0 4742	----------Atoms In Plane----------					
					C(41)	10 0880	12 0993	-0 4532	-0 023	0 006
					C(42)	10 9303	12 9369	-1 1720	0 014	0 009
					C(43)	11 6772	13 9520	-0 4756	0 005	0 009
					C(44)	11 5092	14 0731	0 8806	-0 014	0 008
					C(45)	10 6582	13 2931	1 5266	0 004	0 009
					C(46)	9 9325	12 3215	0 8972	0 015	0 008
					Chi Squared =	24				

TABLE 2.3.7
continued

8	0 0950	-0 9649	-0 2560	-9 4551

Atoms In Plane					
C(51)	8 9252	11 0975	-2 9772	0 003	0 006
C(52)	9 9531	11 4052	-3 8834	-0 005	0 007
C(53)	9 6666	11 7225	-5 1922	0 009	0 007
C(54)	8 3767	11 7856	-5 6217	-0 012	0 007
C(55)	7 3578	11 4747	-4 7571	0 010	0 007
C(56)	7 6263	11 1547	-3 4383	-0 005	0 006

Chi Squared = 8

Other Atoms					
P(2)	9 2528	10 6315	-1 2242	0 020	0 001

9	0 4384	0 7445	-0 5035	12 5822

Atoms In Plane					
C(61)	10 7642	9 5676	-1 4647	-0 003	0 006
C(62)	11 7719	9 6042	-0 5413	0 001	0 007
C(63)	12 9358	8 8220	-0 6965	0 007	0 009
C(64)	13 0141	7 9921	-1 8101	-0 015	0 009
C(65)	12 0426	7 9693	-2 7483	0 014	0 007
C(66)	10 8839	8 7419	-2 5771	-0 005	0 007

Chi Squared = 8

Other Atoms					
P(2)	9 2528	10 6315	-1 2242	0 006	0 002

Dihedral Angles Between Planes

Plane No	Plane No	Dihedral Angle	Plane No	Plane No	Dihedral Angle
1	2	6 60 +- 0 77	1	3	6 56 +- 0 77
1	4	113 26 +- 0 19	1	5	38 04 +- 0 25
1	6	75 63 +- 0 17	1	7	60 51 +- 0 22
1	8	73 17 +- 0 17	1	9	87 24 +- 0 17
2	3	0 05 +- 9 61	2	4	114 48 +- 0 18
2	5	44 06 +- 0.20	2	6	71.11 +- 0 16
2	7	67 10 +- 0 20	2	8	66.91 +- 0 17
2	9	89 41 +- 0.16	3	4	114 46 +- 0.18
3	5	44 02 +- 0 20	3	6	71.13 +- 0 16
3	7	67 06 +- 0 20	3	8	66.95 +- 0 17
3	9	89 39 +- 0 16	4	5	87.94 +- 0.21
4	6	66 39 +- 0 25	4	7	95.22 +- 0 18
4	8	123 84 +- 0.22	4	9	26.91 +- 0 45
5	6	89 44 +- 0.21	5	7	31.74 +- 0 42
5	8	110 89 +- 0.22	5	9	61.84 +- 0 24
6	7	120 62 +- 0.29	6	8	61.69 +- 0 28
6	9	63 16 +- 0 27	7	8	128.73 +- 0 25
7	9	76 05 +- 0 22	8	9	124.40 +- 0 20

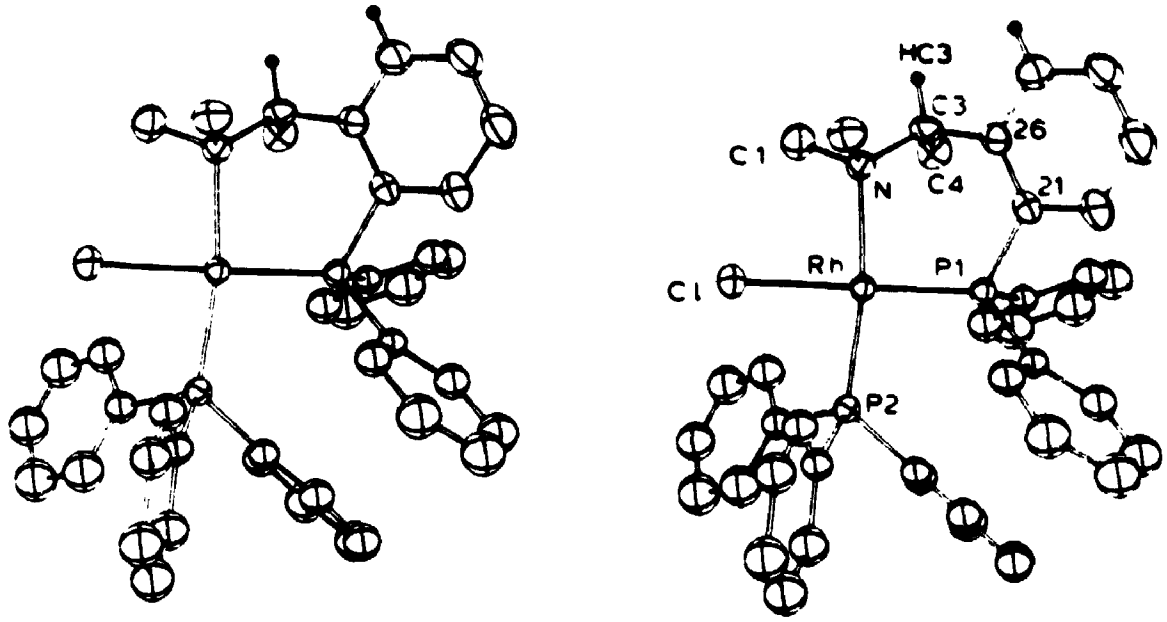

Figure 2.4.1 One stereoview of the whole molecule with atoms drawn as 40% probability thermal ellipsoide showing the atom numbering scheme.

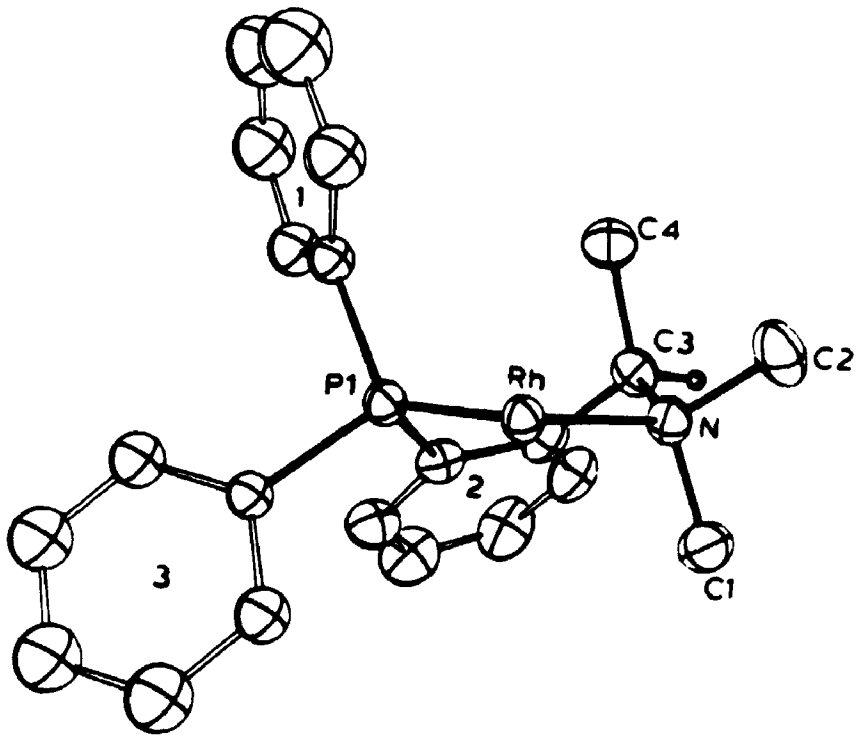

Figure 2.4.2 A part of the molecule with the triphenyl-phosphine ligand removed.

Table 2.4.1 Selected Bond Distances in Angstroms

Atom 1	Atom 2	Distance	Atom 1	Atom 2	Distance
Rh	Cl	2.416(1)	C(25)	C(26)	1.399(8)
Rh	P(1)	2.197(1)	C(31)	C(32)	1.381(8)
Rh	P(2)	2.245(1)	C(31)	C(36)	1.377(8)
Rh	N	2.250(4)	C(32)	C(33)	1.38(1)
P(1)	C(11)	1.818(5)	C(33)	C(34)	1.33(1)
P(1)	C(21)	1.853(5)	C(34)	C(35)	1.36(1)
P(1)	C(31)	1.841(6)	C(35)	C(36)	1.41(1)
P(2)	C(41)	1.856(6)	C(41)	C(42)	1.39(1)
P(2)	C(51)	1.843(6)	C(41)	C(46)	1.377(9)
P(2)	C(61)	1.864(6)	C(42)	C(43)	1.44(1)
N	C(1)	1.487(7)	C(43)	C(44)	1.37(1)
N	C(2)	1.491(7)	C(44)	C(45)	1.32(1)
N	C(3)	1.519(6)	C(45)	C(46)	1.37(1)
C(3)	C(4)	1.550(8)	C(51)	C(52)	1.405(8)
C(3)	C(26)	1.512(8)	C(51)	C(56)	1.379(8)
C(11)	C(12)	1.407(8)	C(52)	C(53)	1.38(1)
C(11)	C(16)	1.389(8)	C(53)	C(54)	1.361(9)
C(12)	C(13)	1.376(9)	C(54)	C(55)	1.372(9)
C(13)	C(14)	1.38(1)	C(55)	C(56)	1.383(8)
C(14)	C(15)	1.38(1)	C(61)	C(62)	1.367(8)
C(15)	C(16)	1.396(9)	C(61)	C(66)	1.391(8)
C(21)	C(22)	1.395(7)	C(62)	C(63)	1.411(9)
C(21)	C(26)	1.388(7)	C(63)	C(64)	1.39(1)
C(22)	C(23)	1.391(8)	C(64)	C(65)	1.36(1)
C(23)	C(24)	1.40(1)	C(65)	C(66)	1.403(9)
C(24)	C(25)	1.364(9)			

Numbers in parentheses are estimated standard deviations in the least significant digits.

Table 2.4.2 Selected Bond Angles in Degrees

Atom 1	Atom 2	Atom 3	Angle	Atom 1	Atom 2	Atom 3	Angle
CL	Rh	P(1)	168.04(6)	C(3)	C(26)	C(25)	116.2(5)
CL	Rh	P(2)	85.72(5)	C(21)	C(26)	C(25)	119.0(5)
CL	Rh	N	86.7(1)	P(1)	C(31)	C(32)	122.7(5)
P(1)	Rh	P(2)	96.82(5)	P(1)	C(31)	C(36)	119.0(4)
P(1)	Rh	N	91.9(1)	C(32)	C(31)	C(36)	118.3(6)
P(2)	Rh	N	170.3(1)	C(31)	C(32)	C(33)	120.4(6)
C(11)	P(1)	C(21)	99.5(2)	C(32)	C(33)	C(34)	121.1(8)
C(11)	P(1)	C(31)	104.5(2)	C(33)	C(34)	C(35)	120.6(9)
C(21)	P(1)	C(31)	101.2(2)	C(34)	C(35)	C(36)	119.7(9)
C(41)	P(2)	C(51)	106.0(3)	C(31)	C(36)	C(35)	120.0(7)
C(41)	P(2)	C(61)	98.1(3)	P(2)	C(41)	C(42)	122.3(5)
C(51)	P(2)	C(61)	99.5(2)	P(2)	C(41)	C(46)	118.9(5)
C(1)	N	C(2)	106.7(4)	C(42)	C(41)	C(46)	118.7(7)
C(1)	N	C(3)	106.9(4)	C(41)	C(42)	C(43)	119.3(7)
C(2)	N	C(3)	107.9(4)	C(42)	C(43)	C(44)	118.5(9)
N	C(3)	C(4)	110.9(5)	C(43)	C(44)	C(45)	120.6(9)
N	C(3)	C(26)	112.4(4)	C(44)	C(45)	C(46)	122.4(8)
C(4)	C(3)	C(26)	114.4(5)	C(41)	C(46)	C(45)	120.4(7)
P(1)	C(11)	C(12)	124.9(4)	P(2)	C(51)	C(52)	122.7(4)

Table 2.4.2 continued

Atom 1	Atom 2	Atom 3	Angle	Atom 1	Atom 2	Atom 3	Angle
P(1)	C(11)	C(16)	116.5(4)	P(2)	C(51)	C(56)	119.7(4)
C(12)	C(11)	C(16)	118.7(5)	C(52)	C(51)	C(56)	117.7(5)
C(11)	C(12)	C(13)	120.5(6)	C(51)	C(52)	C(53)	120.8(6)
C(12)	C(13)	C(14)	120.6(7)	C(52)	C(53)	C(54)	120.5(7)
C(13)	C(14)	C(15)	119.7(7)	C(53)	C(54)	C(55)	119.6(7)
C(14)	C(15)	C(16)	120.4(7)	C(54)	C(55)	C(56)	120.7(6)
C(11)	C(16)	C(15)	120.1(6)	C(51)	C(56)	C(55)	120.7(6)
P(1)	C(21)	C(22)	119.9(4)	P(2)	C(61)	C(62)	119.7(5)
P(1)	C(21)	C(26)	120.8(4)	P(2)	C(61)	C(66)	120.8(5)
C(22)	C(21)	C(26)	119.4(5)	C(62)	C(61)	C(66)	119.5(6)
C(21)	C(22)	C(23)	121.2(6)	C(61)	C(62)	C(63)	121.3(6)
C(22)	C(23)	C(24)	118.6(6)	C(62)	C(63)	C(64)	117.7(8)
C(23)	C(24)	C(25)	120.7(6)	C(63)	C(64)	C(65)	121.8(8)
C(24)	C(25)	C(26)	121.2(6)	C(64)	C(65)	C(66)	120.0(7)
C(3)	C(26)	C(21)	124.7(5)	C(61)	C(66)	C(65)	119.8(6)

Numbers in parentheses are estimated standard deviations in the least significant digits.

$$\lambda = |q_1 - q_2| / (\sigma d)$$

q_1 and q_2 are the two values compared,

$$\sigma d = (\sigma_1^2 + \sigma_2^2)^{\frac{1}{2}}$$

and σ_1 and σ_2 are the errors of the two values compared. A λ value which is less than 1.96 indicates a probability which is greater than 5% that such a difference will occur by chance. It is then assumed that the two measurements belong to the same population, and are not significantly different. If a λ value which is between 1.96 to 2.58 is obtained, this means a probability that is less than 5% and greater than 1%, in which case the difference is possibly significant. If the λ value that is greater than 2.58, the probability is less than 1%, and the difference is probably significant. Values greater than 3 are considered significant. In the following discussion, the λ value has been used to identify significant differences in the values compared.

The geometry about the Rh atom is tetrahedrally distorted square planar. The Rh-Cl distance of 2.416(1) Å is the same as the mean Rh-Cl distance of 2.39(1) Å in $[Rh(cyclo\text{-}C_8H_{12})\ Cl]_2$ [65], λ=2.6, but is somewhat longer, λ=12, than the Rh-Cl(2) distance of 2.390(2) Å in $[Rh(C_{22}H_{37}NP)CL(C_7H_8)]ClO_4$ [56b], and mean Rh-Cl distance of 2.398(5) Å in [RhCl-$([(t\text{-}C_4H_9)_2P(CH_2)_2CH]_2)]$ λ=3.5, [66]. This result is attributable to the phosphorus donor atom of amphos being trans to chloride, so that the interaction between Rh and Cl is decreased.

The Rh-P(1) distance of 2.197(1) Å is shorter than that of

2.279(1) Å in [Rh{(*R*)-o[$(C_6H_5)_2P$](C_6H_4)$CHCH_3N(CH_3)_2$}(C_7H_8)]-ClO_4 (A), λ=59, [32] and the mean value of 2.271(1) Å in [Rh(η-C_8H_{12})-{(2*S*,3*S*)-[$(C_6H_5)_2PCHCH_3]_2$}ClO_4.C_4H_8O (B), λ=53 [57]. This too can be explained by the presence of the chloride ligand trans to the phosphorus of amphos, while the complex A has a π acceptor ethylene of the NBD ligand trans to the phosphorus of amphos, which is consistent with ethylene exerting the stronger trans influence [32]. The Rh-P(2) distance of 2.245(1) Å is somewhat shorter than those of (A), λ=25, and (B), λ=19, because the σ-donor N atom on amphos is trans to P(2) on triphenylphosphine. The Rh-P(2) distance of 2.245(1) Å is somewhat longer than the Rh-P(1) distance of 2.197(1) Å in this complex, λ=47.

The Rh-N distance of 2.250(4) Å is longer than the corresponding bonds in (A), 2.178(3) Å, λ=14.6, and in [Rh(S-amars)(NBD)]ClO_4 (C) 2.182(14) Å, λ=14.7 [31]. It has been found that alkene ligands usually exert a greater trans influence than phosphine ligands [86b]. However, this is only an empirical relationship and the order can be reversed depending on the trans group being influenced. Thus, it has been observed that alkene ligands do not show a trans influence on nitrogen ligands [86b,113]. Similarly, we found that a comparison of the Rh-N bond distances of these two complexes shows the opposite order, in that the Rh-N distance is shorter when trans to NBD than when trans to PPh_3.

The mean P-C bond of 1.846(5) Å is the same as the mean P-Csp^2 distance of 1.826(3) Å, λ =2.1, in (A), and that of

1.817(5) Å, λ = 0.4, in [Ni{(*R*)-o-[cyclo-$(C_6H_{11})_2$P]C_6H_4CHCH$_3$-N$(CH_3)_2$}$(NCS)_2$] (D) [56a]. For the phenylene ring in the aminophosphine ligand, C-C distances range from 1.364(9) to 1.40(1) Å, with an average of 1.389(1) Å and C-C-C angles range from 116.2(5) to 121.2(6). These values are in close agreement with the corresponding values in (A). Within the remaining portion of the chelate ring, distances are C(3)-C(4), 1.550(8); C(3)-C(26), 1.512(8); N-C(3), 1.519(6); N-C(1), 1.487(7); and N-C(2), 1.491(7) Å. These distances are quite similar to those of 1.513(6), 1.517(7), 1.502(6), 1.487(7) and 1.486(6) Å for the corresponding bonds in (A), which contains the same amphos ligand.

A system of labelling the two gauche conformations, i.e. δ and λ, of five membered chelate rings was introduced by Corey and Bailar [11,101], for work with ethylenediamine complexes. The δ-conformation is pictured in Figure 2.4.3. Its mirror image is the λ-conformation. In our molecule, the six membered chelate ring adopts a twist-boat conformation that is not bound by the same rules as those in the original work, but if we define the N-P connector as the N-N connector and the C(26)-C(3) bond as the bond corresponding to the C(1)-C(2) bond in Figure 2.4.3, then we have a quasi-δ conformation (Figure 2.4.4).

In the δ-conformations of puckered five membered rings, e.g. (2*S*)-prophos, and (2*S*,3*S*)-chiraphos, the methyl groups prefer the equatorial positions [11]. In our molecule, the methyl group C(4) on the chiral centre is axially situated with

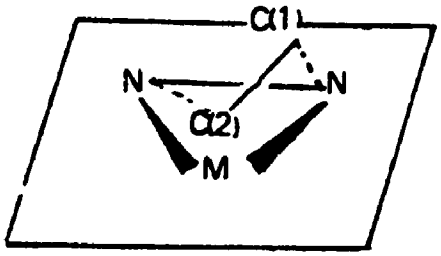

Figure 2.4.3 The δ-conformation of the MNC(1)C(2)N five membered ring.

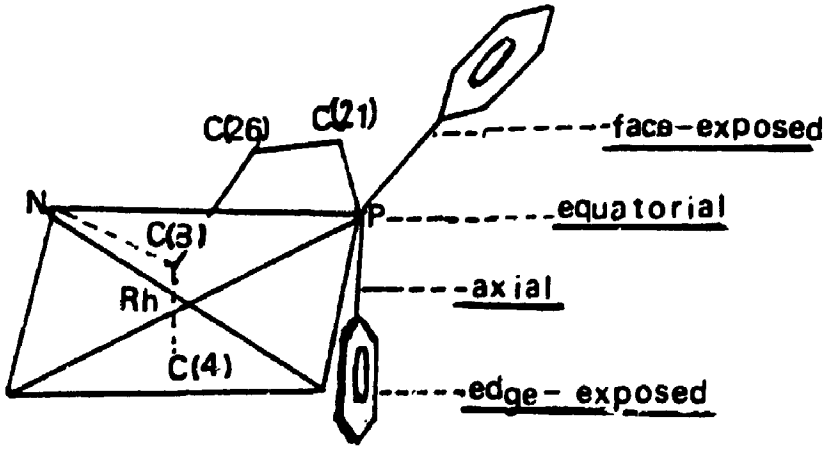

Figure 2.4.4 Equatorial and axial position of the face-exposed and edge-exposed phenyl moieties in the δ-conformation of the Rh-(R)-amphos complex

respect to the Rh-P-N plane. The distance between C(4) and Rh-P-N plane is 1.5 Å longer than that between C(3) and the plane (see Table 2.3.7). The hydrogen atom HC3 on the chiral centre is equatorial to the plane and 2.16(3) Å away from hydrogen atom HC25 of the syn phenyl ring on the chelate ring of amphos. This conformation for six membered rings has less steric hindrance than for five membered rings. The major interaction responsible for this is between the hydrogen atoms of the axial methyl C(4) on the chiral centre, and the hydrogen atoms of the syn phenyl ring on the chelate ring of amphos. The interaction is at a minimum in this configuration.

The two methyl substituents on the N atom are disposed such that the six protons in the methyl groups are staggered. The edge-exposed phenyl ring in amphos is axial to the plane of the chelate ring on the amphos roughly face on to this methyl group C(4). The one of the phenyl ring on the triphenyl-phosphine ligand is roughly parallel to the edge-exposed phenyl ring in order to reduce steric hindrance. The arrangment of the three phenyl rings of the triphenylphosphine ligand is such that the phenyl ring roughly parallel to the edge-exposed phenyl ring on amphos sits axially on the rhodium square plane (the dihedral angle between the planes of phenyl rings is 26.9°; the two planes are 3.2 Å away each other), and the other two phenyl rings are equatorial to the square plane; one is roughly parallel to the syn phenyl ring on the

chelate ring of amphos. This neutral Rh-amphos complex has only one conformation as determined from the X-ray structure, while the Rh-amars complex exhibits two conformations in the solid state. For this compound, a reversal of the phenyl ring orientations is probably strongly hindered, because of the cis triphenylphosphine restraint.

2.5 Discussion and Conclusions.

The six membered chelate ring, which adopts a twist boat conformation in the Rh-amphos complex, influences the arrangement of the phenyl rings at the donor phosphorus atom, one becoming axial and the other equatorial. Furthermore, as the two phenyl rings sit in this way, one is edge-exposed and one face-exposed (Figure 2.4.2). In this way the sense of chirality of the PPh_2 "ears" is enforced by the chiral center in the ligand backbone [70]. The distance between the chiral center in the amphos backbone and the coordination sites of the metal atom, where the prochiral substrates are converted into the optically active products, is approximately 6 Å. It is mainly by transmission through the PPh_2 groups that the chiral information reaches the point where it is needed within the catalyst.

In solution, the formation of a dimer complex (up to 30%, dependent on concentration) indicated that dissociation of the Rh-PPh_3 and the Rh-N bonds occurs. The dissociation of the Rh-N bond can be attributed to the trans-influence of the PPh_3 ligand. The data from our X-ray crystal structure

determination show that the Rh-N bond distance of 2.250(4) Å is longer than that of [Rh(*R*-amphos)(NBD)]ClO_4 (2.182 Å). Therefore the breakage of the Rh-N bond is more likely in this case.

Pearson [86b] proposed a principle for predicting the stability of complexes formed between acids and bases: hard acids prefer to bind hard bases and soft acids prefer to bind to soft bases. Rh(I) belongs to the class of soft acids, and the amine ligand is a harder base than the phosphine ligand. So Rh(I) binds more strongly to the phosphine rather than the amine.

A question remains as to why we found only the isomer with the phosphine ligands cis to each other, since this is obviously sterically unfavorable, the six phenyl rings being constrained with little free rotation for each phenyl ring. The formation of this configuration arises from the initial formation of two geometric isomers from the [Rh(I)Cl(amphos)-solvent] complexes in which the cis isomer is present in greater abundance (70%) than the trans isomer (Figure 2.1.1) [54]. So the addition of PPh_3 ligand leads to a cis isomer as the major product. The bond energy between the Rh atom and the solvent molecule is low and the bond breaks easily, so the solvent site is almost a vacant site for an incoming PPh_3 ligand. The isomer which has a P atom cis to the solvent molecule (70% abundance) can easily trap the PPh_3 ligand. However, not even a 30% abundance of the trans-PPh_3 isomer could be seen with NMR in the product mixtures,

indicating that equilibration is complete within a few hours and that the cis isomer is thermodynamically favoured in spite of the steric factor. As a result, only the cis isomer was crystallized and characterized. However, this steric hindrance still could affect the strength of the bond between Rh(I) and the PPh_3 ligand, favouring dissociation of the Rh-PPh_3 bond.

Thus it is possible to rationalize both the Rh-N bond dissociation necessary for dimer formation, and the Rh-P bond dissociation necessary to start the catalytic cycle. In this case, a change for the phenyl ring orientations is probably possible in solution.

Chapter 3

The Crystal and Molecular Structure of [Rh(III)Cl$_3$(*R*-diamphos)]

3.1 Introduction.

The complex [Rh(I)Cl(*R*-amphos)PPh$_3$] was prepared and isolated as red hexagonally-shaped crystals. The crystal and molecular structure of this compound was determined by X-ray diffraction techniques, which showed that the Cl atom and the P atom of the aminophosphine are trans to each other (see Chapter 2). Since we believe that the synthesis of a new chiral centre is mediated by the spatial arrangement of the phenyl rings, it was of interest to design a ligand which would force the substrate molecule to coordinate cis to the P atom. A chiral, tridentate ligand, the diaminophosphine [$(C_6H_5)_2PC_6H_4CH(CH_3)N(CH_3)$-$(CH_2)_2N(CH_3)_2$], diamphos, was synthesized by I.D. McKay [32], and a catalyst precursor complex [Rh(I)Cl(*R* or *S*-diamphos)] was prepared by the addition of diamphos to a solution of $[RhCl(C_2H_4)_2]_2$. The hydrosilylation of prochiral ketones catalyzed by a mixture of diamphos and $[RhCl(C_2H_4)_2]_2$ was tested by I.D. Mckay [32]. The results were poor, in that all the optical yields were 0%, although the chemical yields ranged from 4% to 75%. To explain this disappointing result, we decided to study the orientations of the phenyl rings on the chelate ring by means of an X-ray structural examination. However,

Rh(I)Cℓ(*R*-amphos) could not be crystallized from various solvents. Finally we found that a Rh(III) complex could be prepared easily by direct reaction of diamphos with $RhCℓ_3.xH_2O$ [32], and after several attempts, crystals suitable for X-ray diffraction studies were grown.

3.2 Experimental.

1. Preparation of [Rh(III)$Cℓ_3$(*R*-diamphos)] crystals.

50 mg $RhCℓ_3.xH_2O$ (0.192 mmole) was dissolved in 25 mL of absolute methanol. 2.12 mL (0.192 mmole) of 0.0906 M *R*-diamphos in methanol was then added, and the solution was heated on a steam bath for 15 minutes. The solvent was removed and the residue was recrystallized from hot $CH_2Cℓ_2$/MeOH. Orange, cubic-shaped crystals of [Rh(III)$Cℓ_3$(*R*-diamphos)] formed, M.P. 236-238°C (dec.).

Elemental analysis: found: C 49.93, H 5.48, N 4.73%; calc. C 50.07, H 5.21, N 4.67%. Analyses performed by Guelph Chemical Laboratories Ltd., Guelph, Ontario.

^{1}H NMR spectrum showed signals at 7.90-7.20(m), 6.09(q), 4.68(d of t), 4.30(d of t), 3.63(d of q), 3.34(t of t), 3.16(s), 3.14(s), 3.08(s), 3.06(s), 2.78(t of t), 2.62(s), 2.38-2.14(m), 1.95(s), 1.59(d) and 1.53(d) ppm; $^3J_{HC-CH_3}$=7.0 Hz, $^3J_{PC-CH}$=2.0 Hz, as recorded in $CDCℓ_3$.

^{31}P NMR spectrum is reported in section 3.5 (Discussion) of this Chapter. All ^{31}P and ^{1}H NMR spectra were recorded on Varian XL-300 and XL-200 spectrometers respectively.

2. X-ray Structure determination.

A photographic examination using Weissenberg and precession techniques showed the crystals to be monoclinic, Laue symmetry 2/m. In the presence of a chiral ligand, observation of the systematic absences 0k0 for k odd lead to an unambiguous assignment of the acentric space group $P2_1$, C^2_2, No.4 [64]. The calculated cell volume was 2557.4(3) $Å^3$. The crystal density, as determined by flotation in a mixture of methylene chloride and hexanes, was 1.57(2)g cm^{-3}. These data indicate Z=4, for which the calculated density is 1.550 g cm^{-3}. There are, therefore, two independent molecules in the asymmetric unit.

The crystal selected for data collection was of approximate dimensions 0.24 x 0.21 x 0.26 mm^3, with six faces revealed by optical goniometry to be {001}, {210} and {2-10}. The crystal dimensions were carefully measured to permit an absorption correction. A perspective view of the crystal, produced by the program ORTEP, is presented in Figure 3.2.1.

Intensity data were recorded on an Enraf-Nonius CAD4F diffractometer using an incident beam graphite monochromator. Accurate cell parameters and an orientation matrix were obtained from refinement of 24 reflections with $24° < 2\theta < 36°$. ω-scans of several intense, low angle reflections, (-112), (020), (004) and (-211), with a wide open counter, had an average width at base of 0.18° and at half height of 0.12°. 8434

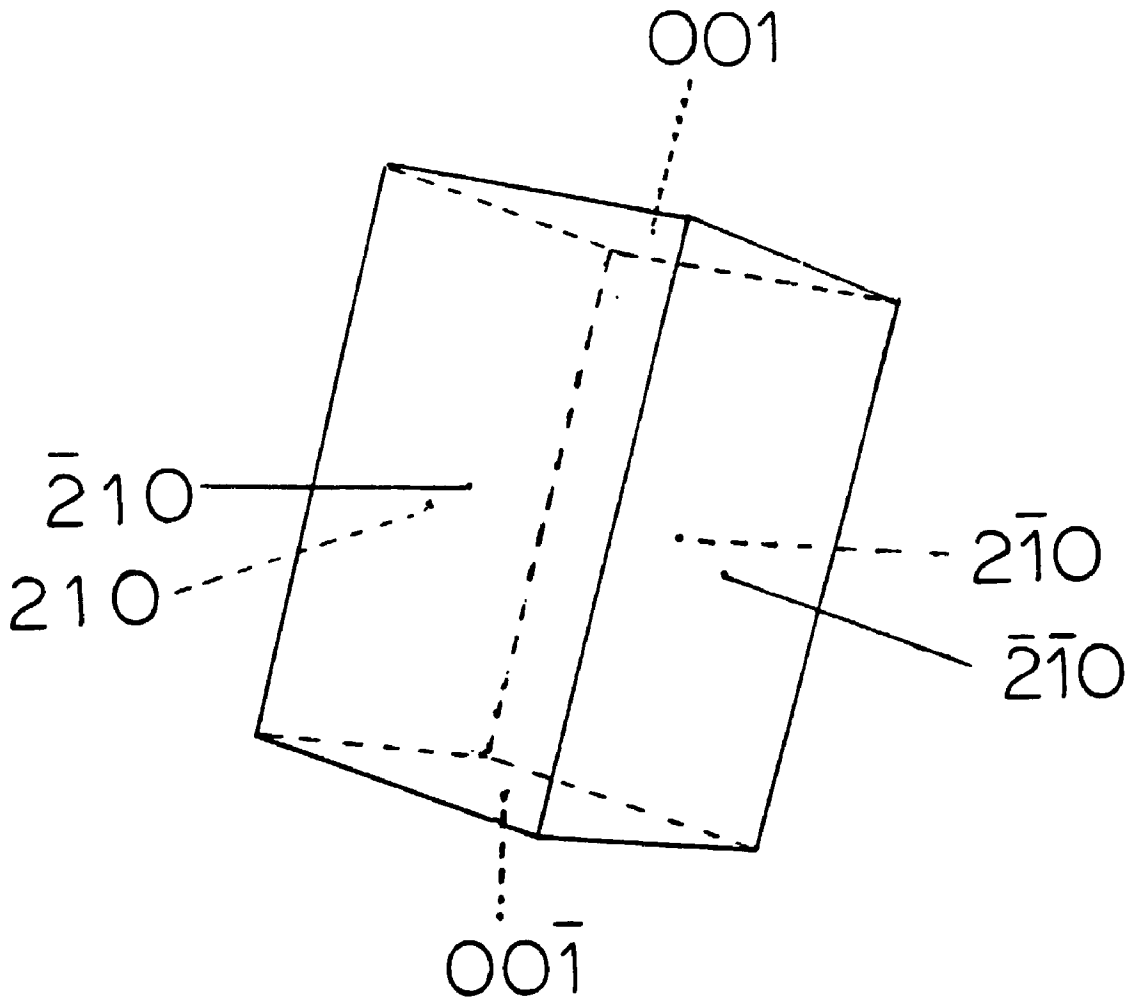

Figure 3.2.1 A Drawing of the Data Crystal. Dotted edges are hidden from view.

reflections ($-28 \leq h \leq 28$, $0 \leq k \leq 13$, $0 \leq \ell \leq 11$) were collected using a θ-2θ scan, up to a maximum 2θ of 60°. Dispersion corrected scans of width 0.70° and variable scan rates within a maximum time per datum of 75 sec. were used. Standard reflections -112, 020, 004 and -211 were recorded every 10,600 sec. of X-ray exposure time and showed an average decay of 0.5%; thus a decay correction was not applied. An orientation check, using three reflections, was done at 200 reflection intervals throughout data collection. Deviation of the observed position of the reflection from the calculated position by an amount equal to or greater than 0.02° resulted in recentering and recalculation of the orientation matrix. Crystal data and experimental conditions are summarized in Table 3.2.1.

3.3 Data Reduction, Structure Solution and Refinement.

Background, monochromator polarization, Lorentz, and polarization corrections were made and standard deviations assigned based on counting statistics. A Gaussian absorption correction was applied.

The structure was solved using Patterson and difference Fourier methods to locate first the two Rh atoms, and subsequently the remaining 62 non-hydrogen atoms and 62 hydrogen atoms of the two molecules in the structure. Refinement proceeded smoothly for all non-hydrogen atoms using the SDP software package [63] running on a DEC-PDP

Table 3.2.1 Summary of Crystal Data and Experimental conditions

compound	$C_{25}H_{31}Cl_3PN_2Rh$
mol. wt.	599.78
unit cell dimens.	a=23.676(2) Å; b=11.580(1) Å
	c=9.329(2) Å; β=91.17(1)°
cell volume.	2557.4(3) Å^3
Z	4
density obsd.;calcd.	1.57(2) g cm^{-3};1.550 g cm^{-3}
abs. coefficient	μ 8.68 cm^{-1}
radiation	MoKα, λ=0.71069 A°
temperature	18°C
crystal-counter distance	205 mm
rec. aperture horiz.;vert.	6.00+0.35*tanθ;4.0mm
scan range(deg.)	0.70+0.35*tanθ
background	at 25% scan extensions
scan type	θ-2θ
data collected	$-28 \leq h \leq 28$, $0 \leq k \leq 13$,
	$0 \leq l \leq 11$ for $0 < 2\theta < 60°$
standard reflections	(-112), (020), (004),(-211).
crystal faces	{001}, {210}, {2-10}.
absorption grid	12x10x12
transmission factors	max. 0.8650. min. 0.8360
# data collected	8438
# standard reflections	220
# unique data $I_o > 3\sigma(I_o)$	5900

11/23+ computer [63]. The Rh, P, Cl and N atoms were refined with anisotropic thermal ellipsoids, and the C atoms were refined as isotropic spheres. This model converged at residuals of R_1=0.059 and R_2=0.088, where

$$R_1=[\Sigma||F_o|-|F_c||]/[\Sigma|F_o|] \quad (1)$$

$$R_2=[(\Sigma\omega(|F_o|-|F_c|)^2)/\Sigma\omega(F_o)^2)]^{\frac{1}{2}} \quad (2)$$

$$\omega=4F_o^2/[\sigma^2(F_o^2)] \quad (3)$$

All 62 H atoms were located in a difference Fourier synthesis with peak heights between 0.5(1) and 0.6(2) eÅ^{-3}, and were included in calculations of F_c, in idealized positions with isotropic temperature factors. After several cycles of refinement, updating the hydrogen atom positions, the model converged at agreement factors R_1=0.047 and R_2=0.071 (446 variables, 4578 observations, $I_o > 3\sigma(I_o)$, the error in an observation of unit weight was 1.70 electrons, p=0.06). However, an inspection of the molecular dimensions showed several unsatisfactory aspects. Aromatic C-C bond lengths varied from 1.28 to 1.51 Å, C-C distances from 1.27 to 1.59 Å and N-C distances from 1.35 to 1.55 Å. We therefore decided to impose rigid group constraints on the phenyl rings, and the refinement was completed using the SHELX 76 software [117].

D_{6h} symmetry (C-C 1.392 Å, C-H 0.95 Å) was imposed on the six phenyl groups. All the methyl hydrogen atoms were fixed in staggered, idealized positions during the refinement, which progressed until no shifts greater than 10^{-4} Å were observed for the atomic positional parameters

and all shifts were less than $10^{-2}\sigma$. In the final cycle, 5843 unique reflections with $F_o \geq 5\sigma(F_o)$ were used to refine 256 variables. Convergence was achieved at residuals of R_1=0.0422, R_2=0.0437, R_G=0.0502, R_M=0.0502 [117]. R_1 and R_2 have the same definitions, given as equations (1) and (2), while $R_G=[\Sigma(\omega(||F_o|-|F_c||)^2)]^{\frac{1}{2}}/\Sigma(\omega|F_o|^2)$ (4) and $R_M=R_G$ (calculated for the scale factor which minimizes R_G)(5) and $\omega=k/[\sigma^2(F_o) + |g| \times (F_o)^2]$ (6)
k is redetermined after each structure factor calculation.

In the final cycle, the k value reached 2.67 under a weighting scheme with a |g| value of 0.000130. A total difference Fourier synthesis showed that the highest peak, at fractional coordinates (0.2709, 0.3380, -0.4807), with an electron density of 1.10(1) $e\text{Å}^{-3}$, is situated 0.70 Å from the C(25) atom. It was considered of no chemical significance. Statistical analyses of R_1 and R_2 in terms of data collection order, F_o, $\lambda^{-1}\sin\theta$ and classes of indices showed no unusual trends, indicating a satisfactory weighting scheme and the absence of significant secondary extinction.

Final positional and U(equivalent) thermal parameters for the non-hydrogen atoms are given in Table 3.3.1. Anisotropic thermal parameters, H atom parameters, root-mean-square amplitudes of thermal vibration, selected torsional angles, and least-squares plane calculations are given in Tables 3.3.2, 3.3.3, 3.3.4, 3.3.5 and 3.3.6.

Table 3.3.1 Atomic Positional ($\times 10^4$) and Thermal ($\times 10^3$) Parameters.

Atom	X	Y	Z	U or U_{eq}($Å^2$)
Rh(1)	826.2(4)	5000	-2627.9(8)	26.4(3)
Rh(2)	5816.2(4)	3432.0(5)	-2667.8(7)	24.4(2)
Cl(1)	196(1)	3515(3)	-1945(3)	37.2(8)
Cl(2)	938(2)	4008(3)	-4793(3)	45(1)
Cl(3)	1447(2)	6426(3)	-3394(3)	42.5(9)
Cl(4)	5180(1)	4899(3)	-1995(3)	35.7(8)
Cl(5)	5943(2)	4460(3)	-4796(3)	39.5(9)
Cl(6)	6453(2)	2063(3)	-3543(3)	41.6(8)
P(1)	1569(1)	4005(3)	-1678(3)	27.3(7)
P(2)	6563(1)	4320(3)	-1569(3)	26.1(7)
N(1)	83(4)	5996(10)	-3486(9)	44(3)
N(2)	661(4)	5903(9)	-684(8)	35(2)
N(3)	5093(4)	2418(9)	-3641(8)	34(3)
N(4)	5648(4)	2420(8)	-796(8)	31(2)
C(1)	-420(6)	5330(12)	-3876(12)	61(4)
C(2)	251(5)	6815(10)	-4739(11)	51(3)
C(3)	-64(6)	6788(11)	-2274(11)	48(3)
C(4)	34(5)	6150(10)	-853(9)	43(3)
C(5)	986(4)	6983(8)	-387(10)	44(2)
C(6)	765(3)	5079(8)	597(7)	32(2)
C(7)	387(4)	5346(9)	1866(10)	56(2)
C(8)	5194(5)	1847(10)	-4965(12)	54(3)
C(9)	4618(5)	3203(11)	-4096(12)	53(3)
C(10)	4916(5)	1645(11)	-2495(11)	47(3)
C(11)	1795(2)	4618(6)	59(6)	27(2)
C(12)	2365(2)	4562(6)	456(6)	43(2)
C(13)	2541(2)	4920(6)	1818(6)	49(2)
C(14)	2148(2)	5334(6)	2781(6)	45(2)
C(15)	1579(2)	5390(6)	2384(6)	37(2)
C(16)	1403(2)	5032(6)	1023(6)	29(2)
C(17)	5035(4)	2112(9)	-1017(9)	34(2)

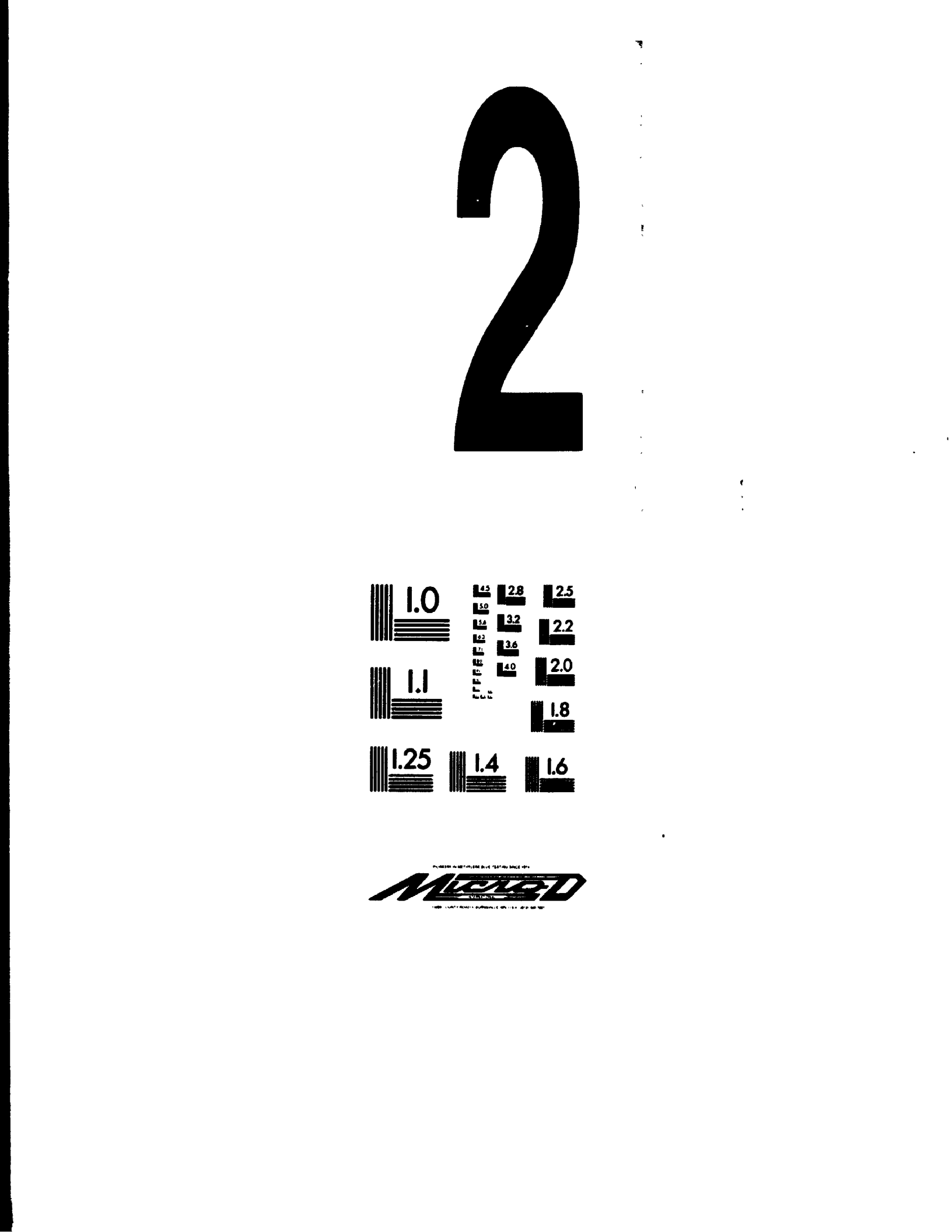
2
1.0
1.1
1.25
1.4
1.6
1.8
2.0
2.2
2.5
2.8
3.2
3.6
4.0
5.0
4.5
MICROCOPY

Table 3.3.1 continued

Atom	X	Y	Z	U or U_{eq}(Å^2)
C(18)	5941(4)	1246(8)	-760(10)	40(2)
C(19)	5751(3)	2876(7)	706(7)	29(1)
C(20)	5417(3)	3938(7)	1159(8)	39(2)
C(21)	2210(3)	3976(5)	-2736(7)	39(2)
C(22)	2548(3)	4954(5)	-2860(7)	46(2)
C(23)	3020(3)	4929(5)	-3726(7)	50(2)
C(24)	3154(3)	3926(5)	-4468(7)	66(3)
C(25)	2816(3)	2948(5)	-4345(7)	93(5)
C(26)	2344(3)	2973(5)	-3478(7)	86(5)
C(31)	1447(3)	2509(6)	-1235(5)	35(2)
C(32)	1220(3)	1798(6)	-2304(5)	40(2)
C(33)	1139(3)	628(6)	-2036(5)	51(3)
C(34)	1285(3)	168(6)	-701(5)	53(3)
C(35)	1512(3)	879(6)	368(5)	52(2)
C(36)	1593(3)	2049(6)	101(5)	42(2)
C(41)	6758(2)	3658(6)	143(6)	31(2)
C(42)	7303(2)	3880(6)	657(6)	37(2)
C(43)	7464(2)	3536(6)	2035(6)	48(2)
C(44)	7080(2)	2971(6)	2900(6)	51(3)
C(45)	6535(2)	2749(6)	2387(6)	42(2)
C(46)	6373(2)	3092(6)	1009(6)	31(2)
C(51)	7221(3)	4345(5)	-2607(6)	32(2)
C(52)	7567(3)	3374(5)	-2577(6)	42(2)
C(53)	8042(3)	3331(5)	-3430(6)	50(2)
C(54)	8171(3)	4259(5)	-4313(6)	51(3)
C(55)	7824(3)	5230(5)	-4343(6)	63(3)
C(56)	7350(3)	5273(5)	-3490(6)	52(3)
C(61)	6449(3)	5864(5)	-1079(6)	32(2)
C(62)	6581(3)	6234(5)	307(6)	42(2)
C(63)	6504(3)	7387(5)	679(6)	50(2)

Table 3.3.1 continued

Atom	X	Y	Z	U or U_{eq}(Å^2)
C(64)	6296(3)	8169(5)	-335(6)	49(2)
C(65)	6165(3)	7798(5)	-1721(6)	46(2)
C(66)	6241(3)	6645(5)	-2093(6)	38(2)

Anisotropically refined atoms are given in the form of the isotropic equivalent thermal parameter defined as:
$(1/6\pi^a)[a^2*B(1,1)+b^2*B(2,2)+c^2*B(3,3)+ab(\cos\gamma)*B(1,2)-$
$+ac(\cos\beta)*B(1,3)+bc(\cos\alpha)*B(2,3)]$

Table 3.3.2 Anisotropic Thermal Parameters ($\times 10^3$)

Name	U(1,1)	U(2,2)	U(3,3)	U(1,2)	U(1,3)	U(2,3)
Rh(1)	28.7(6)	27.8(4)	22.8(4)	-1.5(4)	0.6(4)	0.4(4)
Rh(2)	26.7(6)	23.8(4)	22.9(4)	2.2(4)	3.0(3)	0.5(4)
Cl(1)	36(2)	39(2)	37(1)	-7(2)	5(1)	3(1)
Cl(2)	62(3)	47(2)	27(1)	1(2)	-3(1)	-4(1)
Cl(3)	45(2)	35(1)	47(1)	-10(1)	10(1)	8(1)
Cl(4)	33(2)	31(1)	43(1)	9(1)	0(1)	1(1)
Cl(5)	45(2)	48(2)	25(1)	7(2)	8(1)	9(1)
Cl(6)	44(2)	37(2)	45(1)	4(1)	11(1)	-6(1)
P(1)	28(2)	28(1)	26(1)	-2(1)	-1(1)	-4(1)
P(2)	31(2)	22(1)	26(1)	2(1)	3(1)	3.9(9)
N(1)	36(6)	58(7)	39(5)	-1(5)	-7(4)	12(5)
N(2)	33(6)	39(5)	34(4)	-4(4)	-4(4)	-3(4)
N(3)	39(6)	33(5)	30(4)	-13(4)	7(4)	-4(4)
N(4)	45(6)	22(4)	26(4)	-4(4)	12(4)	4(3)

The form of the anisotropic thermal parameter is : $\exp[-2\pi^2(h^2a^2U(1,1) + k^2b^2U(2,2) + l^2c^2U(3,3) + 2hkabU(1,2) + 2hlacU(1,3) + 2klbcU(2,3))]$ where a, b, c are reciprocal lattice constants.

Table 3.3.3 Hydrogen Atomic Positional ($\times 10^4$) and Thermal ($\times 10^3$) Parameters

Atom	X	Y	Z	U(Å^2)
H1A	-336	4821	-4641	80
H1B	-714	5840	-4166	80
H1C	-536	4893	-3071	80
H2A	349	6365	-5548	80
H2B	564	7275	-4444	80
H2C	-59	7299	-4986	80
H3A	168	7456	-2298	80
H3B	-450	7010	-2365	80
H4A	-171	5445	-862	80
H4B	-87	6617	-81	80
H5A	930	7508	-1158	80
H5B	1376	6805	-286	80
H5C	857	7324	474	80
H6	657	4326	292	80
H7A	467	4816	2621	80
H7B	2	5275	1574	80
H7C	458	6110	2191	80
H8A	5493	1308	-4838	80
H8B	5294	2400	-5668	80
H8C	4861	1452	-5274	80
H9A	4503	3649	-3300	80
H9B	4308	2752	-4441	80
H9C	4740	3701	-4835	80
H10A	4521	1515	-2601	80
H10B	5112	933	-2590	80
H12	2633	4279	-202	99
H13	2930	4882	2089	99
H14	2269	5578	3711	99
H15	1311	5673	3042	99

Table 3.3.3 continued

Atom	X	Y	Z	U(Å²)
H17A	4812	2785	-883	80
H17B	4935	1544	-333	80
H18A	6336	1351	-622	80
H18B	5870	855	-1641	80
H18C	5798	798	5	80
H19	5611	2264	1274	80
H20A	5025	3809	972	80
H20B	5537	4591	630	80
H20C	5477	4074	2153	80
H22	2456	5638	-2353	99
H23	3250	5596	-3810	99
H24	3475	3909	-5059	99
H25	2908	2264	-4852	99
H26	2114	2306	-3394	99
H32	1121	2112	-3215	99
H33	984	143	-2766	99
H34	1229	-631	-518	99
H35	1611	565	1280	99
H36	1748	2534	830	99
H42	7565	4266	66	99
H43	7836	3687	2386	99
H44	7190	2736	3841	99
H45	6272	2363	2977	99
H52	7480	2740	-1974	99
H53	8279	2668	-3410	99
H54	8495	4230	-4896	99
H55	7912	5864	-4946	99
H56	7113	5936	-3510	99
H62	6723	5701	999	99
H63	6594	7640	1625	99

Table 3.3.3 continued

Atom	X	Y	Z	U(Å²)
H64	6244	8956	-81	99
H65	6022	8331	-2413	99
H66	6151	6392	-3039	99

H1A, H1B, H1C are bonded to C(1); H2A, H2B, H2C are bonded to C(2); H3A, H3B are bonded to C(3); H4A, H4B are bonded to C(4) etc.

Table 3.3.4 Root-Mean-Square Amplitudes of Thermal Vibration (Å)

Atom	Min.	Int'med.	Max.
Rh(1)	0.151	0.163	0.173
Rh(2)	0.146	0.152	0.170
Cl(1)	0.165	0.200	0.211
Cl(2)	0.159	0.218	0.249
Cl(3)	0.153	0.221	0.235
Cl(4)	0.151	0.203	0.208
Cl(5)	0.144	0.200	0.240
Cl(6)	0.166	0.207	0.233
P(1)	0.148	0.169	0.177
P(2)	0.140	0.162	0.181
N(1)	0.168	0.202	0.254
N(2)	0.164	0.195	0.202
N(3)	0.149	0.168	0.227
N(4)	0.124	0.164	0.225

Table 3.3.5 Selected of Torsion Angles in Degree

Atom 1	Atom 2	Atom 3	Atom 4	Angle
N(1)	Rh(1)	N(2)	C(4)	26.25(64)
N(2)	Rh(1)	N(1)	C(3)	5.14(74)
Rh(1)	N(2)	C(4)	C(3)	-55.03(90)
N(1)	C(3)	C(4)	N(2)	65.04(115)
C(4)	C(3)	N(1)	Rh(1)	-36.37(103)
N(2)	Rh(1)	P(1)	C(11)	-13.04(36)
P(1)	Rh(1)	N(2)	C(6)	-37.47(57)
Rh(1)	P(1)	C(11)	C(16)	37.99(62)
Rh(1)	N(2)	C(6)	C(16)	82.84(68)
N(2)	C(6)	C(16)	C(11)	-62.68(91)
P(1)	C(11)	C(16)	C(6)	-5.12(92)
N(4)	Rh(2)	P(2)	C(41)	9.83(35)
P(2)	Rh(2)	N(4)	C(19)	33.58(71)
Rh(2)	P(2)	C(41)	C(46)	-28.85(62)
Rh(2)	N(4)	C(19)	C(46)	-65.17(86)
N(4)	C(19)	C(46)	C(41)	46.64(99)
P(2)	C(41)	C(46)	C(19)	2.48(99)
Rh(2)	N(4)	C(17)	C(10)	49.04(91)

TABLE 3.3.6 Results of Least-Squares Plane Calculations

The equation of the plane is of the form $Ax + By + Cz - D = 0$

where A, B, C & D are constants and x, y & z are orthogonalized coordinates

Plane No	A	B	C	D	Atom	x	y	z	Distance	Esd
1	0.6237	0.7317	-0.2749	6.1611						
					----------Atoms In Plane----------					
					RH(1)	2.0058	5.7814	-2.4514	0.000	0.001
					P(1)	3.7474	4.6378	-1.5651	0.000	0.003
					N(2)	1.5778	6.8354	-0.6382	0.000	0.010
					----------Other Atoms----------					
					C(5)	2.3410	8.0857	-0.3608	1.315	0.010
					C(6)	1.7990	5.8810	0.5567	-0.889	0.008
					C(7)	0.8819	6.1899	1.7406	-1.560	0.010
					C(11)	4.2501	5.3473	0.0550	0.387	0.006
					C(16)	3.3021	5.8267	0.9543	-0.100	0.006
2	0.6146	-0.7169	-0.3291	6.4649						
					----------Atoms In Plane----------					
					RH(2)	13.8219	3.9738	-2.4886	0.000	0.001
					P(2)	15.5704	5.0021	-1.4631	0.000	0.003
					N(4)	13.3896	2.8018	-0.7425	0.000	0.009
					----------Other Atoms----------					
					C(18)	14.0824	1.4423	-0.7089	1.390	0.009
					C(19)	13.6050	3.3304	0.6586	-0.708	0.007
					C(20)	12.8042	4.5599	1.0809	-2.220	0.008
					C(41)	15.9978	4.2353	0.1338	0.287	0.006
					C(46)	15.0718	3.5805	0.9407	-0.078	0.006
3	0.6156	0.7367	-0.2797	6.1856						
					----------Atoms In Plane----------					
					RH(1)	2.0058	5.7894	-2.4514	0.000	0.001
					N(1)	0.2624	6.9424	-3.2517	0.000	0.011
					N(2)	1.5778	6.8354	-0.6382	0.000	0.010
					----------Other Atoms----------					
					C(1)	-0.9218	6.1712	-3.6154	-1.195	0.014
					C(2)	0.6831	7.8905	-4.4204	1.284	0.011
					C(3)	-0.1097	7.8598	-2.1214	0.131	0.013
					C(4)	0.0968	7.1208	-0.7961	-0.657	0.011
					C(5)	2.3410	8.0857	-0.3608	1.313	0.010
4	0.6480	-0.6969	-0.3074	6.9514						
					----------Atoms In Plane----------					
					RH(2)	13.8219	3.9738	-2.4886	0.000	0.001
					N(3)	12.1288	2.8001	-3.3966	0.000	0.010
					N(4)	13.3896	2.8018	-0.7425	0.000	0.009
					----------Other Atoms----------					
					C(8)	12.3929	2.1387	-4.6318	1.012	0.012
					C(9)	11.0107	3.7081	-3.8210	-1.227	0.012
					C(10)	11.6879	1.9042	-2.3275	0.010	0.013
					C(17)	11.9406	2.4454	-0.9491	-0.627	0.010
					C(18)	14.0824	1.4423	-0.7089	1.386	0.009

TABLE 3.3.6
continued

5	0 6202	0 7325	-0 2805	6 1647
	Chi Squared =	2		

----------Atoms In Plane----------					
RH(1)	2 0058	5 7894	-2 4514	0 008	0 001
P(1)	3 7474	4 6378	-1 5651	-0 004	0 003
N(2)	1 5778	6 8354	-0 6382	0 000	0 010
N(1)	0 2624	6 9424	-3 2517	-0 004	0 011
----------Other Atoms----------					
C(11)	4 2501	5 3473	0 0550	0 373	0 006
C(16)	3 3021	5 8267	0 9543	-0 116	0 006
C(6)	1 7990	5 8810	0 5567	-0 897	0 008
C(4)	0 0968	7 1208	-0 7961	-0 665	0 011
C(3)	-0 1097	7 8598	-2 1214	0 120	0 013

6	0 6290	-0 7149	-0 3055	6 6467
	Chi Squared =	2062		

----------Atoms In Plane----------					
RH(2)	13 8219	3 9738	-2 4886	-0 034	0 001
P(2)	15 5704	5 0021	-1 4631	0 017	0 003
N(4)	13 3896	2 8018	-0 7425	-0 001	0 009
N(3)	12 1288	2 8001	-3 3966	0 018	0 010
----------Other Atoms----------					
C(41)	15 9978	4 2353	0 1338	0 347	0 006
C(46)	15 0718	3 5805	0 9407	-0 014	0 006
C(18)	13 6050	3 3304	0 6586	-0 672	0 007
C(17)	11 9406	2 4454	-0 9491	-0 595	0 010
C(10)	11 6879	1 9042	-2 3275	0 054	0 013

7	0 6222	0 7247	-0 2962	6 1409
	Chi Squared =	46		

----------Atoms In Plane----------					
CL(2)	2 3122	4 6412	-4 4710	-0 015	0 004
N(1)	0 2624	6 9424	-3 2517	0 016	0 011
N(2)	1 5778	6 8354	-0 6382	-0 017	0 010
P(1)	3 7474	4 6378	-1 5651	0 015	0 003
----------Other Atoms----------					
RH(1)	2 0058	5 7894	-2 4514	0 028	0 001

8	0 6309	-0 7075	-0 3184	6 7280
	Chi Squared =	114		

----------Atoms In Plane----------					
CL(5)	14 1622	5 1645	-4 4733	-0 022	0 003
N(3)	12 1288	2 8001	-3 3966	0 025	0 010
N(4)	13 3896	2 8018	-0 7425	-0 026	0 009
P(2)	15 5704	5 0021	-1 4631	0 023	0 003
----------Other Atoms----------					
RH(2)	13 8219	3 9738	-2 4886	-0 026	0 001

Dihedral Angles Between Planes

Plane No	Plane No	Dihedral Angle
1	2	92 91 +- 0 18
1	6	92 68 +- 0 18
2	3	93 31 +- 0 24
2	7	92 27 +- 0 16
3	6	93 10 +- 0 25
4	5	91 28 +- 0 23
5	6	92 74 +- 0 20
6	7	92 08 +- 0 17

Plane No	Plane No	Dihedral Angle
1	4	91 22 +- 0 22
1	8	92 10 +- 0 16
2	5	92 96 +- 0 19
3	4	91 64 +- 0 28
3	8	92 51 +- 0 23
4	7	90 62 +- 0 21
5	8	92 16 +- 0 17
7	8	91 48 +- 0 14

The absolute configuration, *R*, for the chiral center on the C atom, was known from the ligand synthesis. In order to confirm this, three cycles of refinement were carried out on the inverted hand of the model under the same conditions. Agreement factors of R_1=0.0428, R_2=0.0444, R_G=0.0518 and R_{WF}=0.0518 were obtained, slightly poorer than those observed for the *R* model. No attempt could be made to compare Friedel pairs, since these had not been recorded.

3.4 Structure Description.

The lack of significant residual electron density in the final difference Fourier synthesis confirms that the model chosen is appropriate. Stereoviews of the complex on the two independent molecules in the unit cell, and showing the atom numbering scheme, are given in Figures 3.4.1(a) and (b). Stereoviews of the two independent Rh-ligand fragments, with the three Cl atoms removed, are presented in Figures 3.4.2(a) and (b), to illustrate the conformations adopted by the chelate rings, and the arrangements of the phenyl groups. Atoms are drawn as 50% probability thermal ellipsoids. Selected intramolecular distances and angles are given in Tables 3.4.1 and 3.4.2.

The unit cell contains two independent molecules, with a Rh(1)....Rh(2) separation of 11.955(1) Å. The shortest intermolecular distances in adjacent cells are the c axis repeat of 9.329(2)Å for Rh(1)....Rh(1), and Rh(2)....Rh(2). The shortest non-bonding H....H contacts

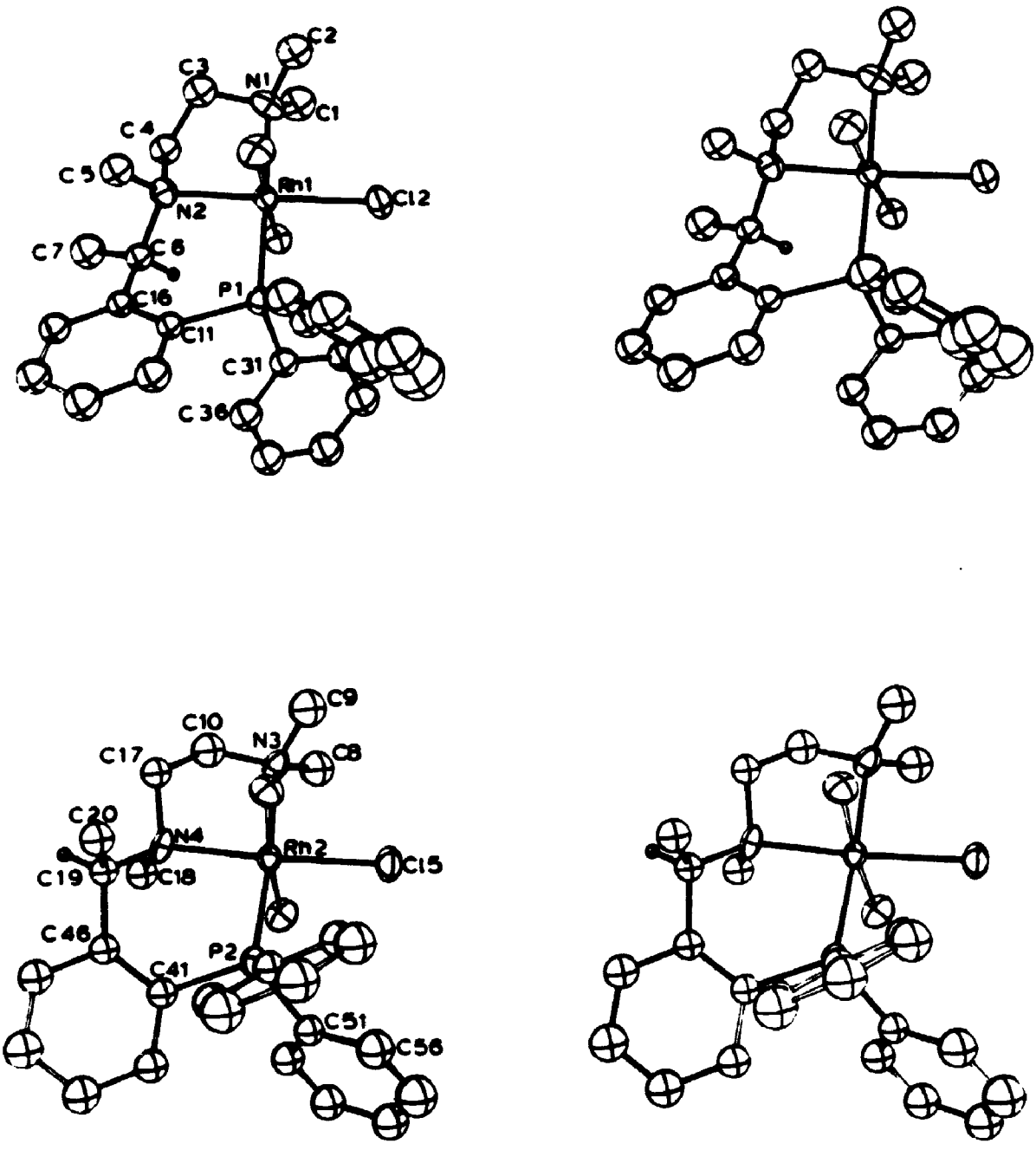

Figure 3.4.1 Stereoviews of the Two Molecules of [Rh(III)Cl$_2$(*R*-diamphos)] showing the Atom Numbering Scheme. (top) Molecule I (bottom) molecule II.

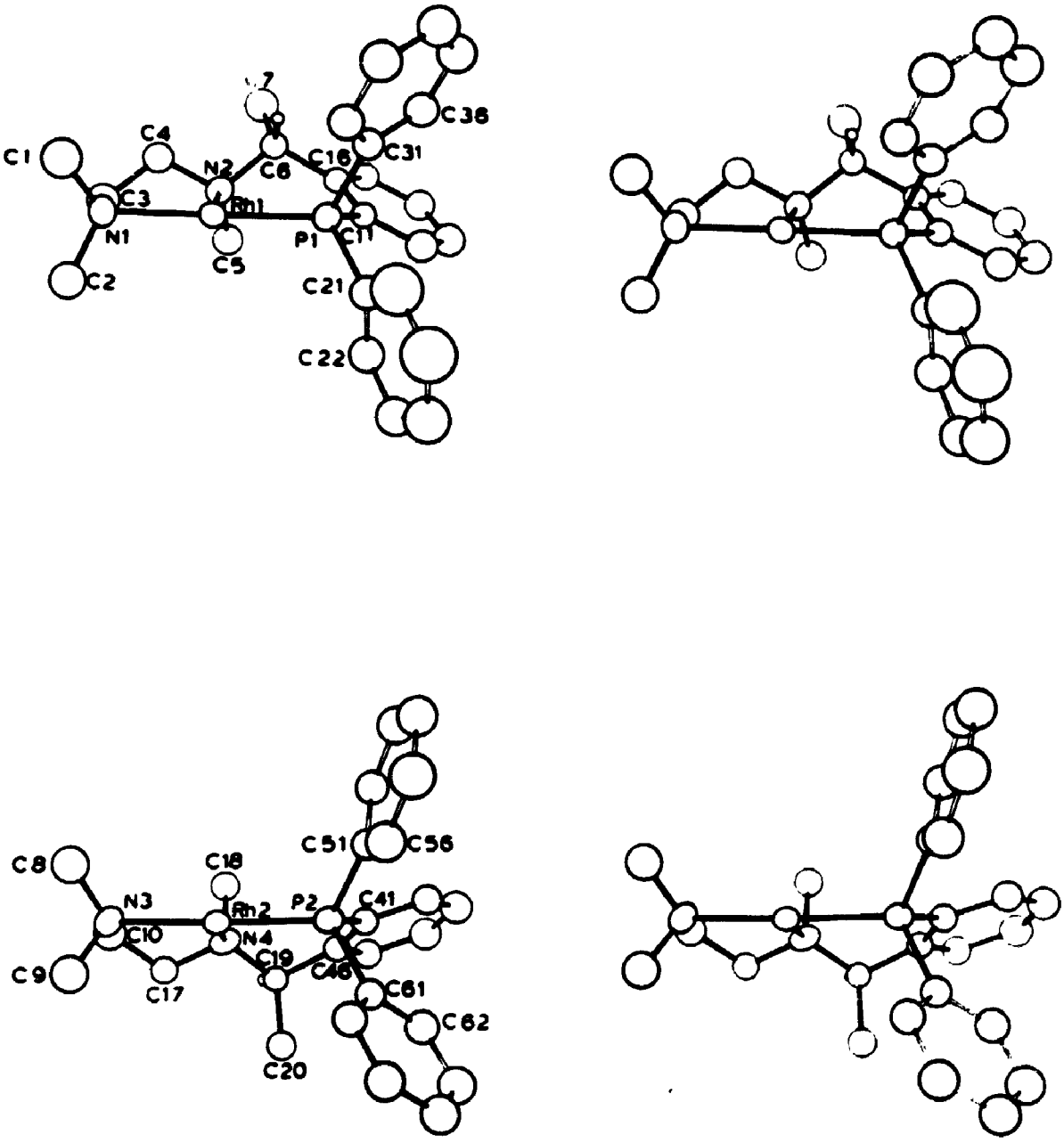

Figure 3.4.2 Stereoviews of the Two Molecules of [Rh(III)Cl$_3$(*R*-diamphos)] complex, in which three Cl atoms were removed from each molecule. (top) Molecule I (bottom) Molecule II.

Table 3.4.1 Selected Bond Distances in Angstroms

Atom 1	Atom 2	Distance	Atom 1	Atom 2	Distance
Rh(1)	Cl(1)	2.373(3)	Rh(1)	Cl(2)	2.343(3)
Rh(1)	Cl(3)	2.336(3)	Rh(1)	P(1)	2.268(3)
Rh(1)	N(1)	2.238(10)	Rh(1)	N(2)	2.147(8)
Rh(2)	Cl(4)	2.364(3)	Rh(2)	Cl(5)	2.339(3)
Rh(2)	Cl(6)	2.346(3)	Rh(2)	P(2)	2.273(3)
Rh(2)	N(3)	2.251(19)	Rh(2)	N(4)	2.147(8)
P(1)	C(11)	1.839(6)	P(1)	C(21)	1.828(7)
P(1)	C(31)	1.806(7)	P(2)	C(41)	1.822(6)
P(2)	C(51)	1.851(7)	P(2)	C(61)	1.866(7)
N(1)	C(1)	1.459(16)	N(1)	C(2)	1.563(14)
N(1)	C(3)	1.503(15)	N(2)	C(4)	1.516(13)
N(2)	C(5)	1.491(13)	N(2)	C(6)	1.545(11)
N(3)	C(8)	1.426(14)	N(3)	C(9)	1.501(15)
N(3)	C(10)	1.463(13)	N(4)	C(17)	1.506(13)
N(4)	C(18)	1.527(13)	N(4)	C(19)	1.513(10)
C(3)	C(4)	1.531(14)	C(6)	C(16)	1.555(9)
C(10)	C(17)	1.502(13)	C(6)	C(7)	1.529(12)
C(19)	C(46)	1.514(9)	C(19)	C(20)	1.527(11)

all phenyl C-C distances were constrained to 1.392 Å

Numbers in parentheses are estimated standard deviations in the least significant digits.

Table 3.4.2 Selected Bond Angles in Degrees

Atom 1	Atom 2	Atom 3	Angle	Atom 1	Atom 2	Atom 3	Angle
Cl(1)	Rh(1)	Cl(2)	87.7(1)	Cl(1)	Rh(1)	Cl(3)	177.6(1)
Cl(1)	Rh(1)	P(1)	90.8(1)	Cl(1)	Rh(1)	N(1)	88.6(3)
Cl(1)	Rh(1)	N(2)	90.0(3)	Cl(2)	Rh(1)	Cl(3)	90.0(1)
Cl(2)	Rh(1)	P(1)	89.3(1)	Cl(2)	Rh(1)	N(1)	92.7(3)
Cl(2)	Rh(1)	N(2)	175.9(3)	Cl(3)	Rh(1)	P(1)	89.5(1)
Cl(3)	Rh(1)	N(1)	91.2(3)	N(4)	C(19)	C(20)	117.6(7)
Cl(3)	Rh(1)	N(2)	92.3(3)	N(4)	C(19)	C(46)	111.6(6)
P(1)	Rh(1)	N(1)	178.0(3)	C(20)	C(19)	C(46)	108.9(6)
P(1)	Rh(1)	N(2)	94.1(3)	P(1)	C(21)	C(22)	120.9(3)
N(1)	Rh(1)	N(2)	84.0(4)	P(1)	C(21)	C(26)	119.0(2)
Cl(4)	Rh(2)	Cl(5)	87.3(1)	Cl(4)	Rh(2)	Cl(6)	174.7(1)
Cl(4)	Rh(2)	P(2)	92.8(1)	Cl(4)	Rh(2)	N(3)	89.9(3)
Cl(4)	Rh(2)	N(4)	92.7(3)	Cl(5)	Rh(2)	Cl(6)	87.4(1)
Cl(5)	Rh(2)	P(2)	92.3(1)	P(1)	C(31)	C(32)	117.7(2)
Cl(5)	Rh(2)	N(3)	91.9(2)	P(1)	C(31)	C(36)	122.3(2)
Cl(5)	Rh(2)	N(4)	175.7(3)	Cl(6)	Rh(2)	P(2)	87.9(1)
Cl(6)	Rh(2)	N(3)	89.8(3)	Cl(6)	Rh(2)	N(4)	92.6(3)
P(2)	Rh(2)	N(3)	175.1(2)	P(2)	Rh(2)	N(4)	92.0(3)

Table 3.4.2 continued.

Atom 1	Atom 2	Atom3	Angle	Atom 1	Atom 2	Atom 3	Angle
N(3)	Rh(2)	N(4)	83.8(3)	P(2)	C(41)	C(42)	116.1(2)
C(11)	P(1)	C(21)	104.7(3)	P(2)	C(41)	C(46)	123.4(2)
C(11)	P(1)	C(31)	102.3(3)	C(21)	P(1)	C(31)	104.1(3)
C(41)	P(2)	C(51)	105.4(3)	C(41)	P(2)	C(61)	102.9(3)
C(51)	P(2)	C(61)	104.0(3)	C(1)	N(1)	C(2)	110.7(8)
C(1)	N(1)	C(3)	108.0(10)	C(19)	C(46)	C(45)	111.9(3)
C(2)	N(1)	C(3)	105.0(10)	C(19)	C(46)	C(41)	127.9(3)
C(4)	N(2)	C(5)	111.2(9)	P(2)	C(51)	C(52)	118.6(2)
C(4)	N(2)	C(6)	109.7(7)	P(2)	C(51)	C(56)	121.2(2)
C(5)	N(2)	C(6)	107.5(7)	C(8)	N(3)	C(9)	100.0(8)
C(8)	N(3)	C(10)	113.9(9)	C(9)	N(3)	C(10)	110.6(9)
C(17)	N(4)	C(18)	103.2(8)	C(17)	N(4)	C(19)	110.3(7)
C(18)	N(4)	C(19)	103.1(7)	P(2)	C(61)	C(62)	119.5(2)
N(1)	C(3)	C(4)	108.8(10)	P(2)	C(61)	C(66)	120.5(2)
N(2)	C(4)	C(3)	108.2(9)	N(2)	C(6)	C(7)	112.8(7)
N(2)	C(6)	C(16)	110.9(6)	C(7)	C(6)	C(16)	112.9(6)
N(3)	C(10)	C(17)	113.5(9)	P(1)	C(11)	C(12)	118.7(4)
P(1)	C(11)	C(16)	121.1(2)	C(6)	C(16)	C(15)	119.7(3)
N(4)	C(17)	C(10)	111.9(8)				

Numbers in parentheses are estimated standard deviations in the least significant digits.

are 2.17 Å for H25....H56, (1+X,1-Y,1-Z), 2.28 Å for H26....H55, (1+X,1-Y,1-Z), 2.38 Å for H18C....H64, (X,1-Y,Z), 2.34 Å for H5A....H34, (X,1-Y,Z), and 2.46 Å for H45....H23, (1+X,1-Y,Z). The shortest non-bonding H....Cl contacts are 2.91 Å for Cl(1)....H4B, (X,Y-1,Z), 2.88 Å for Cl(2)....H2C, (X,Y-1,Z-1), 2.80 Å for Cl(2)....H7A, (X,Y,Z-1), 2.94 Å for Cl(2)....H(15), (X,Y,Z-1), 2.90 Å for Cl(4)....H17B, (1+X,Y,Z), and 2.99 Å for Cl(5)....H8C, (1+X,Y,Z-1). All are close to the sums of the van der Waals radii.

The geometry at the Rh atoms is octahedral, with two trans Cl atoms on the axis, and P, N, N and Cl atoms on the equator. The Rh(1)-Cl(2) (equatorial) distance of 2.343(3) Å in molecule I is the same (λ=1.0) as the Rh(2)-Cl(5) distance of 2.339(2) Å in molecule II; both are trans to N atoms, and cis to Cl, Cl, P and N atoms. The Cl(3) and Cl(6) atoms are trans to the Cl(1) and Cl(4) atoms respectively. Of the four such Rh-Cl bonds, two are short, and two are long, the Rh(1)-Cl(3) distance of 2.336(3) Å is the same as the Rh(2)-Cl(6) distance of 2.346(3) Å, λ=2.5, and the Rh(1)-Cl(1) distance of 2.373(3) Å is the same as the Rh(2)-Cl(4) distance of 2.364(3)Å, λ=2.25. However, the Rh(1)-Cl(3) bond length is shorter than the Rh(1)-Cl(1) distance of 2.373(3) Å, λ=8.72, and the Rh(2)-Cl(6) distance is shorter than the Rh(2)-Cl(4) distance of 2.364(3) Å, λ=4.24. The probable explanation for these differences lies in the positions of the methyl

substituents C(5) and C(18) on the chiral N atoms. Cl(3) and Cl(6) are close to the H atoms of the methyl on the chiral N atom (H5A, H5B, H5C) in molecule I and (H18A, H18B, H18C) in molecule II respectively. The shortest, intramolecular non-bonding H....Cl contacts are 2.74 Å for Cl(3)....H5A, 2.94 Å for Cl(3)....H5B, 2.87 Å for Cl(6)....H18A and 2.66 Å for Cl(6)....H18B, close to the sum of the van der Waal's radii, 2.9 Å. The Cl(1)-H6 distance of 2.52 Å in molecule I and the Cl(4)-H9A distance of 2.46 Å in molecule II are much shorter than the sum of the the van der Waal's radii, 2.9 Å. A replusive interaction between them would be dominant, so the distances of Rh(1)-Cl(1) and Rh(2)-Cl(4) are slightly longer. The Rh(1)-Cl(1) distance of 2.373(3) Å and the Rh(2)-Cl(4) distance of 2.364(3)Å are the same as mean Rh-Cl distance of 2.364(2) Å in $[Rh(III)Cl(n\text{-}P_3Cy)H]^+$-$[BPh_4]^-\cdot(CH_3)_2CO$, ($nP_3Cy$ is tri(2-dicyclohexylphosphino-ethyl)amine) [123].

The Rh(1)-P(1) distance of 2.268(3) Å in molecule I is the same as the Rh(2)-P(2) distance of 2.273(3) Å in molecule II, λ=1.2. The mean Rh-P distance of 2.271(3) Å is somewhat shorter than the mean Rh-P distance of 2.285(1) Å in $[Rh(III)_2Cl_3(COCH_3)_2(PMe_2Ph)_4]PF_6$ [118] and the Rh-P(2) distance of 2.285(1) Å in $[Rh(III)Cl(COCH_3)$-$(PMe_2Ph)_3]PF_6$ [119], λ=3.8. In these two complexes, the P atoms are trans to the Cl atoms. But in our complex, the P atom is trans to a N atom.

The two Rh-N distances in each molecule are different. The Rh(1)-N(1) distance of 2.238(10) Å is longer than the Rh(1)-N(2) distance of 2.137(8) Å, λ=7.9; the Rh(2)-N(3) distance of 2.251(19) Å is longer than the Rh(2)-N(4) distance of 2.147(8) Å, λ=5.0. This result is attributable to the P(1) and P(2) donor atoms being trans to the N(1) and N(3) atoms, while there are Cl(2) and Cl(5) atoms trans to the N(2) and N(4) atoms respectively, so that the interactions between Rh(1) and N(1), and Rh(2) and N(3) are decreased and the distance between those are increased, which are due to the greater trans influence of the P atom. The Rh(1)-N(1) distance of 2.238(10) Å is the same as the Rh(2)-N(3) distance of 2.251(19) Å, λ=0.6, in both molecule I and II. The Rh(1)-N(2) distance of 2.137(8) Å is the same as the Rh(2)-N(4) distance of 2.147(8) Å, λ=0.88, in molecules I and II. The Rh(1)-N(2) and Rh(2)-N(4) distances of 2.137(8) Å and 2.147(8) Å are the same as the Rh(1)-N(1) and Rh(2)-N(2) distances of 2.116(5) Å and 2.114(5) Å in $[Rh(III)_2(Ph_2PPy)_2(\mu\text{-}CO)Cl_2]$ [120], λ=2.23; and the same as the mean Rh-N distance of 2.130(10)Å in $[Rh(III)_2(C_5Me_5)_2[N_3C_2(CF_3)_2]_2(N_3)]$ [122], λ=0.55; but are longer than the mean Rh-N distance of 2.095(8) Å in $[Rh(III)(NCMe)_2(NO)(PPh_3)_2][PF_6]_2$, λ=7.2, in which the N atom is trans to a N atom, while in our molecule, the P atom and Cl atom are both trans to a N atom [121].

The mean P-C bond of 1.835(3) Å in both molecules is the

same as the mean P-Csp^2 distance of 1.825(2) Å, λ=2.8, in [Rh(I)[(*R*)-o-[$(C_6H_5)_2$P](C_6H_4)CHCH$_3$N(CH_3)$_2$](C_7H_8)]-ClO_4] (A) [32]; and the same as the mean P-C bond of 1.837(3) Å, λ=0.47, in [Rh(I)Cl[(*R*)-o-[$(C_6H_5)_2$P](C_6H_4)CHCH$_3$-N(CH_3)$_2$]P(C_6H_5)$_3$] (B) [see Chapter 2].

The mean N-C bond distance of 1.505(4) Å is indistinguishable from the mean N-C bond of 1.492(4) Å, λ=2.3, in (B), and the same as that of 1.501(4) Å, λ=0.53, in (A). The mean C-C bond distance of 1.528(4) Å in the chelate ring is quite similar with that of 1.531(6) Å, λ=0.42, in the chelate ring of (B) and 1.515(7) Å, λ=1.61, in (A).

There are two chelate rings in the [Rh(III)Cl_3(diamphos)] complex with the tridentate ligand. One is a six-membered ring and the other is a five-membered ring. The six-membered ring adopts a twist boat (skew) conformation with Rh(1), P(1) and N(2), and Rh(2), P(2) and N(4) forming the planes, while the five-membered ring takes an envelope conformation. The two molecules of [Rh(III)Cl_3-(*R*-diamphos)] (Figures 3.4.1(a) and (b), Figures 3.4.2(a) and (b)) differ in several ways. The secondary N atoms N(2) and N(4) become chiral centres when the diamphos ligand coordinates to a metal atom. Whereas the chirality at C(6) and C(19) is always *R*, the chirality at N(2) for molecule I is *S*, while that for N(4) in molecule II is *R*. The phenyl rings at the P atom are face-edge in molecule I, but edge-face in molecule II (in Figure 3.4.2(a), the

phenyl ring which is given atom numbers from 31-36 is face-exposed, while that from 21-26 is edge-exposed; in Figure 3.4.2(b), the phenyl ring which is numbered from 51-56 is edge-exposed, while that from 61-66 is face-exposed). Molecule I has a λ-configuration, but molecule II has a δ-configuration in the six-membered chelate rings. The orientations of the methyl groups attached to the chiral C and N atoms are of particular interest. The methyl group and the hydrogen atom on the chiral C atom ride equally upon the six-membered ring, being neither axial nor equatorial. The methyl group on the chiral N atom hangs down towards the chelate ring in molecule I (see Figure 3.4.2(a)). In molecule II, the methyl group and the hydrogen atom on the chiral C atom are located in this way: the methyl group points axially down from the chelate ring; the hydrogen atom is equatorial, while the methyl group in the chiral N atom is axial (up) (see Figure 3.4.2(b)). The methyl group in molecule II in the [Rh(III)Cl_3(*R*-diamphos)] complex is very similar to those in the complexes (A) and (B) with the bidentate amphos ligand. The complex with bidentate amphos ligand showed an axial orientation of the methyl group on the chiral C atom and staggering of the N-methyl groups. This arrangment minimizes steric repulsions between methyl-H atoms and the nearest neighbour on the phenylene ring in the chelate back bone.

3.5 Discussion.

The ^{31}P NMR spectral results for the Rh(III) diamphos complex indicate that two conformations, in roughly equal proportions, exist in solution (δ_1=29.8 (d) ppm, δ_2=25.7 (d) ppm, $^1J_{Rh-P}$=11.0 Hz) [32]. In the crystal structure, we see two pairs of different molecules in a cell, which is consistent with two diastereomers existing in both solid and solution: *RS* and *RR*. The unchanging *R* conformation represents chirality at the C atom, while the other describes the chirality at the N atom. The optical yields for the hydrosilylation of prochiral ketones catalyzed with the [Rh(I)Cl(diamphos)] complex were very low [32].

When the silane oxidatively added to the [Rh(I)Cl(diamphos)] complex, a Rh(III)-hydridosilyl complex was formed. So we assume that addition of the silane could produce a ratio of conformers similar to that observed in the [Rh(III)Cl_3(diamphos)] complex. The X-ray structure of the [Rh(III)Cl_3(diamphos)] complex can still be used to explain why the optical yield is zero. This tridentate ligand which is coordinated to the Rh metal forms a flexible six-membered chelate ring. The size and the flexibility of the chelate ring would be expected to influence the arrangement of the phenyl rings at the P atom. Therefore, we can expect the two molecules to have different conformations, especially the two different arrangements of the phenyl rings (face-edge, edge-face). As discussed on the Chapter 2, it is mainly by transmission

through the PPh_2 groups that the chiral information reaches the point where it is needed at the substrate molecule. So the induction of chirality by this complex fails.

The presence of a small amount of a Rh(III) species in a solution of the Rh(I) diamphos complex was detected in the ^{31}P NMR spectrum [32]. In the ^{31}P NMR spectrum of the Rh(I) diamphos complex, the Rh(I) complex also exhibits two conformations in solution, but they are present in unequal amounts, one conformation being adopted by roughly 85% of the complex present (δ_1^*=43.8 (d) ppm, δ_2=38.0 (d)ppm, $^1J_{Rh-P^*}$=167.8 Hz, $^1J_{Rh-P}$=151.1 Hz, P^* being the 85% amount) [32]. From this result, we deduce that the axial Cl atoms might play an important role in the absolute configuration of the chiral N atom, and the orientation of the phenyl rings at the P atom (face-edge, edge-face). The H atoms at the methyl group bound to the chiral N atom, the H atom at the chiral C atom and one of the H atoms in each of the phenyl rings are all in close proximity to the axial Cl atoms (about 2.5-3.0 Å). These non-bonding H....Cl contacts are shorter or close to the sum of the van der Waal's radii, 2.9 Å. They are 2.52 Å for Cl(1)....H6, 2.99 Å for Cl(1)....H32, 2.74 Å for Cl(3)....H5A, 2.94 Å for Cl(3)....H5B, 2.72 Å for Cl(3)....I22, 2.60 Å for Cl(4)....H20B, 2.87 Å for Cl(6)....H18A, 2.66 Å for Cl(6)....H18B and 2.92 Å for Cl(6)....H52, where H6 is the H atom at the chiral C atom in molecule I, H32 is the H atom at phenyl ring (face-exposed) in molecule I, H5A and

H5B are the H atoms of the methyl group at the chiral N atom in molecule I, H22 is the H atom at phenyl ring (edge-exposed) in molecule I, H20B is the H atom of the methyl group at the chiral C atom in molecule II, H18A and H18B are the H atoms of the methyl group at the chiral N atom in molecule II, and H52 is the H atom of the phenyl ring (edge-exposed) in molecule II.

Non-bonded atoms (or groups) that just touch each other - that is, that are about as far apart as the sum of their van der Waal's radii - attract each other. If brought any closer together, they repel each other: such crowding together is accompanied by van der Waal's strain (steric strain) [114]. Thus non-bonded interactions can be either repulsive or attractive, and as a result when formed can either destabilize or stabilize a conformation. These interactions between H atoms and axial Cl atoms could lead to the two arrangements seen for the methyl groups at the chiral C atom and the chiral N atom, as well as the face-edge, edge-face on the phenyl ring groups, in order to form as far as is possible stable conformations.

3.6 Conclusions.

The two molecules in the [Rh(III)Cl_3(R-diamphos)] complex exist in equal amounts in both solid and solution. Particularly, in the solid state, the different orientations could be observed. Consequently, the function of inducing chirality was not achieved with this

catalyst. In fact, McKay [32] observed very low optical yields for the hydrosilylation of prochiral ketones [32], a situation strongly reminiscent of that found by Stephan for the amars ligand. In both of these cases, the ligand has formed a rather flexible chelate ring and it is clear that a tightly-bonded, rigid arrangement is required for successful chiral induction.

Chapter 4

The Preparation and Spectroscopic Properties of Intermediates in the Reaction of [Rh(I)Cl(S-amphos)(PPh_3)] With $HSiCl_3$.

4.1 Introduction.

The catalytic, asymmetric reduction of prochiral ketones by rhodium(I) complexes of chiral amphos, amars, diamphos and other chiral phosphines [32,54] has been studied in our group for ten years. But the exact nature of the process of enantiomeric discrimination is still unknown. In this chapter, various spectroscopic studies which have provided considerable insight into the mechanism will be described.

We had hoped that crystal structure analyses of the reactive intermediates of the oxidative-addition of a hydrosilane to the chiral Rh-amphos species might assist in understanding the causes of enantiomeric discrimination. Ever since the crystal structure of one of the reactive intermediates derived from Wilkinson's catalyst, Rh(I)Cl-(PPh_3)$_3$, was determined in 1969, Rh(III)HCl(PPh_3)$_2$($SiCl_3$), [44,45,71] no further examples of hydrosilylation intermediates of rhodium complexes have been isolated and crystallized. We worked hard for two years trying to isolate and crystallize hydrosilylation adducts of the Rh(I)Cl(S-amphos)(PPh_3) catalyst using $HSiCl_3$ as reagent. A yellow powder, Rh(III)HCl(S-amphos)($SiCl_3$)(PPh_3), was

prepared and characterized by ^{31}P and ^{1}H NMR.

Yellow crystals were obtained by slow diffusion of hexane into a CH_2Cl_2 solution of powder, but it was too air and moisture sensitive to do an X-ray structure determination. We tried to use another method to crystallize the compound by mixing $HSiCl_3$ diluted with hexane with Rh(I)Cl(S-amphos)(PPh_3) crystals, and adding a small amount of CH_2Cl_2 to dissolve the starting material. A complex was crystallized in 15 days at 1°C and was less air and moisture sensitive than before. An X-ray analysis was undertaken and successfully completed, but unfortunately the pale yellow single crystal was found to be Rh(III)HCl(PPh_3)$_2$($SiCl_3$), (I), from which the amphos ligand had been lost and still remained in solution. The crystal and molecular structure of this complex I will be described in Chapter 5.

Prompted by the known utility of ^{31}P NMR spectroscopy in studies of the solution chemistry of tertiary phosphine complexes of Rh(I) [38,72-75], we started to study the reactions of the Rh(I)Cl(S-amphos)(PPh_3) complex, (II), by adding $HSiCl_3$ and $(CH_3)HSiCl_2$ in solution, and monitoring by ^{31}P, ^{1}H and UV-visible spectroscopies in order to elucidate the structures of the species present in solution. The investigation initially involved treating $[RhCl(C_2H_4)_2]_2$ with varying mole-ratios of amphos ligand with and without PPh_3. The ^{31}P NMR spectra of so-generated species could be the references for study of

the hydrosilylation intermediates of the complex II.

Assignments were made largely on the basis of two general considerations: (a) that for a given phosphine in a series of Rh complexes, ^{31}P resonances shift to lower field and values of $^{1}J(Rh-P)$ increase as the trans influence of the ligand trans to the phosphine decreases. These criteria have been used with some success by Tolman et al [38] and Baird [72-75]. A survey of some of the pertinent literature [38,72-80] shows that $^{1}J(Rh-P)$ normally increases by 30-40% on going from trans P to trans Cl in otherwise similar complexes. Carbonyl, alkyl groups, and hydride ligands appear to have effects similar to those of phosphines. Similarly, chemical shift differences between P trans to P and P trans to Cl can amount to as much as 20 ppm. Data comparisons between Rh(I) and Rh(III) compounds seem to hold the same general trends within each oxidation state. (b) that ring strain contributions to the ^{31}P chemical shifts of coordinated phosphines have been discussed by Garrou [81]. He was able to show that, in a wide variety of compounds, coordinated P atoms in five and six membered rings are deshielded 24-55 ppm and shielded 2-12 ppm, respectively, relative to the similar monodentate complexes.

The decrease in $^{1}J(Rh-P)$ on going from four-coordinated to five- and six-coordinated is consistent with an increase in coordination number [76]. Both ^{31}P chemical shifts and $^{1}J_{Rh-P}$ coupling constants can thus provide information

concerning stereochemistry, coordination number and the trans influences of other ligands.

4.2 Experimental Methods (general).

All syntheses and reactions were performed under a dry, O_2-free Ar Atmosphere. ^1H NMR spectra were recorded on a Varian XL-200 Spectrometer using $Si(CH_3)_4$ as a reference. ^{31}P NMR spectra were recorded on a Varian XL-300 spectrometer with $OP(OCH_3)_3$ as the external reference. Elemental analyses were performed by Guelph Chemical Laboratories, Guelph, Ont., CANADA. The Visible spectra were measured on a Hewlett-Packard 8451A U.V. spectrophotometer. The Infrared spectra were recorded on a Beckman (AcculabI) I.R. spectrometer using Nujol mull. The mass spectra were obtained on a Finnigan-mat 8230 mass spectrometer.

4.3 Reaction of 1 Mole of $[RhCl(C_2H_4)_2]_2$, "Cramer's Compound", with 3 Moles of (*R*)-amphos.

This reaction with the 1 mole excess of (*R*)-amphos ligand was used to investigate the ^{31}P NMR spectrum of Rh(I)Cl(*R*-amphos)(L) complexes in solution (L-solvent, excess (*R*)-amphos ligand, or oxidized *R*-amphos ligand).

Treatment of a stirred suspension of 50 mg (0.129 mmole) $[RhCl(C_2H_4)_2]_2$ in degassed, dry CH_2Cl_2, with 128.9 mg (0.387mmole) *R*-amphos resulted in evolution of ethylene and the formation of an orange solution. The ^{31}P NMR spectrum

of the solution was recorded in CD_2Cl_2 at 243K. The reaction mixture contained several species formulated below. Peak assignments of the ^{31}P NMR data are listed in Table 4.3.1, in which the structural formulas of compounds III, IV, V, VI, VII are as follows,

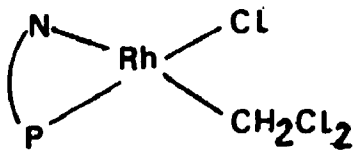

(III)

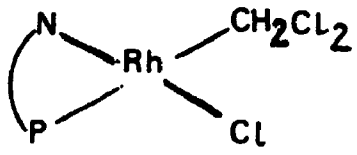

(IV)

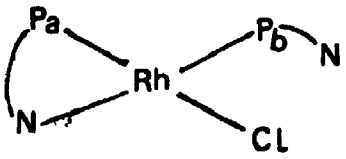

(V)

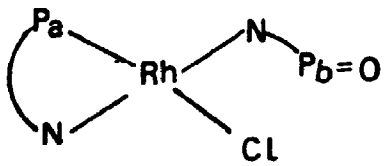

(VI)

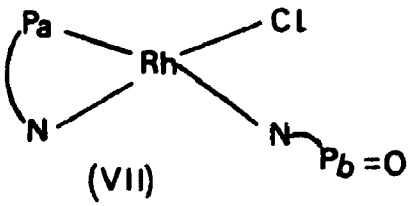

(VII)

Table 4.3.1 ^{31}P NMR data and assignment for a reaction of "Cramer compound" with *R*-amphos ligand (ratio 1:3).

Assignment	Chemical Shifts (ppm)	Coupling Constant (Hz)
III [54]	43.30 (d)	J(Rh-P)=184
IV [54]	50.25 (d)	J(Rh-P)=183
V	P_a=26.22 (d of d); P_b=13.06 (d of d).	J(Rh-P_a)=150; J(Rh-P_b)=125; J(P_a-P_b)=22.5
VI	P_a=34.91 (d); P_b=28.35 (s).	J(Rh-P_a)=175
VII	P_a=39.30 (d); P_b=28.35 (s).	J(Rh-P_a)=160

Complex III (58% yield) and IV (9% yield) were first identified by Stephan [54]; the chemical shift is always at higher field for the complex of a P atom trans to a chloride atom than in a complex with a P atom trans to a solvent molecule. Complex V (6% yield) has two P atoms

cis to each other. The four-line signals which appear at 26.22 ppm indicate a Rh to P_a coupling ($^1J_{Rh-Pa}$ = 150 Hz), and P_b to P_a coupling ($^2J_{Pa-Pb}$ = 22.5 Hz). The other four-line signals located at 13.06 ppm were assigned to an amphos ligand in which the nitrogen end of the amphos was not coordinated to the Rh atom, for which the Rh to P_b coupling ($^1J_{Rh-Pb}$ = 125 Hz) and the P_a to P_b cis coupling ($^2J_{Pa-Pb}$ = 22.5Hz) were evident. For complexes, VI (10% yield) and VII (12% yield), having both signals only doublets indicated only one P atom which was coordinated to the Rh atom in both complexes. The nitrogen atom of the amphos which was oxidized might be coordinated to the Rh atom to form the four-coordination complexes in the VI and VII. The single signal of uncoordinated, oxidized amphos is usually located at 27.80 ppm in CD_2Cl_2 solvent. The single signal at 28.35 ppm could be more down field because the nitrogen end of the amphos was coordinated to the Rh atom, the P end of the amphos having been oxidized during the ^{31}P NMR measurement [84]. This was consistant with the presence of a signal at 3.52 ppm in the ^1H NMR spectrum, which was assigned to the N-methyl groups in an amphos in which only the nitrogen end was coordinated to the Rh atom. For complex VII, with a P atom trans to the nitrogen, the signal of P atom was similar to that in the complex Rh(I)Cl(R-diamphos) (δP=38.0 ppm; $^1J_{Rh-P}$=152 Hz).

4.4 Reaction of 1 Mole of "Cramer's Compound" with 4 Moles

of (R)-amphos and 2 Moles of $NaPF_6$.

In this reaction, the effect of removal of the chloride ligand by addition of $NaPF_6$ solution was examined.

Treatment of a stirred suspension of 50 mg (0.128 mmole) "Cramer's compound" in degassed, dry CH_2Cl_2 with 171.3 mg (0.515 mmole) R-amphos ligand and 43.9 mg (0.257 mmole) $NaPF_6$ in MeOH resulted in evolution of ethylene and formation of a dark red solution and a white precipitate of NaCl (a $AgNO_3$ test performed). After filtration, a red solid was precipitated from the dark red solution by adding hexane. The red powder was dissolved in $CDCl_3$ and CD_3CN for ^{31}P NMR spectra; different ^{31}P NMR spectra were obtained in the different solvents (Figure 4.4.1). The ^{31}P NMR data and assignments are summarized in Table 4.4.1, in which the possible structures of compounds VIII and IX are pictured as follows,

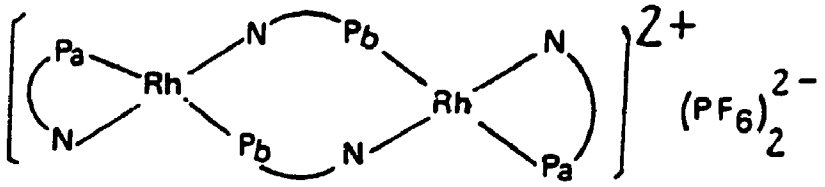

(VIII) $CDCl_3$

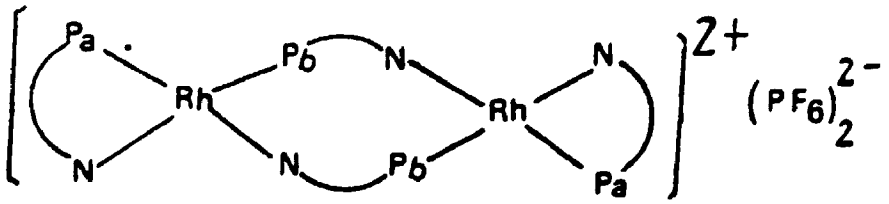

(IX) CD_3CN

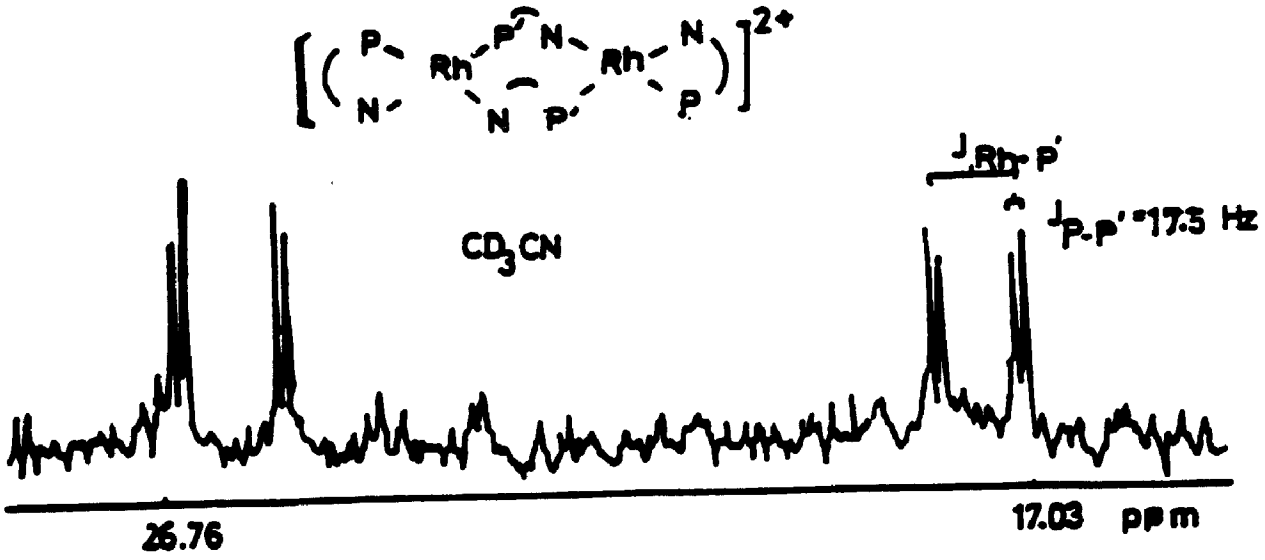

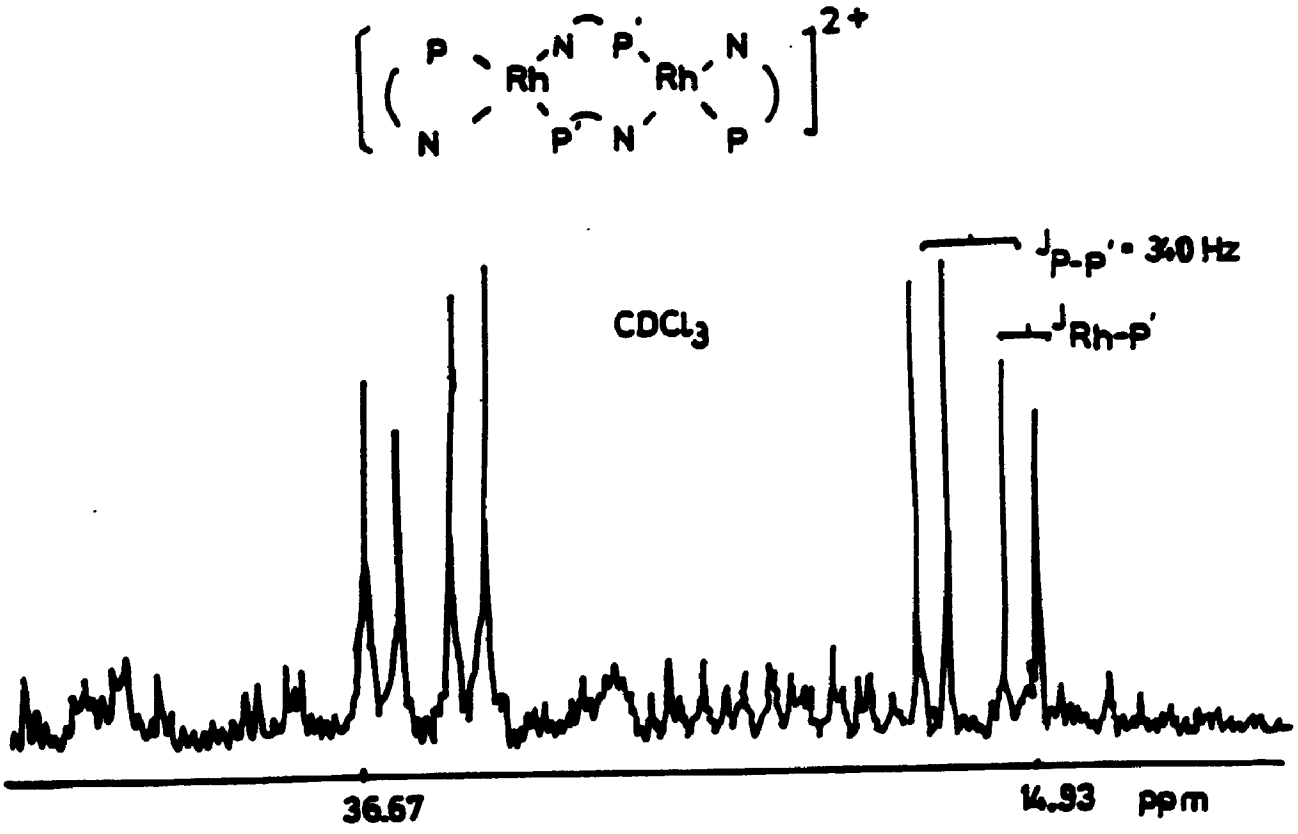

Figure 4.4.1 ^{31}P NMR Spectra of $[Rh_2(amphos)_4]^{2+}$ in CD_3CN and $CDCl_3$ solvent at 293 K.

Table 4.4.1 ^{31}P NMR data and assignments for reaction of "Cramer's compound" with *R*-amphos (ratio 1:4) in $CDCl_3$ and CD_3CN solvents at 295 K.

Assignment	Chemical Shifts (ppm)	Coupling Constant (Hz)
VIII	P_a=34.67 (d of d);	J(Rh-P_a)=140
$CDCl_3$	P_b=16.88 (d of d).	J(Rh-P_b)=140
		J(P_a-P_b)=340
IX	P_a=26.10 (d of d);	J(Rh-P_a)=154
CD_3CN	P_b=17.57 (d of d).	J(Rh-P_b)=115
		J(P_a-P_b)=17.5

For the dimeric complexes VIII and IX, the P atom of the amphos at the terminal position was named as P_a, the P atom at the bridging position was labelled P_b. The eight-line signals of complex VIII, which are centred at 34.67 ppm and 16.88 ppm, indicated P_a trans to P_b, because of the same $^1J_{Rh-P}$ coupling constant (140 Hz), and the large coupling constant (up to 340 Hz) between the two P atoms (P_a and P_b) [82].

For the dimer complex IX, the eight-line signals occur at 26.10 ppm and 17.57 ppm. The small coupling constant between the two P atoms (P_a and P_b) is 17.5 Hz, and the

different coupling constant between $^1J_{Rh-Pa}$ and $^1J_{Rh-Pb}$ (154 Hz and 115 Hz respectively) show P_a cis to P_b in dimer complex IX [82].

The mass spectra of both complex VIII and IX are consistent with the cationic molecular formulas assigned. The M^+ parent peaks, m/e 1538, are due to ions of formula $[(C_{22}H_{24}NP)_4Rh_2]^{2+}$.

4.5 Reaction of [Rh(I)Cl(*S*-amphos)(PPh_3)], II, with $HSiCl_3$.

This reaction was carried on at least 30 times under varying conditions; the most successful method is described here.

Treatment of 100 mg of red crystalline compound II (1.364×10^{-4} mole) in a minimum of degassed, dry methylene chloride with 5 mL excess $HSiCl_3$ (2.77×10^{-2} mole) resulted in an immediate yellow precipitate and a pale yellow solution. The solvent was removed by passage of a stream of dry nitrogen gas. The yellow solid was dissolved in degassed dry $CDCl_3$ and frozen in dry ice-acetone before the sample was measured by ^{31}P and ^1H NMR. The initial ^{31}P NMR spectrum at 213 K showed only sixteen lines which were centred at 14.07 ppm and 14.85 ppm; the $^1J_{Rh-P}$ coupling constants were 120 Hz and 114 Hz, the $^2J_{P-P}$ coupling constant was 24 Hz and the $^2J_{P-H}$ coupling constants were 12 Hz and 20 Hz. This information indicated that the formation of a Rh(III) complex (complex X), with cis coupling between the P atom at the amphos

ligand and the P atom at the triphenylphosphine ligand had occurred. After the sample had been measured for 45 minutes, the signals of the ^{31}P NMR spectrum became more complicated (Figure 4.5.4). These ^{31}P NMR data and the peak assignments are summarized in Table 4.5.1.

The probable structures of complexes X, XI, XII, and the compound XIII are pictured as follows, that of complex I is included.

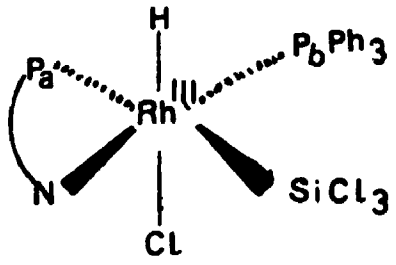

(X)

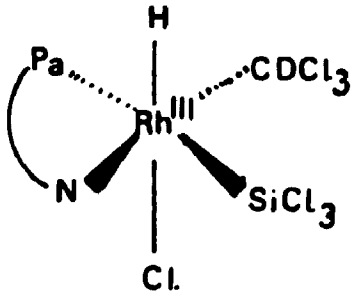

(XI)

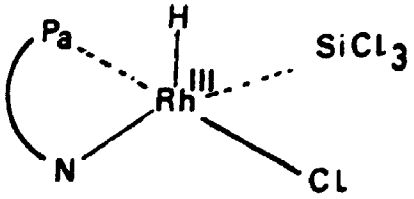

(XII)

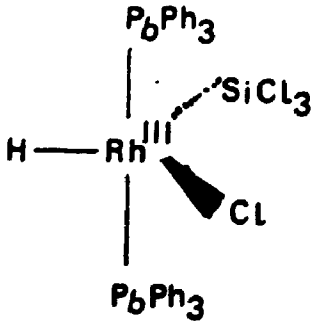

(I)

(XIII)

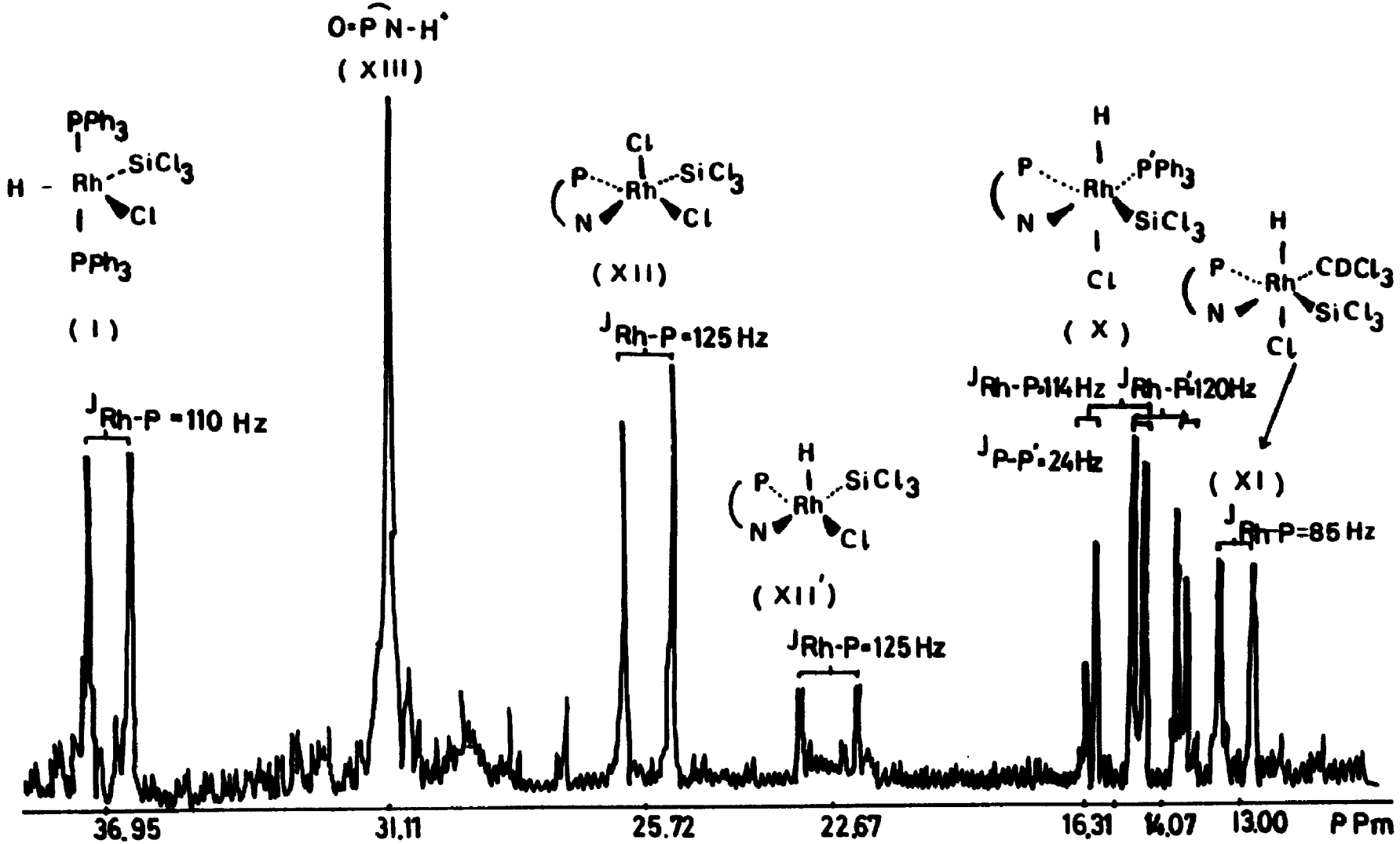

FIGURE 4.5.4 ^{31}P NMR Spectrum of [Rh(I)Cl(S-amphos)(PPh_3)] with $HSiCl_3$ added at 213 K.

Table 4.5.1 ^{31}P NMR data, assignment and hydride data from ^{1}H NMR for a reaction of [Rh(I)Cℓ(*R*-amphos)(PPh_3)] with excess $HSiCℓ_3$ in $CDCℓ_3$ solvent at 213 K.

assignment	^{31}P NMR data	
	Chemical shift (ppm)	Couplinging constant (Hz).
X	P_a=14.85 (q of d);	J(Rh-P_a)=114
	P_b=14.07 (q of d).	J(Rh-P_b)=120
		J(P_a-P_b)=24
		J(P_a-H)=12
		J(P_b-H)=20.8
XI	P_a=13.00 (d of d)	J(Rh-Pa)=85
		J(P_a-H)=12
XII	P_a=22.67 (d)	J(Rh-P_a)=125
	P_a^*=25.72 (d)	J(Rh-P_a^*)=125
I	P_b=36.95 (d of d)	J(Rh-P_b)=110
		J(P_b-Rh-H)=12
XIII	P=31.11 (S).	

* - The hydride was replaced by the chloride atom of $CDCℓ_3$.

Assignment	^{1}H NMR data (hydride)	
	Chemical shifts (ppm)	Coupling constant (Hz)
X	-20.89 (t of d d)	J(Rh-H)=20 J(P_b-Rh-H)=20.8 J(P_a-Rh-H)=12
XI	-22.75 (t)	J(Rh-H)=16 J(P_a-Rh-H)=12
XII	-32.70 (single broad)	
I	-14.37 (t of d)	J(Rh-P_b)=19.6 J(P_b-Rh-H)=12

The ^{1}H NMR spectra showed several high-field metal hydride resonances (Figure 4.5.5). The inital signal in the hydride region in the ^{1}H NMR spectrum at 213 K, six lines of a double doublet triplet pattern at -20.89 ppm (Figure 4.5.1) was consistent with the formation of hydride complex X [34]. Two inequivalent P atoms were indicated by the hydride region of the ^{1}H NMR.

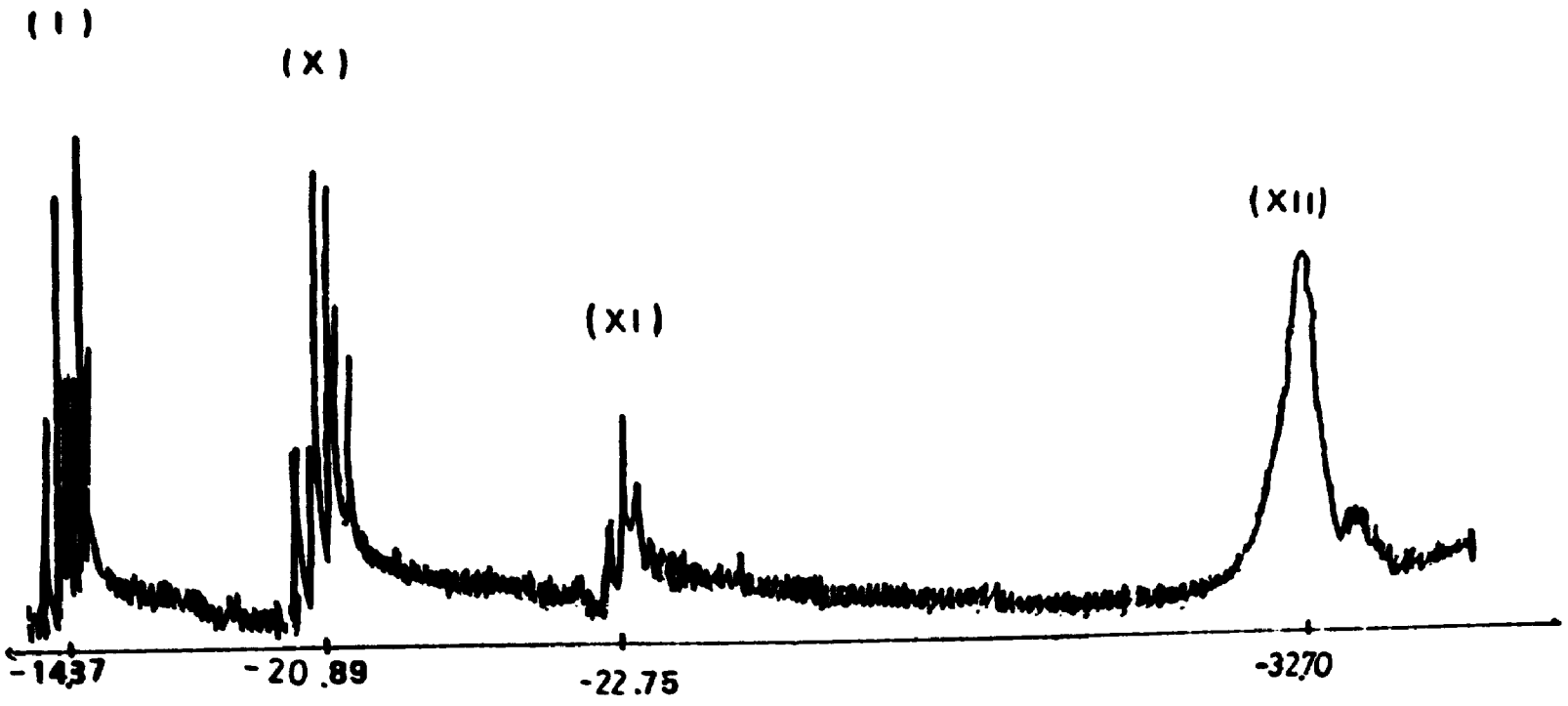

FIGURE 4.5.5 ^{1}H NMR Spectrum for Hydrides of [Rh(I)Cl(S-amphos)(PPh_3)] with $HSiCl_3$ added. at 213 K.

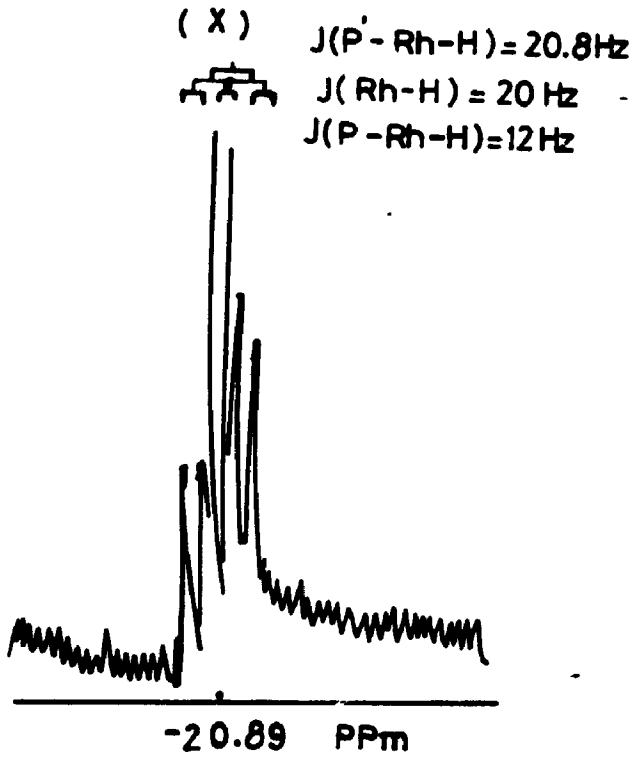

Figure 4.5.1 ^{1}H NMR Spectrum for Hydride of [Rh(III)Cℓ-(S-amphos)H($SiCℓ_3$)(PPh_3)] Complex in $CDCℓ_3$ at 213 K.

After the sample had been measured for 45 minutes, three new signals appeared in the hydride region of the spectrum, two new sets of signals and one broad single signal, while the original multiplet decreased in intensities. One set was located at -22.75 ppm (Figure 4.5.2). It was assigned to the hydride complex XI. Only coupling from one P_a atom appeared in a hydride region of ^{1}H NMR, and it was more up field.

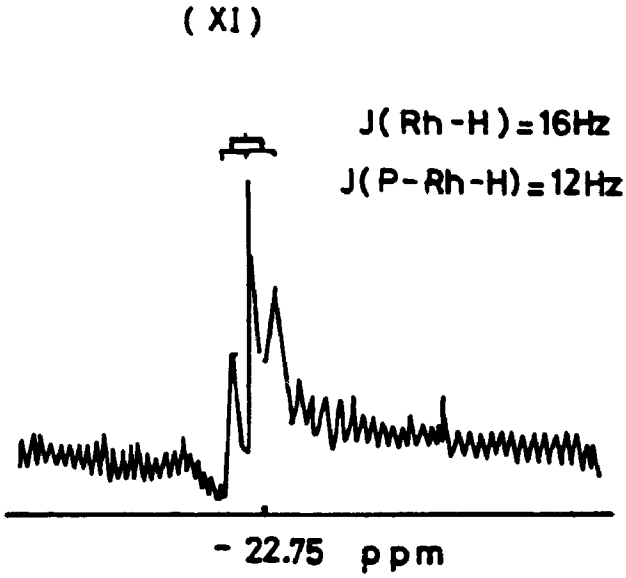

Figure 4.5.2 ^{1}H NMR Spectrum for Hydride of [Rh(III)Cℓ-(*S*-amphos)H($SiCℓ_3$)] Complex in $CDCℓ_3$ at 213 K.

Another set of hydride signals appeared at -14.37 ppm (Figure 4.5.3). These were assigned to hydride complex I. Complex I was similar with the complex which was crystallized from reaction of the Rh(I)Cℓ(*S*-amphos)(PPh_3) complex with diluted $HSiCℓ_3$ (in hexane). Two chemically equal, trans P_b atoms (PPh_3) made a double triplet pattern [44].

Inspection of the ^{31}P NMR data in Table 4.5.1 indicates that X and XI are six-coordinate Rh(III) complexes. Moreover, the $^{1}J_{Rh-P}$ coupling is always larger for a P atom trans to a chloride than for the P atoms cis to the same chloride. It is agreed that the coupling constants

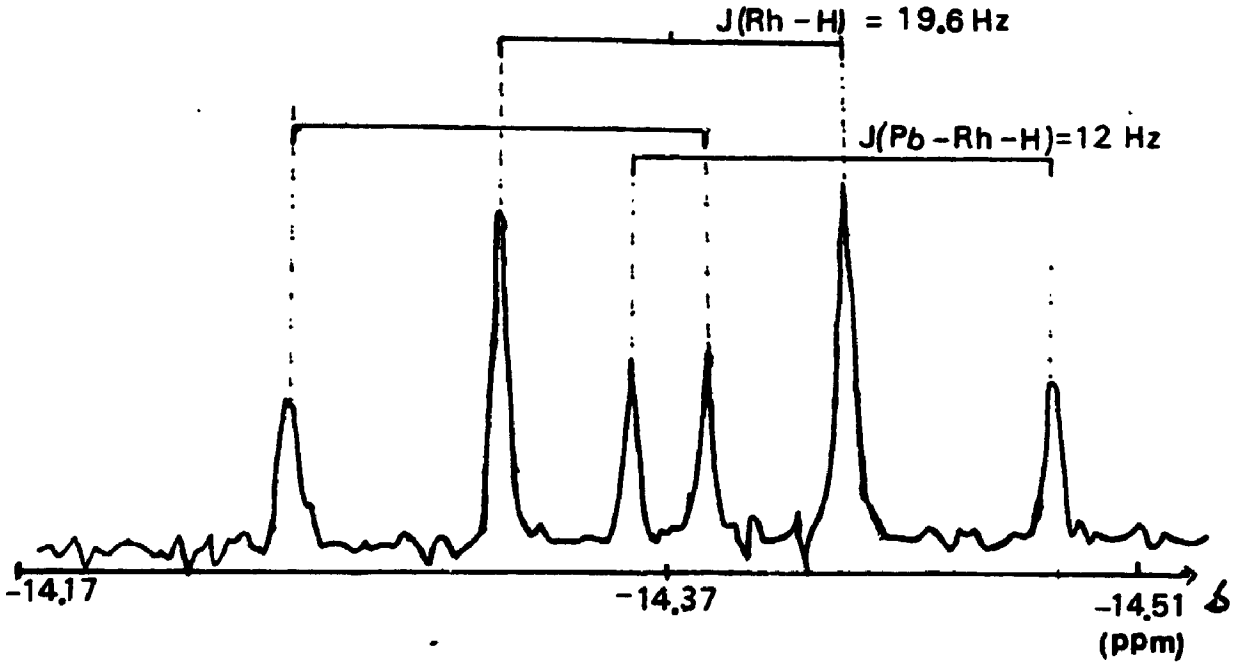

Figure 4.5.3 ^{1}H NMR Spectrum for Hydride of [Rh(III)H-Cℓ(SiCℓ$_3$)(PPh$_3$)$_2$] Complex CDCℓ$_3$ at 213 K.

depend on the electronic distributions in the vicinity of both nuclei; since the contact term is predicted to dominate the coupling, increased s character of the valence orbitals on either atom should lead to an increase in the coupling constant. Therefore σ-bond effects should be predominant. However, greater π-bonding may also indirectly increase the coupling constant by strengthening the bond. The large value of $^{1}J_{Rh-P}$ can possibly be explained by a directed greater π character of the P atom trans to the chloride atom [76].

In complex XI, the chemical shift of P_a in the ^{31}P NMR spectrum was at 13.00 ppm, which indicated the formation of six-coordinate complex by loss of the triphenylphosphine

ligand and incorporation of solvent, $CDC\ell_3$, during the measurement [42,83]. The $^1J_{Rh-P_a}$ coupling constant was only 85 Hz, showing that P_a was trans to the $SiC\ell_3$. The intensity ratio between the complex XI and the complex XII was one to two in $CDC\ell_3$ solution, but the intensity ratio was two to one in CD_3CN solution. This is good evidence for solvent coordination to the Rh atom, because CD_3CN solvent is more polar than $CDC\ell_3$ solvent. In benzene solution we did not observe the presence of complex XI. Complex XI showed a small $^2J_{P_a-H}$ coupling constant (12 Hz) that indicates a P_a atom cis to the hydride atom. The triplet pattern in the hydride region of the ^1H NMR confirmed that only one P_a atom was coordinated.

Complex X was the initial product. The intensities of the complex X signals decreased by 60% as the signals of the new complexes XI, XII and I were formed in solution at 213 K after 45 minutes. The yields of XI, XII and I were approximately 10%, 20% and 30% respectively.

For complex XII, after long time periods (20 minutes), no hydride resonance could be observed because the chloride of the deuterated chloroform replaced the hydride with time. At shorter time periods, another doublet signal with the same $^1J_{Rh-P_a}$ coupling constant of 125 Hz was observed at 22.67 ppm, which may have been the hydride not replaced by chloride. The single broad signal of the hydride of complex XII from ^1H NMR was located at -32.70 ppm. The intensity of the 22.67 ppm doublet signal was

always smaller than that of 25.72 ppm doublet signal. A signal due to $CHDC\ell_2$ at 5.32 ppm always appeared in the ^1H NMR spectra in $CDC\ell_3$, because $CDC\ell_3$ reacted with $HSiC\ell_3$ to form $CHDC\ell_2$ [71].

In order to verify that complex XII was formed, we added $HSiC\ell_3$ to the Rh(I)Cℓ(*S*-amphos)(solvent) complex in $CH_2C\ell_2$ solution to get a ^{31}P NMR spectrum with CD_3CN as a solvent at 293 K (δP=29.00 ppm (d), $^1J_{Rh-P}$=122 Hz.). This doublet signal in the ^{31}P NMR spectrum could be assigned to complex XII, present in 20% yield. When the ligand amphos was oxidized, the signal of the oxidized P atom was located at 27.00 ppm. In compound XIII, the signal at 31.1 (S) ppm is assigned to an amphos ligand with oxidized P atom and nitrogen atom protonated, perhaps by HCℓ contamination [84]. The compound XIII was present in 10% amount.

The elemental analysis for the yellow powder agreed with the formulation of complex X as ($C_{40}H_{40}P_2N_1C\ell_1Si_1Rh_1$): calculated C: 55.24%; H: 4.58%; found C: 53.91%; H: 4.83%. A small deficiency in carbon percentage is normally due to the formation of silicon carbide during the analysis [71]. The mass spectrum of the yellow powder showed as the highest peak, m/e 867, the expected molecular weight of the complex, but the base peak was m/e 852 (one N-methyl lost) in which the carbon and hydrogen percentages were in agreement with the results from the elemental analysis.

An attempt was made to recrystallize the yellow powder by slow diffusion of hexane into a CH_2Cl_2 solution of the solid. A few crystals grew, but they were too few in numbers, and too air and moisture sensitive to do an X-ray crystal structure determination.

When trichlorosilane was added to the solution of complex II, an immediate colour change from orange to lemon yellow was observed. Visible spectroscopy was used to monitor the oxidative addition of trichlorosilane [32,96]. The spectra, before and after addition, are presented in Figure 4.5.6 (a, b).

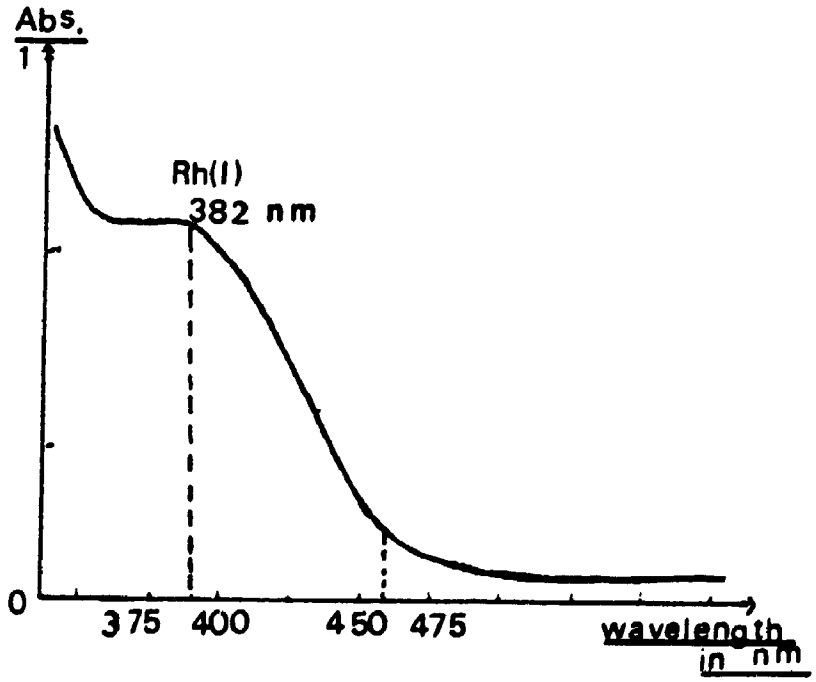

Figure 4.5.6 (a) Visible spectrum recorded the complex Rh(I)Cl(S-amphos)(PPh_3) without addition of $HSiCl_3$.

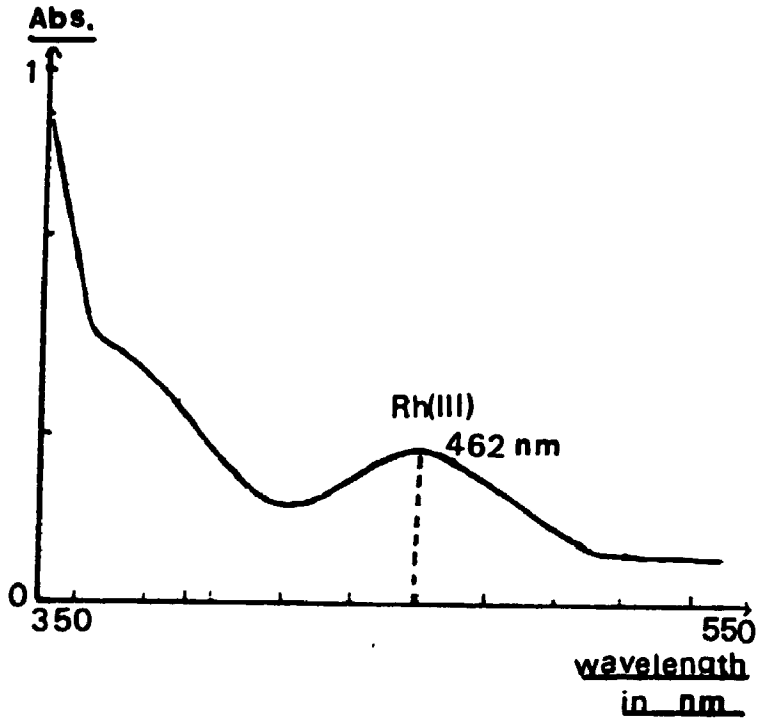

Figure 4.5.6 (b) Visible spectrum recorded the reaction between Rh(I)Cl(S-amphos)(PPh_3) and $HSiCl_3$ after 5 minutes.

Complex II has a maximum absorption at 382 nm in the visible spectrum (Rh(I) at 382 nm) before adding $HSiCl_3$ (Figure 4.5.6 (a)). Spectra were recorded at five minute intervals after adding 1 drop of $HSiCl_3$. The spectrum showing 5 minute's reaction between the Rh(I) species and $HSiCl_3$ is presented in Figure 4.5.6 (b). After 5 minutes, a new maximum appeared at 462 nm (Rh(III)) and the band at 382 nm decreased. After 10 minutes, the Rh(I) species was no longer observed and the Rh(III) species absorption had only a small increase. The reaction was followed for 30 minutes, but the spectrum showed little change. The results from the visible spectra are consistent with the

results from the ^{31}P NMR spectra.

In conclusion, it was found that the isolation and characterization of products from the Rh-amphos complex oxidative addition reaction with $HSiCl_3$ as solids was difficult. Many species are formed. The products are labile, readily dissociating from six-coordinate to five-coordinate species in solution. This behaviour is the basis of catalytic activity, a vacancy being needed for the incoming substrate molecule.

4.6 Reaction of Complex II With $HSiCl_3$ Diluted With Hexane.

4.6 mg (6.27×10^{-3} mmole) of red crystals of Rh(I)Cl-(*S*-amphos)(PPh_3), II, dissolved in a minimum amount of CH_2Cl_2 solvent were added to a degassed, dry $HSiCl_3$ solution (10% in hexane). After 15 days at 1°C, yellow crystals and a powdery yellow precipitate had appeared.

The yellow crystals were characterized by ^{31}P and ^{1}H NMR in $CDCl_3$ solution, and Infrared spectroscopy. (^{31}P: δP=37.26 ppm (d), $^{1}J_{Rh-P}$=110 Hz; ^{1}H hydride: δH=-14.37 ppm (t of d), $^{1}J_{Rh-H}$=19.6 Hz, $^{2}J_{P-H}$=12Hz.). The spectrum was similar to that of the complex I. The Infrared spectrum displayed a stretching frequency at 2020-2130 cm^{-1} (ν_{Rh-H}) (nujol). The yellow precipitate showed similarities in the NMR to the complexes XI and XII, and, too, had a small amount of protonated nitrogen.

In the present study, it was found that complex I formed crystals on addition of $HSiCl_3$ to complex II, but that an

oxidative-addition product containing the amphos ligand could not be crystallized with $HSiCl_3$ as solvent. Instead, a bis(triphenylphosphine) species was obtained. The detailed crystal structure of this complex will be described in Chapter 5.

4.7 Reaction of Complex II With $(CH_3)HSiCl_2$ Diluted With Hexane.

The synthetic procedure has been described above in section 4.6. The yellow-green crystals of $Rh(III)Cl(PPh_3)_2(CH_3SiCl_2)$ were more air and moisture sensitive than the crystals containing the $SiCl_3$ ligand. The complex was characterized by ^{31}P and ^1H NMR (^{31}P: δP=36.55 ppm (d), $^1J_{Rh-P}$=110 Hz; ^1H hydride: δH=-14.45 ppm (t of d), $^1J_{Rh-H}$=22.5 Hz, $^2J_{P-H}$=13.5Hz; ^1H: Si-CH_3 δH=0.86 ppm).

4.8 Discussion

The oxidative-addition of $HSiCl_3$ to complex II occurs by cis addition. The four stereoisomers formed by cis addition of $HSiCl_3$ to complex II are shown in Figure 4.8.1 [85].

For oxidative addition along the P-Rh-Cl axis, pathway i, two diastereomers are possible, the first with hydride trans to Cl, labelled as the H...Cl model, and the second with hydride trans to P on amphos labelled as the H...P_a model. These two diastereomers correspond respectively to the $HSiCl_3$ approaching complex II shown as Q and R in

Figure 4.8.2. Similarly, for pathway ii (addition along the N-Rh-PPh_3 axis), diastereomers with hydride trans to PPh_3 (H...P_b model) and hydride trans to N (H...N model) are possible, corresponding to the substrate approaches shown as T and S in Figure 4.8.3.

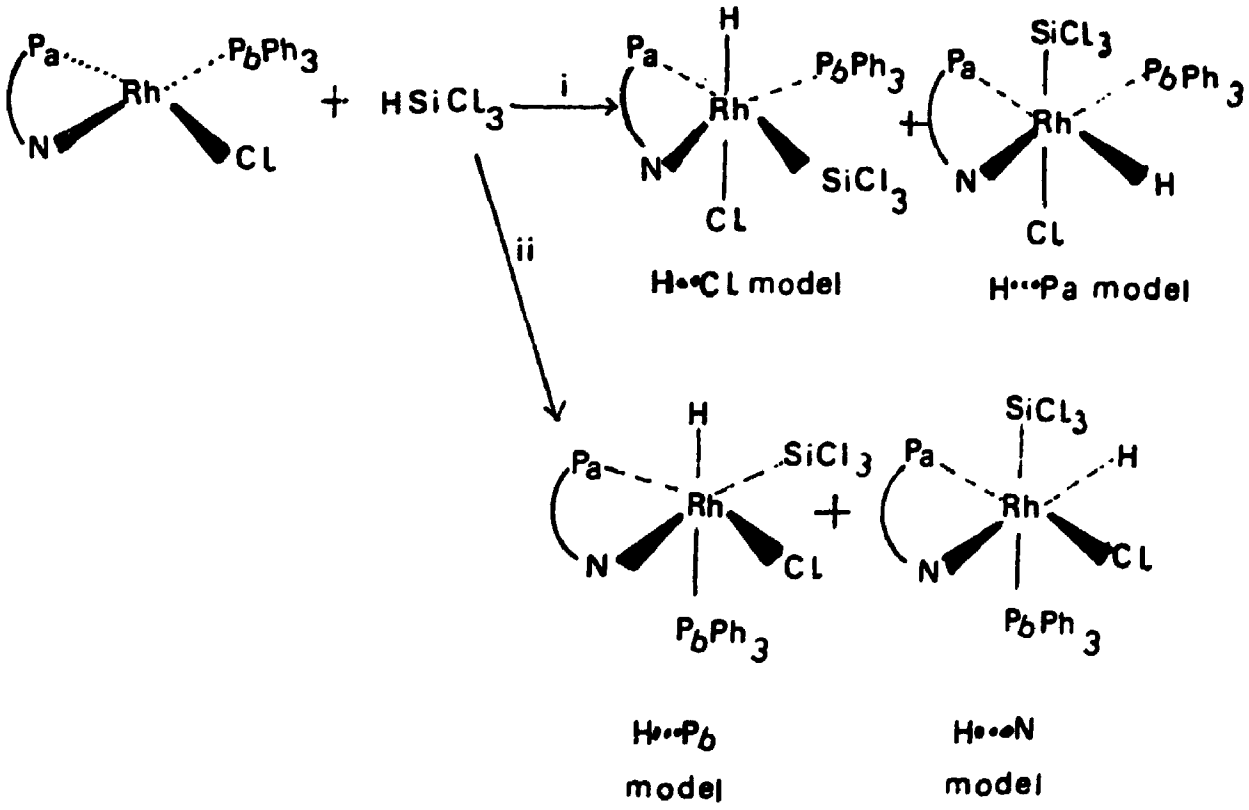

Figure 4.8.1 The four diastereomers for cis addition $HSiCl_3$ to Rh(I)Cl(S-amphos)(PPh_3).

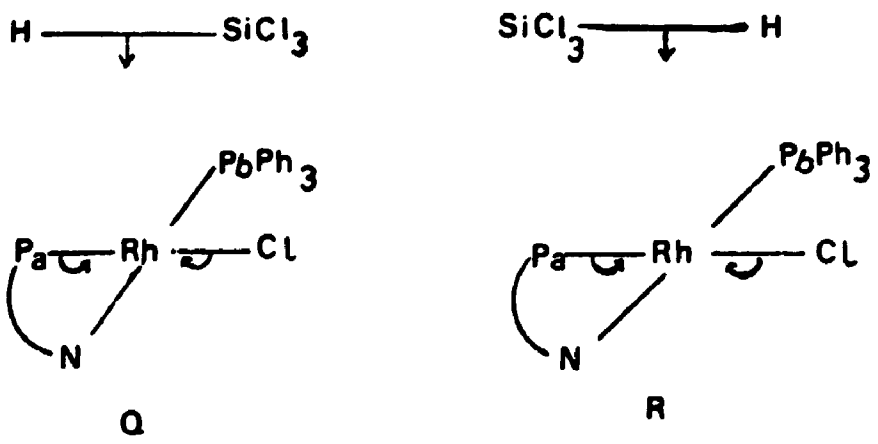

Figure 4.8.2 The two diastereomers Q and R.

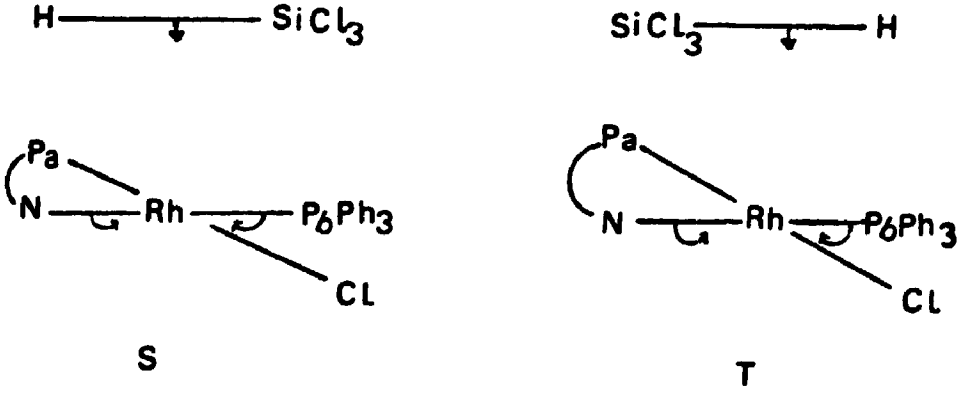

Figure 4.8.3 The two diastereomers S and T.

From the ^{1}H and ^{31}P NMR spectra, we found an initial complex X which had hydride cis to two inequivalent P atoms. Only two diastereomers (H...Cl and H...N models) (Q and T) are possible, because the H...P_a and H...P_b models (R and S) have the hydride trans to one of the two P atoms. The first isomer (H....Cl model)(Q) seems to be

more likely because of lesser steric hindrance.

We can now hypothesize on the course of the reaction. For complex II, rapid formation of the H...Cl model(Q) kinetically favored six-coordinate compound is followed by dissociation to form the five-coordinate diastereomers. As the $HSiCl_3$ substrate approaches the metal complex in this addition, one pair of trans ligands bends such that complex + substrate form a trigonal bipyramid in the transition state [85]. The bending ligands and the $HSiCl_3$ substrate occupy the equatorial sites of this trigonal bipyramid. Preference for bonding of the P-Rh-Cl axis over the N-Rh-PPh_3 axis may occur because this places the less crowded chloride in the equatorial plane where it can better stabilize the developing trigonal bipyramid [85]. This view is similar to that used to explain the trans effect in square-planar substitution reactions [86] and relates to the proposal put forward by Harrod [95], showing that deformation of the square-planar complex is a major component of the activation barrier in H_2 oxidative addition. Both of the factors proposed to explain H_2 stereoselectivity can be extended to silane oxidative addition as well.

In the crystal structure of complex I, the Cl, H and $SiCl_3$ ligands occupy the equatorial sites of the trigonal bipyramid (Chapter 5). This supports the H...Cl model (Q) proposed above.

The reaction mechanism can be explained as shown in

Figure 4.8.4. Whether any of the three intermediate configurations possesses enough stability to be regarded as actual intermediates rather than merely a phase of an activated complex remains uncertain. Two regular geometries: sp (square pyramid) and tbp (trigonal bipyramid) are commonly formed in five-coordinate complexes [86-88]. The tbp configuration for complex I is more favorable (see Chapter 5), but the sp configuration for complex XII may be preferred because the amphos chelate ligand must occupy cis sites rather than trans. The hydride ligand in complex XII had a broad signal in which the hydride exchanges rapidly with chloride in $CDCl_3$ solvent. This phenomenon is typical of a hydride located on the axis of the sp configuration [71]. Unfortunately, complex XII which contains a chiral centre could not be isolated and crystallized. However, five-coordinate species resulting from the addition of hydrosilanes are potent catalytic intermediates toward substrates containing multiple interatomic linkages or an active hydrogen atom [36]. The incoming prochiral ketone could occupy the PPh_3 position cis to H, $SiCl_3$ and the P atom of the amphos ligand forming another six coordination complex, of which Rh(III)HCl($SiCl_3$)(RR'CO) is most likely. We performed an experiment in which complex II was dissolved in CH_3CN and then $HSiCl_3$ was added. The colour in solution changed from red to yellow immediately. The ^{31}P NMR (Figure 4.8.5) showed three doublets and one singlet. (δP=10.46 ppm (d),

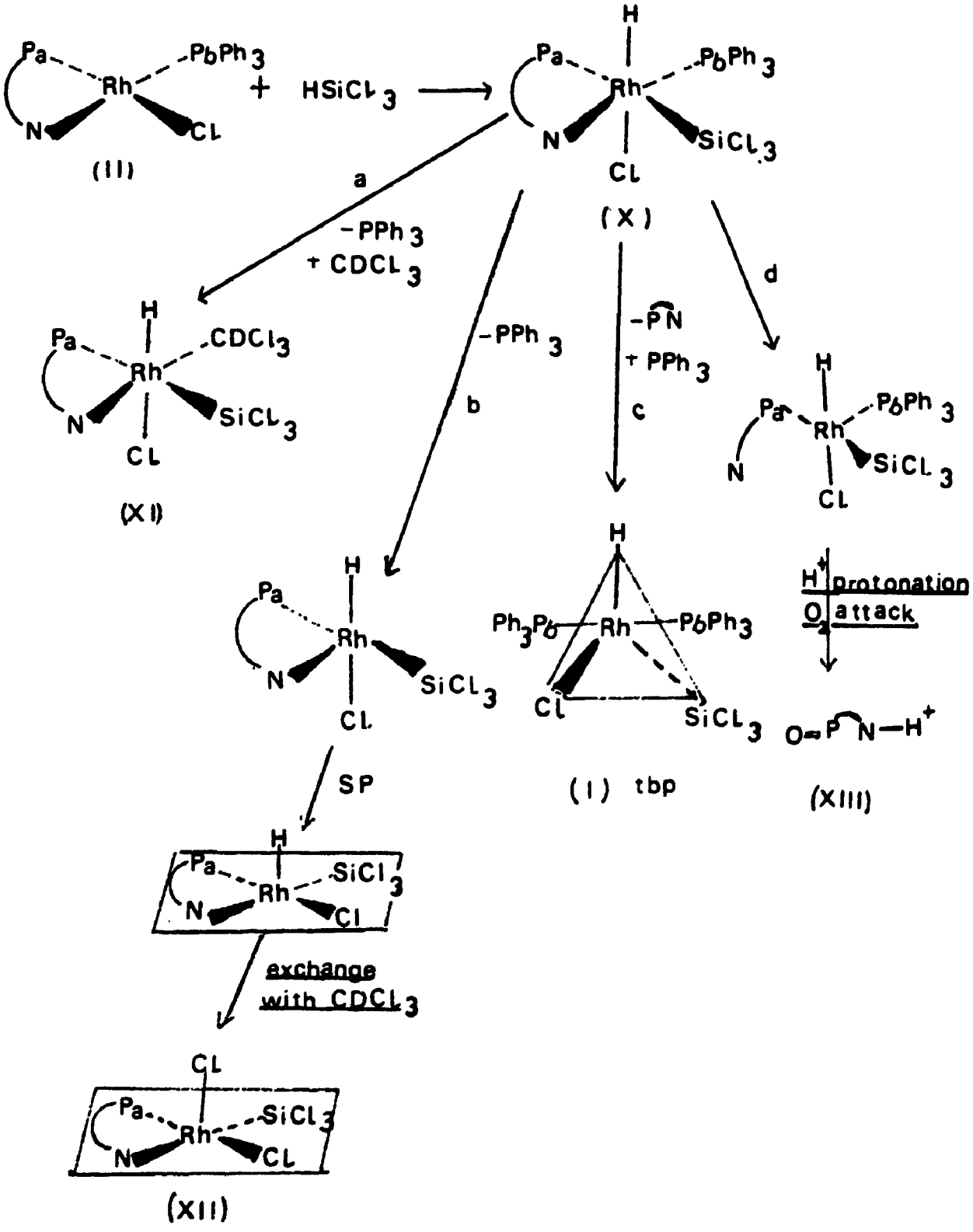

Figure 4.8.4 The reaction mechanism of oxidative addition of $HSiCl_3$ to the complex Rh(I)Cl (S-amphos)(PPh_3).

$^1J_{Rh-P}$=85 Hz; δP=29.52ppm (d), $^1J_{Rh-P}$=85 Hz; δP=35.20ppm (d), $^1J_{Rh-P}$=110 Hz; δP=-18.76 ppm (S); hydride; δH=-15.31 ppm, δH=-12.66 ppm, δH=-12.22 ppm respectively). The signal at 10.46 ppm may be assigned as Rh(III)HCℓ(*S*-amphos)-($SiCℓ_3$)(CH_3CN), XIV, the signal at 29.50 ppm as Rh(III)HCℓ-(*S*-amphos)($SiCℓ_3$), XV, the signal at 35.20 ppm as complex I and the signal at -18.76 ppm as free PPh_3. The ratio of the intensities between complex XIV and complex XV was two to one. Therefore complex XIV, in which the solvent has coordinated to the Rh to form a six coordinate species, was predominant in CH_3CN solution. We assume that the incoming prochiral ketone would occupy the solvent position (i.e. the PPh_3 position). In Chapter 2 (Figure 2.4.1), it can be seen that the chirality at the carbon atom of the amphos ligand is separated by three bonds through nitrogen from the centre of the substrate which becomes the new asymmetric centre (originally the PPh_3 site), i.e. by ca. 6 Å. However, the distance is still so large that the question must be asked as to how the prochiral centre in the coordinated substrate "feels" the chiral influence upon being converted to the chiral centre. Certainly, the chiral information in the catalyst complex could also be transmitted by the surrounding solvent cage. It appears, however, that the real transmitters are the phenyl rings at the P atom, according to a proposal by Knowles et al [89], and this has since been supported by numerous X-ray structure analyses. These equatorial/axial positions of

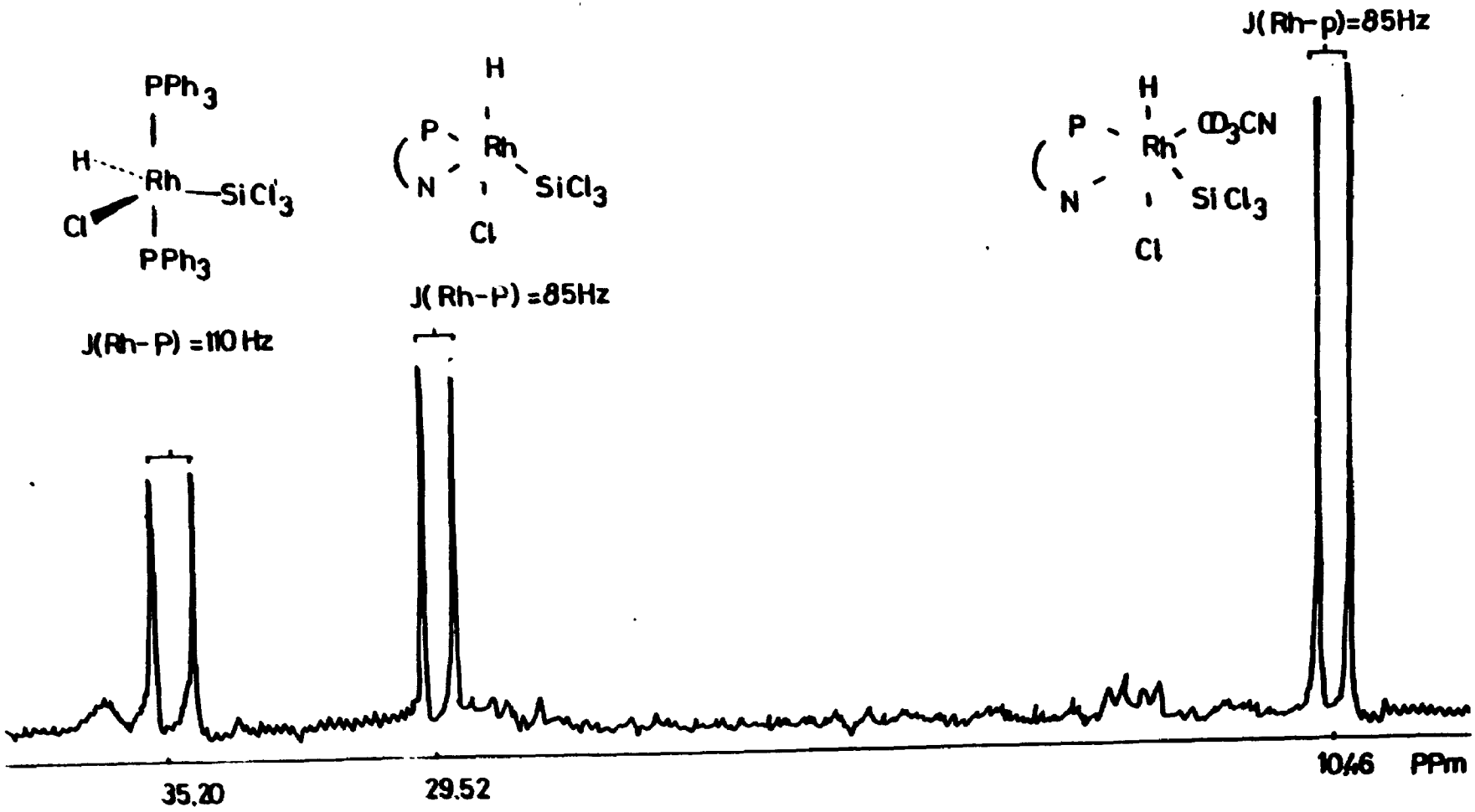

FIGURE 4.8.5 ^{31}P NMR Spectrum of [Rh(I)Cl(S-amphos)(PPh_3)] with $HSiCl_3$ in CD_3CN solvent at 293 K.

the phenyl rings in the $P(C_6H_5)_2$- groups of the amphos arise because the chelate ring is puckered. Positioning the two phenyl rings at the P atom (axial/equatorial and face/edge exposed) causes chirality, which is determined by the puckering of the chelate ring and thus by the configuration of the asymmetric centres in the chelate skeleton. The chiral information is transmitted from the asymmetric centre in the chelate frame work through the $P(C_6H_5)_2$- groups of the amphos to the catalytically active coordination sites at the metal atom. A substrate molecule at the empty site (originally the PPh_3 site) of the Rh-square encounters hardly any steric hindrance from the "equatorial" phenyl ring; however, strong steric interactions, especially with the orthohydrogen atom of the "axial" phenyl ring, are to be expected.

Although the chirality transfer through the two phenyl "ears" of the P atom is extraordinarily effective in numerous catalyses, it is not the optimal solution for asymmetric catalysis. The chelating phosphine in amphos has a different centre of chirality than the vast majority of optically active ligands used to date, e.g. the tartaric acid chirality in diop and the proline chirality in BPPM, etc. Moreover, the rigidity of the chelate ring minimizes the axial/equatorial distinction. However, the transfer mechanism for all three specific chiralities is the probably same. The $P(C_6H_5)_2$transmitter can only react to the specific chiral information by positioning its phenyl

rings more or less axial/equatorial and face/edge exposed. The prochiral substrate thus does not "see" the original chirality of the C atom of the amphos, but rather the phenyl "ears" of the transmitter only. Consequently, this mechanism for transfer of chirality leads to a loss of information. One might therefore expect better results in asymmetric catalysis if the inducing centre of chirality in the catalyst were located where the $P(C_6H_5)$- transmitter is situated [11]. A loss of information due to transfer would then be avoided, and the inducing chirality would interact directly with the substrate in the neighboring coordination site. We preferred that the incoming prochiral ketone was cis to the nitrogen rather than trans to the nitrogen. In this way, the distance between the chiral centre carbon atom of the amphos and the centre of the substrate for the incoming would be the shortest. The diamphos ligand we made was designed to achieve this purpose.

The Rh complexes containing various phosphines are very active catalysts from which it is difficult to isolate the reaction intermediates. Most researchers used the Iridium analogue to study the reaction intermediates [90-93], but it was not the real catalytic system, and so the five coordination process was not observed.

4.9 Conclusions.

In the present study, much of the catalytic cycle is

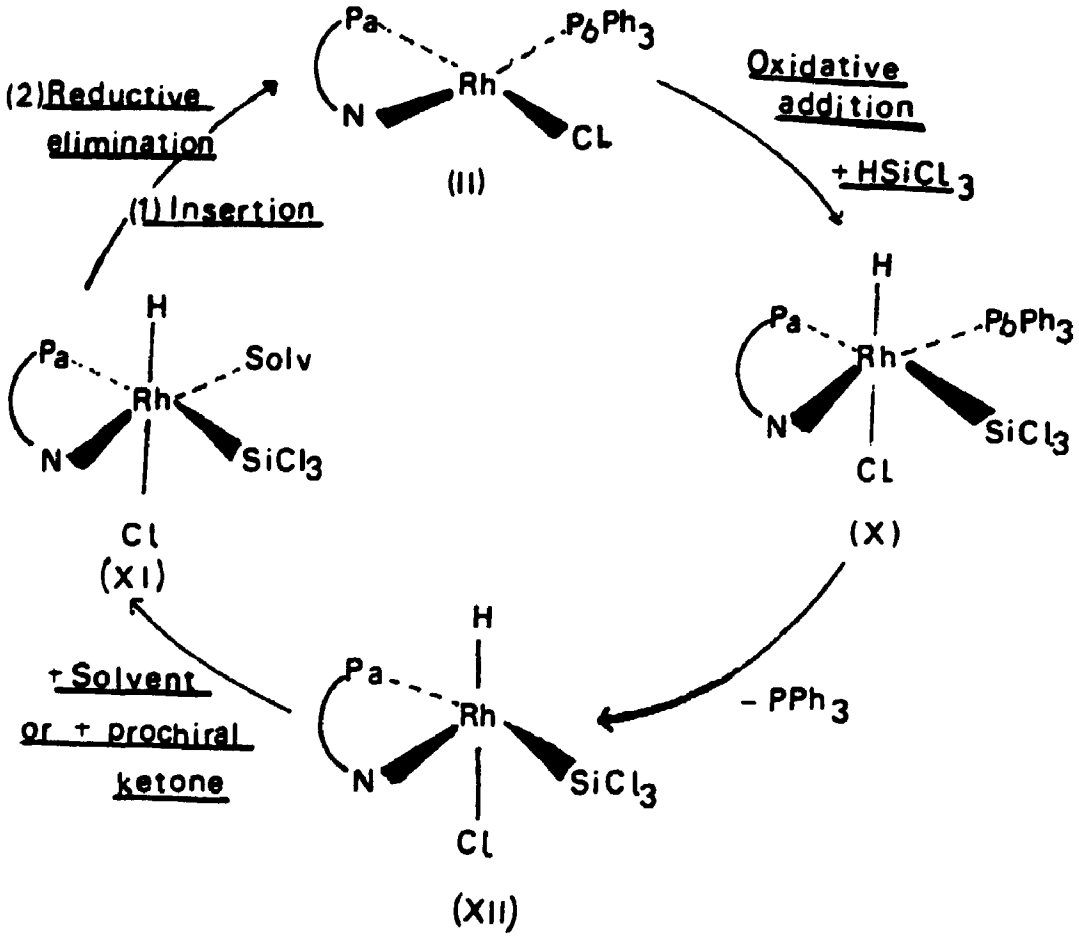

Figure 4.9.1 Mechanism of prochiral ketone hydrosilylation.

very clear from ^{31}P & ^{1}H NMR and the visible spectroscopy.

The catalytic cycle involves initial oxidative addition of $HSiCl_3$ silane to a neutral Rh(I)Cl(*S*-amphos)(PPh_3) complex, II, with cleavage of the Si-H bond, forming a six-coordination complex Rh(III)HCl(*S*-amphos)(PPh_3)($SiCl_3$), X. Then breakage of the Rh-PPh_3 bond to form a five-coordination complex Rh(III)HCl(*S*-amphos)($SiCl_3$), XII, is followed by prochiral ketone or solvent insertion to

form a six-coordination complex Rh(III)HCl(*S*-amphos)($SiCl_3$)-(Solv.), XI. Since the five-coordinate complexes are coordinatively unsaturated, they may complex with an additional ligand, giving an overall three-fragment oxidative addition. Such a process is exemplified by the reaction of Rh(I)Cl(PPh_3)$_3$ with molecular hydrogen in pyridine solution to give the Rh(III)HClH(PPh_3)$_2$Py complex and free PPh_3 ligand [42]. Reactions such as these are important in catalytic cycles, since they enable insertion reactions to take place with a second reactant at the Rh centre. The final steps involve insertion and reductive elimination reactions.

In our attempts to elucidate the mechanism, we used $HSiCl_3$ and $(CH_3)HSiCl_2$ as reactants which are more polar than R_3SiH silanes, because our emphasis was on the isolation and characterization of products of the oxidative addition step. We were not able to observe the proposed insertion and reductive elimination steps, but these may be inferred from the products formed.

CHAPTER 5

The Crystal and Molecular Structure of Hydridochloro(trichlorosilyl)bis(triphenylphosphine)rhodium(III), [Rh(III)HCl(SiCl$_3$)(PPh$_3$)$_2$]

5.1 Introduction

Yellow crystals of a trichlorosilyl complex, Rh(III)H-Cl(SiCl$_3$)(PPh$_3$)$_2$, were made by accident in an attempt to isolate the [Rh(III)HCl(*S*-amphos)(SiCl$_3$)] complex, the proposed intermediate in the reaction of [Rh(I)Cl(*S*-amphos)-(PPh$_3$)] with HSiCl$_3$. Unfortunately, the desired product still remained in solution, while the by-product [Rh(III)H-Cl(SiCl$_3$)(PPh$_3$)$_2$] was crystallized with great difficulty from HSiCl$_3$ solution diluted by hexane and a small amount of CH_2Cl_2.

In 1970, Ibers determined the crystal structure of solvated hydridochloro(trichlorosilyl)bis(triphenyl-phosphine)rhodium(III), Rh(III)HCl(SiCl$_3$)(PPh$_3$)$_2$.xSiHCl$_3$. Since then no other hydridosilylrhodium(III) complex has been isolated and examined by X-ray diffraction. The complex reported by Ibers crystallized in the space group P-1, C_i^1 of the triclinic system with unit cell dimensions a=11.727(5), b=12.952(6), and c=13.365(5) Å, α=104.65(2), β=98.08(2), and γ=94.43(2)°. It was very similar to our complex [Rh(III)HCl(PPh$_3$)$_2$(SiCl$_3$)] in unit cell dimensions (see Table 5.2.1).

5.2 Experimental

1. Photographic analysis

The sample appeared to be air-sensitive, therefore the crystal was mounted in a well-dried 0.3 mm glass capillary with solvent (10% $HSiCl_3$/hexane) under dry nitrogen. A photographic examination using Weissenberg and precession techniques showed the crystals to be triclinic, Laue symmetry -1. Initially, we assigned the space group P1 in the absence of an elemental analysis, on the assumption that *S*-amphos was present. Finally, we found no chiral centre in the complex and the fractional coordinates of all atoms of two molecules in a unit cell were related by a centre of symmetry. So the assignment of the centric space group is P-1, C_i^1, No 2 [64]. The cell volume is 1930.3(3) $Å^3$. The crystal density was determined by flotation in a mixture of methylene chloride and hexanes. The value found was 1.40(3) g cm^{-3}. These data indicate Z=2, for which the calculated density is 1.373 g cm^{-3}. After photography, we found that the crystal was stable in a capillary without added solvent.

Although the reaction was repeated ten times, only two or three crystals were formed on each occasion. We were therefore unable to obtain an elemental analysis on the crystals.

2. Data collection

ω-Scans of three different crystals all gave broad peak widths so that the choice of crystal was made on the basis

of good shape. The crystal selected for data collection was mounted in a well-dried 0.3 mm glass capillary under dry nitrogen without solvent, and was of approximate dimensions 0.26×0.30×0.60 mm^3, with eight faces which were revealed by optical goniometry to be {10-1}, {001}, {010}, (100) and (110). The crystal dimensions were carefully measured with a filar microscope to permit an absorption correction. A perspective view of the crystal, produced by the program Ortep, is presented in Figure 5.2.1.

Intensity data were recorded on an Enraf-Nonius CAD4F diffractometer using an incident beam graphite monochromator. Cell parameters and an orientation matrix were obtained from a least-squares refinement using the setting angles of 24 reflections with $16° < 2\theta < 26°$. ω-scans of several intense, low angle reflections (-32-4), (300), (002) and (020), with a wide open counter, had peak widths at base of 0.39°, 0.30°, 0.58° and 0.38° respectively, and at half height of 0.39°, 0.18°, 0.41° and 0.24° respectively, indicating that the mosaicity of the specimen was relatively high. 9556 reflections ($-16 \leq h \leq 16$, $-17 \leq k \leq 17$, $-15 \leq l \leq 0$) were collected using omega scan, up to a maxmium 2θ of 55°. Dispersion corrected scans of width 1.60° and variable scan rates within a maximium time per datum of 75 sec. were used. Standard reflections (-32-4), (300), (002) and (020) were recorded every 10,600 seconds of X-ray exposure time and showed an average decay of 0.5%; thus a decay correction was not

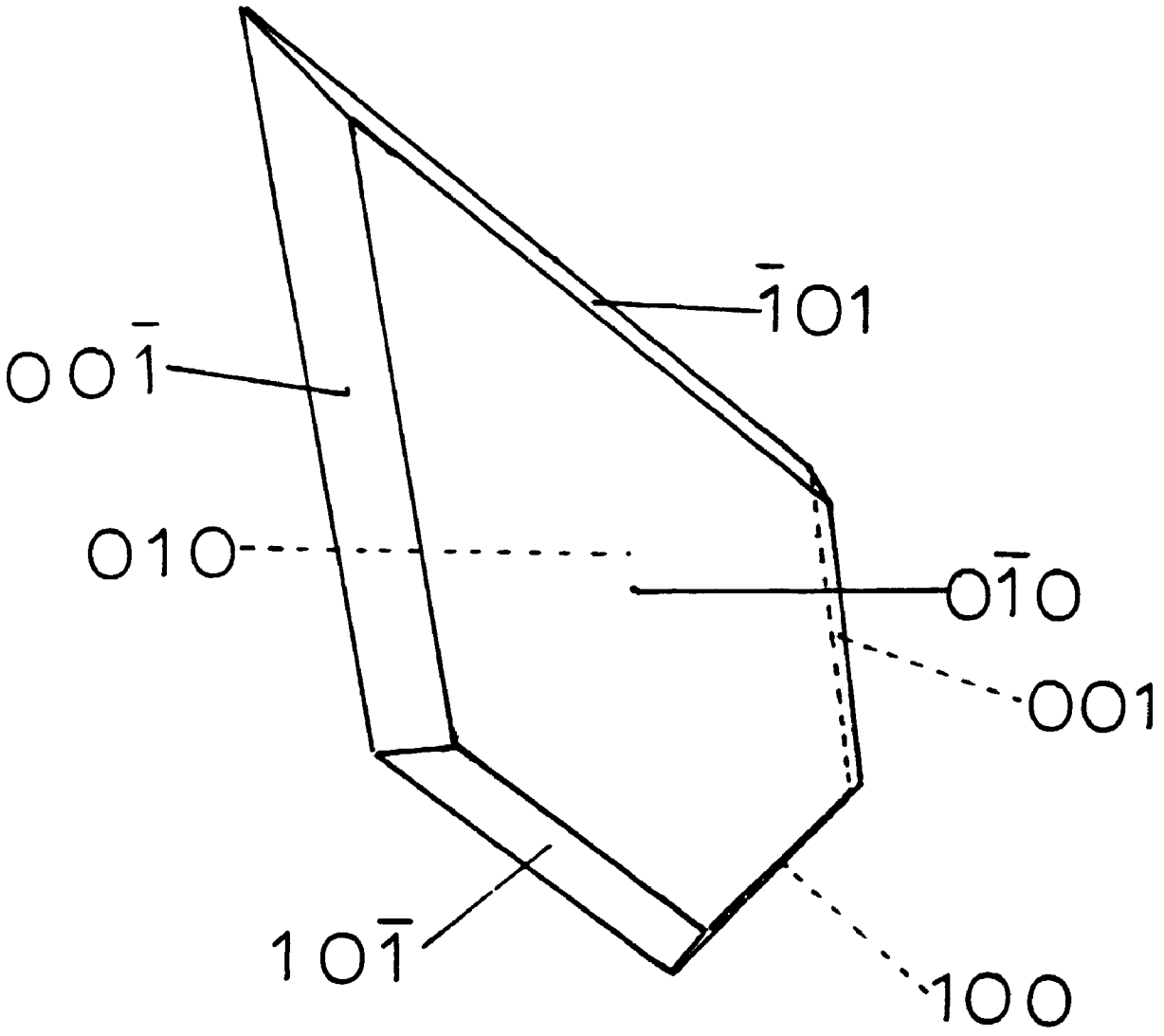

Figure 5.2.1 A drawing of the data crystal. Dotted edges are hidden from view.

required. An orientation check, using three reflections, (-160),(-5-30) and (20-5), was done at 200 reflection intervals throughout data collection. Recentering and recalculation of the orientation matrix were made about 20 times during data collection. Crystal data and experimental conditions are summarized in Table 5.2.1.

5.3 Data Reduction, Structure Solution and Refinement.

Background, monochromator polarization, Lorentz, and polarization corrections were applied and standard deviations were assigned based on counting statistics [63]. A Gaussian absorption correction was applied [63]. 9269 data were averaged using the Paint program [63], which found 25 pairs of data with serious errors among the 619 averaged data with indices $\pm$h, $\pm$k, 0. This was due to a mechanical problem with the Enraf-Nonius CADF diffractometer.

The structure was solved using Patterson and difference Fourier methods in the acentric space group P1 using the SDP software package [63] running on a DEC-PDP 11/23+ computer [63]. Then we found that the complex did not contain *S*-amphos, and that the two molecules in the unit cell were related by a centre of symmetry. The new position of the Rh atom was obtained by averaging the fractional coordinations of two original Rh atoms. The remaining 43 non-hydrogen atoms were moved to new fractional coordinates in the same way.

Table 5.2.1 Summary of Crystal Data and Experimental Conditions

compound; mol. wt.	$C_{36}H_{31}Cl_4P_2SiRh$; 798.0
unit cell dimens.	a=12.961(3) Å; b=13.354(2)Å; c=11.731(2) Å; α=98.00(1)°; β=94.93(2)°; γ=104.47(2)°.
cell volume; Z	1930.0(3) Å^3; 2
density obsd.; calcd.	1.40(3) g cm^{-3}; 1.373 g cm^{-3}
abs. coefficient	μ 7.308 cm^{-1}
radiation	Mo Kα, λ=0.71069 Å
temperature	18°C
crystal-counter distance	205 mm
receiving aperture horiz.	6.00+0.35*tanθ
vert.	4.0 mm
scan range (deg)	1.60+0.35*tanθ
background	at 25% scan extensions
scan type	omega scan
data collected	$-16 \leq h \leq 16$, $-17 \leq k \leq 17$, $-15 \leq l \leq 0$ for $0° < 2\theta < 55°$
standard reflections	(-32-4), (300), (002), (020)
crystal faces	{10-1}, {001}, {010}, (100), (110)
absorption grid	16x10x12
transmission factors	max. 0.805 min. 0.729
# data collected; $I_o > 3\sigma(I_o)$	9556; 6680
# standard reflections	287

The Rh, P, Cl and Si atoms were refined with anisotropic thermal ellipsoids, and the C atoms were refined as isotropic spheres. The model converged at agreement factors R_1=0.075 and R_2=0.104, where R_1 and R_2 have the same definitions as in Chapter 3 (equation 1-3). 30 H atoms of the total 31 H atoms were located in a difference Fourier synthesis with peak heights between 0.5(1) and 0.6(2) $e\text{Å}^{-3}$, and were included in the calculation of F_C, in idealized positions with isotropic temperature factors. After several cycles of refinement, with the hydrogen atom positions regularly updated, we attempted to locate the hydridic hydrogen atom. It was not found, because the map contained residual peaks near the Rh atom. The presence of the hydride atom was based on the ^1H nmr spectrum in Chapter 4 (double triplet at -14.37 ppm) and a vacant position between the Si atom and the Cl(1) atom in the equator of the trigonal bipyramidal configuration. We could not get a position for the hydride ligand, and it was therefore not included in the refinement or structure factor calculations.

An inspection of the aromatic C-C bond lengths, which varied from 1.28 to 1.60 Å, showed the model to be unsatisfactory. Therefore rigid group constraints were imposed on the six phenyl rings, namely D_{6h} symmetry (C-C 1.392 Å, C-H 0.95 Å), and the refinement was completed using the SHELX-76 software [117]. The misaveraged data were edited out before the final five cycles of

refinement. However, we have no guarantee that the remaining majority of the data are free of systematic error. In the final cycles, 6586 unique reflections with $F_O \geq 5\sigma(F_O)$ were used to refine 146 variables. Convergence was achieved at residuals of R_1=0.069, R_2=0.082, R_G=0.122 and R_W=0.122, where R_1, R_2, R_G and R_W have the same definitions as in Chapter 3 (equation 1-6). In the final cycle, the k value reached 1.00 under a weighting scheme with a |g| value of 0.0115 [$w=K/(\sigma^2(F_O) + |g| \times (F_O)^2)$]. No shifts greater than 10^{-4} Å were observed for the atomic positional parameters and all shifts were less than $10^{-2}\sigma$.

A total difference Fourier synthesis showed that the highest peak, at fractional coordinates (0.131, 0.283, 0.185) with an electron density of 1.70(1) $eÅ^{-3}$ is situated 0.15 Å from the Rh atom. It was considered of no chemical significance. Another attempt was then made to find the hydride ligand. Three contoured maps which are the centre section of the Si, Rh and Cl(1) defined plane, and two sections of 0.25 Å up and down from the centre section respectively, are presented in Figures 5.3.1 (a), (b) and (c). One residue peak which is 2.1 Å away from the Rh atom in the map of the centre section can not be assigned as the hydride atom, because the distance of Rh-H is longer than the sum of the covalent radius between the Rh atom and the H atom (1.60 Å). Therefore we cannot find the hydride atom from the difference Fourier synthesis.

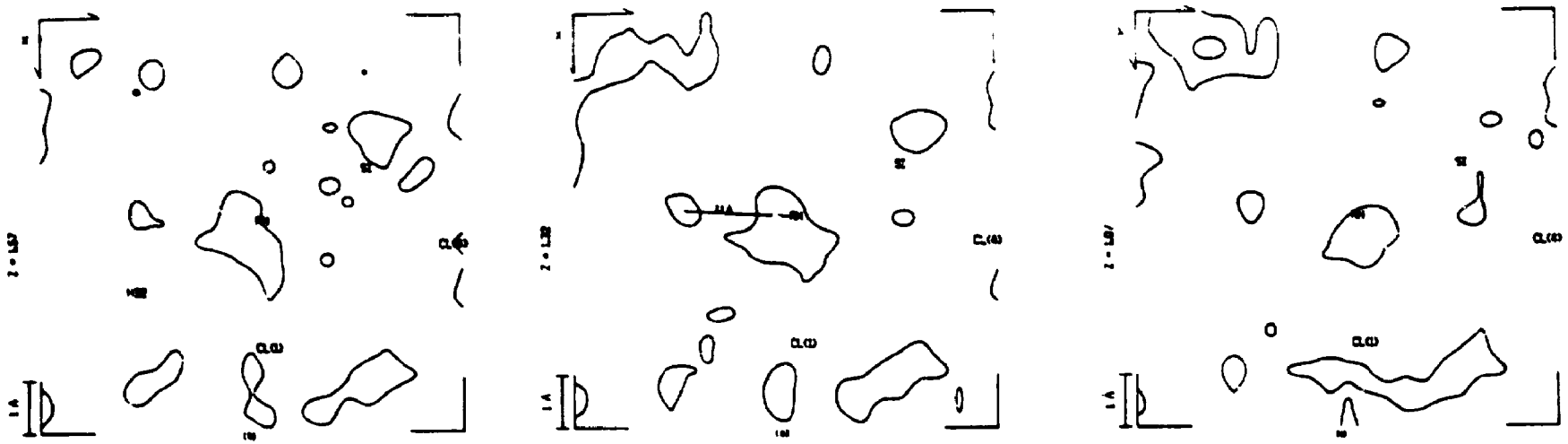

Figure 5.3.1 Three contoured maps of the Si, Rh and Cℓ(1) defined plane (a) the centre section (b) 0.25 Å up from the centre section (c) 0.25 Å down from the centre section.

Statistical analyses of R_1 and R_2 in terms of data collection order, F_o, $\lambda^{-1}\sin\theta$ and classes of indices showed no unusual trends, other than the poorer than usual overall quality of the analysis.

Final positional and U(equivalent) thermal parameters for the non-hydrogen atoms are given in Table 5.3.1. Anisotropic thermal parameters, H atom parameters, root-mean-square amplitudes of thermal vibration, selected torsional angles, and least-squares plane calculations are given in Tables 5.3.2, 5.3.3, 5.3.4, 5.3.5 and 5.3.6.

5.4 Structure Description

The lack of significant residual electron density in the final difference Fourier synthesis confirms that the model chosen is appropriate. Although there were mechanical problems with the diffractometer, it is encouraging to note that 30 of the 31 hydrogen atoms could be located; we therefore can place some confidence in the results obtained. A stereoview of the $Rh(III)Cl(SiCl_3)(PPh_3)_2$ complex showing the atom numbering scheme is given in Figure 5.4.1. A perspective view of the coordination polyhedron around the rhodium atom is given in Figure 5.4.2. Atoms are drawn as 50% probability thermal ellipsoids. Selected intramolecular distances and angles are given in Tables 5.4.1 and 5.4.2.

The crystals are built up from discrete molecules, for which the shortest intermolecular distances are 3.17 Å,

Table 5.3.1 Atomic Positional ($\times 10^4$) and Thermal ($\times 10^3$), for Rh, Cl(1), P(1), P(2) and Si ($\times 10^5$, xyz) and Rh, Cl(1), Cl(2), Cl(3), Cl(4), P(1) and P(2) ($\times 10^4$,U) Parameters

Atom	X	Y	Z	U or U_{eq}($Å^2$)
Rh	12973(3)	27918(3)	19668(4)	324(1)
Cl(1)	10378(14)	45089(12)	24056(15)	475(5)
Cl(2)	3555(2)	1978(2)	3268(2)	789(9)
Cl(3)	1284(3)	868(3)	3939(3)	1269(9)
Cl(4)	2332(2)	3304(3)	4870(2)	918(8)
P(1)	28509(11)	35864(12)	12025(13)	341(4)
P(2)	-4923(12)	19814(12)	21193(13)	368(4)
Si	20573(17)	21981(17)	33957(17)	515(6)
C(11)	3790(4)	2811(3)	802(4)	43(1)
C(12)	4897(4)	3229(3)	1048(4)	55(2)
C(13)	5585(4)	2632(3)	685(4)	70(2)
C(14)	5166(4)	1617(3)	75(4)	86(3)
C(15)	4059(4)	1199(3)	-172(4)	76(2)
C(16)	3371(4)	1796(3)	191(4)	58(2)
C(21)	3690(4)	4826(4)	2029(3)	39(1)
C(22)	3875(4)	5754(4)	1573(3)	55(2)
C(23)	4484(4)	6690(4)	2250(3)	70(2)
C(24)	4908(4)	6698(4)	3383(3)	63(2)
C(25)	4723(4)	5770(4)	3840(3)	73(2)
C(26)	4114(4)	4833(4)	3163(3)	65(2)
C(31)	2414(3)	3902(4)	-210(3)	36(1)
C(32)	1364(3)	3959(4)	-471(3)	47(1)
C(33)	1048(3)	4234(4)	-1522(3)	52(2)
C(34)	1782(3)	4452(4)	-2312(3)	53(2)
C(35)	2832(3)	4396(4)	-2051(3)	55(2)
C(36)	3148(3)	4121(4)	-1000(3)	50(2)
C(41)	-1184(4)	2043(3)	717(4)	42(1)
C(42)	-1194(4)	3026(3)	450(4)	52(2)
C(43)	-1652(4)	3110(3)	-637(4)	66(2)
C(44)	-2102(4)	2212(3)	-1459(4)	80(3)

Table 5.3.1 continued

Atom	X	Y	Z	U or U_{eq}(Å^2)
C(45)	-2092(4)	1229(3)	-1193(4)	75(2)
C(46)	-1633(4)	1145(3)	-105(4)	60(2)
C(51)	-1182(4)	2634(4)	3154(4)	47(1)
C(52)	-2267(4)	2581(4)	2917(4)	68(2)
C(53)	-2780(4)	3061(4)	3741(4)	81(3)
C(54)	-2207(4)	3593(4)	4803(4)	86(3)
C(55)	-1122(4)	3646(4)	5040(4)	95(3)
C(56)	-609(4)	3167(4)	4215(4)	72(2)
C(61)	-889(4)	597(4)	2230(4)	43(1)
C(62)	-1658(4)	212(4)	2932(4)	59(2)
C(63)	-1924(4)	-847(4)	3027(4)	72(2)
C(64)	-1421(4)	-1522(4)	2422(4)	69(2)
C(65)	-651(4)	-1138(4)	1720(4)	66(2)
C(66)	-386(4)	-78(4)	1624(4)	52(2)

Anisotropically refined atoms are given in the form of the isotropic equivalent thermal parameter, defined as:
$(1/6\pi^2)[a^2*B(1,1)+b^2*B(2,2)+c^2*B(3,3)+ab(\cos\gamma)*B(1,2)+ac(\cos\beta)*B(1,3)+bc(\cos\alpha)*B(2,3)]$

Table 5.3.2 Anisotropic Thermal Parameters ($\times 10^3$)

Rh	31.2(3)	29.8(3)	34.5(3)	7.2(2)	1.5(2)	2.9(2)
Cl(1)	48.6(9)	36.8(8)	55.6(9)	15.6(7)	3.1(7)	-3.0(6)
Cl(2)	81(2)	102(2)	73(1)	51(1)	-1(1)	30(1)
Cl(3)	117(2)	122(2)	106(2)	-44(2)	-52(2)	79(2)
Cl(4)	79(2)	135(2)	48(1)	34(2)	-18(1)	-23(1)
P(1)	27.1(7)	33.1(7)	40.7(8)	7.0(6)	-0.8(6)	7.0(6)
P(2)	34.2(8)	33.6(7)	38.9(8)	5.1(6)	6.9(6)	-0.9(6)
Si	52(1)	55(1)	42(1)	4.4(9)	-8.0(8)	13.6(8)

The form of the anisotropic thermal parameter is : $\exp[-2\pi^2(h2a2U(1,1) + k2b2U(2,2) + l2c2U(3,3) + 2hkabU(1,2) + 2hlacU(1,3) + 2klbcU(2,3))]$ where a, b, c are reciprocal lattice contants.

Table 5.3.3 Hydrogen Atomic Positional x(10^4) and Thermal ($x10^3$) Parameters

Atom	X	Y	Z	U(Å²)
H12	5183	3922	1465	60
H13	6341	2917	853	60
H14	5635	1209	-174	60
H15	3773	506	-589	60
H16	2615	1511	23	60
H22	3586	5749	799	60
H23	4610	7324	1938	60
H24	5323	7337	3845	60
H25	5012	5775	4613	60
H26	3988	4200	3474	60
H32	863	3809	68	60
H33	331	4272	-1701	60
H34	1567	4640	-3030	60
H35	3333	4546	-2590	60
H36	3865	4083	-822	60
H42	-887	3639	1011	60
H43	-1659	3780	-819	60
H44	-2415	2269	-2201	60
H45	-2399	616	-1753	60
H46	-1627	475	77	60
H52	-2657	2218	2192	60
H53	-3520	3025	3580	60
H54	-2557	3921	5366	60
H55	-732	4010	5765	60
H56	131	3203	4377	60
H62	-2002	673	3345	60
H63	-2449	-1110	3506	60
H64	-1602	-2245	2487	60
H65	-308	-1599	1307	60
H66	140	184	1146	60

H is bonded to Rh, H11 is bonded to C(11) etc.

Table 5.3.4 Root-Mean-Square Amplitudes of Thermal Vibration (Å)

Atom	Min.	Int'med.	Max.
Rh	0.169	0.178	0.192
Cl(1)	0.177	0.218	0.253
Cl(2)	0.194	0.295	0.339
Cl(3)	0.199	0.245	0.530
Cl(4)	0.185	0.289	0.398
P(1)	0.161	0.181	0.208
P(2)	0.172	0.182	0.218
Si	0.181	0.219	0.272

Table 5.3.5 Selected of Torsion Angles in Degrees

Atom 1	Atom 2	Atom 3	Atom 4	Angle
Cl(1)	Rh	Si	Cl(2)	-113.19(14)
Cl(1)	Rh	Si	Cl(3)	120.28(16)
Cl(1)	Rh	Si	Cl(4)	2.06(15)
P(1)	Rh	Si	Cl(2)	-22.47(14)
P(1)	Rh	Si	Cl(3)	-149.00(16)
P(1)	Rh	Si	Cl(4)	92.78(13)
P(2)	Rh	Si	Cl(2)	149.87(13)
P(2)	Rh	Si	Cl(3)	23.34(17)
P(2)	Rh	Si	Cl(4)	-94.88(13)

Table 5.3.6 Result of Least-Squares Plane Calculations

Orthonormal Equation of Plane

0.8574 X +	0.4447 Y +	-0.2590 Z -	1.3202 = 0
0.0004	0.0007	0.0012	0.0043

Crystallographic Equation of Plane

11.1156 X +	2.8844 Y +	-4.7137 Z -	1.3202 = 0
0.0053	0.0682	0.0559	0.0043

Atom	X	Y	Z	Distance	Esd
Rh	0.5516	3.2254	2.2666	0.0000	+- 0.0004
Cl(1)	-0.4020	5.3585	2.7723	0.0000	+- 0.0018
Si	1.5903	2.1815	3.9133	0.0000	+- 0.0022
	..... Other Atoms				
P(1)	2.3779	4.4000	1.3858	2.3164	+- 0.0015
P(2)	-1.5135	2.1489	2.4424	-2.2949	+- 0.0016
Cl(2)	3.6185	1.9222	3.7661	1.6618	+- 0.0028
Cl(3)	0.9771	0.3575	4.5391	-1.4990	+- 0.0037
Cl(4)	1.4287	3.3246	5.6118	-0.0701	+- 0.0030

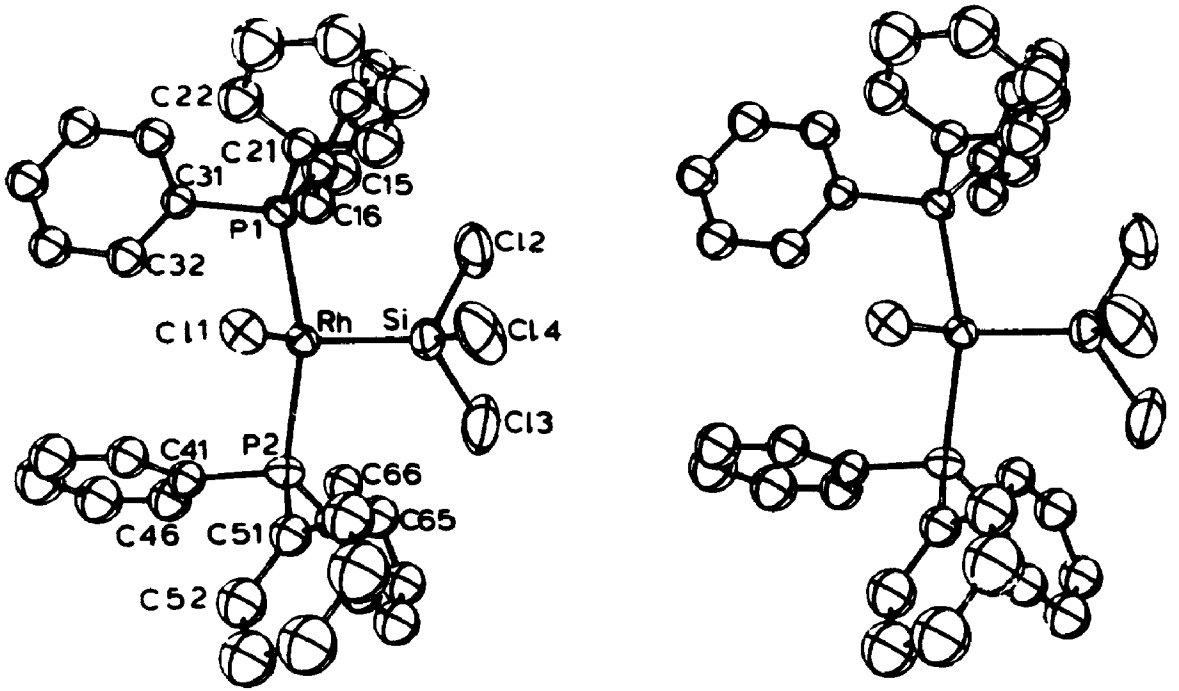

Figure 5.4.1 One stereoview of the [Rh(III)HCl(SiCl$_3$)(PPh$_3$)$_2$] complex showing the atom numbering scheme. Atoms are drawn as 50% probability thermal ellipsoids.

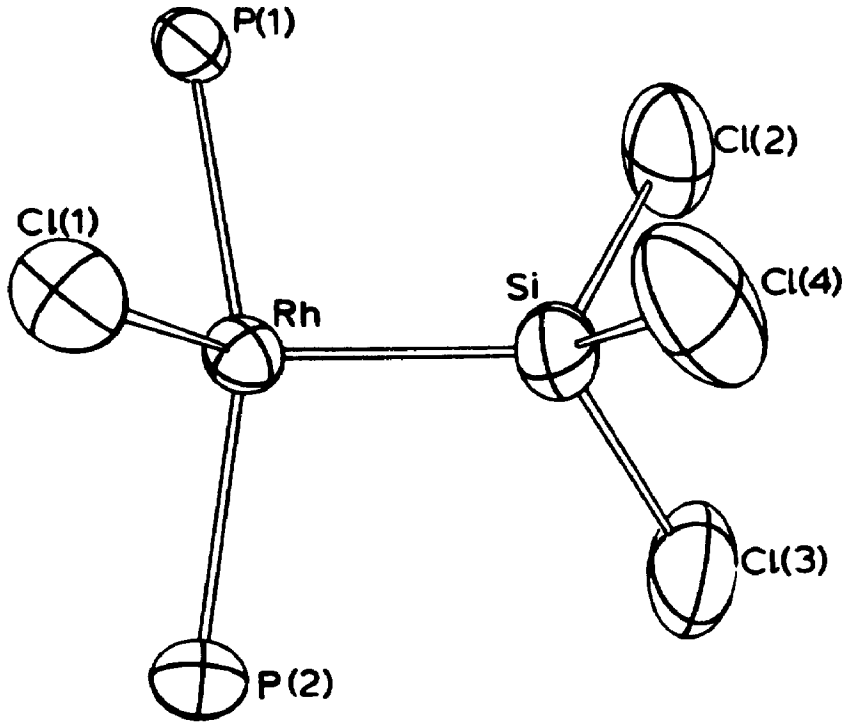

Figure 5.4.2 A perspective view of the coordination polyhedron around the rhodium atom.

Table 5.4.1 Selected Bond Distances in Angstroms

Atom 1	Atom 2	Distance	Atom 1	Atom 2	Distance
Rh	Cl(1)	2.391(2)	Rh	P(1)	2.343(2)
Rh	P(2)	2.335(2)	Rh	Si	2.209(2)
Cl(2)	Si	2.050(4)	Cl(3)	Si	2.024(4)
Cl(4)	Si	2.054(3)	P(1)	C(11)	1.835(5)
P(1)	C(21)	1.825(4)	P(1)	C(31)	1.842(5)
P(2)	C(41)	1.827(5)	P(2)	C(51)	1.820(6)
P(2)	C(61)	1.816(5)			

all phenyl C-C distances were constrained to 1.392 Å

Numbers in parentheses are estimated standard deviations in the least significant digits.

Table 5.4.2 Selected Bond Angles in Degrees

Atom 1	Atom 2	Atom 3	Angle	Atom 1	Atom 2	Atom 3	Angle
Cl(1)	Rh	P(1)	86.74(6)	Cl(1)	Rh	P(2)	92.44(6)
Cl(1)	Rh	Si	116.85(7)	P(1)	Rh	P(2)	16 1.53(6)
P(1)	Rh	Si	98.67(7)	P(2)	Rh	Si	98.16(7)
Rh	P(1)	C(11)	119.1(2)	Rh	P(1)	C(21)	116.9(2)
Rh	P(1)	C(31)	107.1(1)	C(11)	P(1)	C(21)	105.1(2)
C(11)	P(1)	C(31)	101.6(2)	C(21)	P(1)	C(31)	105.2(2)
Rh	P(2)	C(41)	102.8(2)	Rh	P(2)	C(51)	118.6(2)
Rh	P(2)	C(61)	119.7(2)	C(41)	P(2)	C(51)	103.2(2)
C(41)	P(2)	C(61)	103.8(2)	C(51)	P(2)	C(61)	106.4(3)
Rh	Si	Cl(2)	118.1(1)	Rh	Si	Cl(3)	120.9(1)
Rh	Si	Cl(4)	108.4(1)	Cl(2)	Si	Cl(3)	102.1(2)
Cl(2)	Si	Cl(4)	102.0(1)	Cl(3)	Si	Cl(4)	102.8(2)
P(1)	C(11)	C(12)	121.7(3)	P(1)	C(11)	C(16)	118.3(3)
P(1)	C(21)	C(22)	121.8(3)	P(1)	C(21)	C(26)	118.1(3)
P(1)	C(31)	C(32)	120.3(3)	P(1)	C(31)	C(36)	119.7(3)
P(2)	C(41)	C(42)	118.3(3)	P(2)	C(41)	C(46)	121.7(3)
P(2)	C(51)	C(52)	121.5(3)	P(2)	C(51)	C(56)	118.6(4)
P(2)	C(61)	C(62)	121.2(4)	P(2)	C(61)	C(66)	118.8(4)

numbers in parentheses are estimated standard deviations in the least significant digits.

H13....H53 at (X+1, Y, Z); 3.25Å, H22....H36 at (-X-1, -Y-1, -Z). The shortest metal-metal distance is 7.96 Å, Rh....Rh at (-X,-Y,-Z); 11.73 Å, Rh....Rh at (X,Y,Z-1).

The coordination pattern about the rhodium atom is a highly distorted trigonal bipyramid, with apical triphenylphosphines, and H, Cl and $SiCl_3$ in the trigonal plane. If this description is adopted, then the idealized values of the P-Rh-P and P-Rh-Si angles would be respectively 180° and 90°. The departures from these idealized values can then be ascribed to steric repulsion between the bulky triphenylphosphine and silyl ligands. These repulsions caused spreading of the Si-Rh-P(1) and Si-Rh-P(2) to 98.7(1)° and 98.1(1)° respectively, with a corresponding closure of the P(1)-Rh-P(2) angle to 161.5(1)°. As a result, the intramolecular Cl(1)....P(1) and Cl(1)....P(2) contracts are 3.25 Å and 3.41 Å respectively, shorter than the sum of the corresponding van der Waals radii, 3.65 Å. The interactions between Cl(1) atom and two P atoms may probably lead to the closure of the P(1)-Rh-P(2) angle.

The mean Si-Cl distance of 2.042(3) Å is the same as the mean Si-Cl distance of 2.054(5) Å in complex (A) [65], λ=2.06, and the same as the value of 2.035(3) Å found in $Co(SiCl_3)(CO)_4$, (B) [124], λ=1.65, as well as lying within the range of 2.01-2.05 Å found in free chlorosilanes [125]. The coordination around the Si atom is distorted tetrahedral, the Cl(2)-Si-Cl(3), Cl(3)-Si-Cl(4) and Cl(2)-Si-Cl(4) angles being 102.1(2)°, 102.0(1)° and

102.8(2)° respectively, while Cℓ(2)-Si-Rh, Cℓ(3)-Si-Rh and Cℓ(4)-Si-Rh are 118.1(1)°, 121.0(1)° and 108.5(1)° respectively. These angles are the same as that in complex (A) [65]. In complex (B), the mean Co-Si-Cℓ angle is 113.3(1)° and the mean Cℓ-Si-Cℓ angle is 105.4(1)°. The Rh-Si-Cℓ(4) angle found here is 108.4(1)° while the other two Rh-Si-Cℓ angles are 118.1(1)° and 120.9(1)°, because the intramolecular Cℓ(2)....H26 and Cℓ(4)....H56 contacts are 2.85 Å and 2.83 Å respectively, close to the sum of the H....Cℓ van der Waals radii, 2.90 Å.

The Rh-Si distance of 2.210(2) Å is very similar to the Rh-Si distance of 2.203(4) Å in (A), λ=1.6, and shorter than the Co-Si distance of 2.254(3) Å in (B), λ=10.2 [124], as well as shorter than the Fe-Si distance of 2.253(3) Å in $[FeH(CO)(Cp)(SiCℓ_3)_2]$, λ=9.8 [126]. The shortening of Rh-Si bond cannot be simply explained by the covalent radius. The metal-silicon distances might be influenced by many factors such as an electronic effect, d_π-d_π bond contraction, and they still remain open questions [126].

The Rh-P(1) and Rh-P(2) distances of 2.343(2) Å and 2.335(2) Å in this complex are the same as the Rh-P distances of 2.344(4) Å and 2.332(4) Å in complex (A), λ=0.22 [65], but longer than the Rh-P(1) and Rh-P(2) distances of 2.197(1) Å and 2.245(1)Å respectively in [RhCℓ(*R*-amphos)(PPh_3)], (C), λ=65 [Chapter 2], and longer than the mean Rh-P distance of 2.271(3) Å in [$RhCℓ_3$-(*R*-diamphos)],(D), λ=20 [Chapter 3]. In this complex the

two phosphines are trans to each other, while in complex (C) the two phosphines are cis to each other.

5.5 Discussion

It is interesting to note that, on purely steric grounds, one would predict that these five-coordinate complexes would adopt a regular trigonal-bipyramidal configuration, with the phosphine or silyl ligands in the trigonal plane. This occurs in $[RhH(CO)(PPh_3)_3]$, with the three P atoms in the equatorial plane, the hydrogen at one apex, and the carbon of the carbonyl at the other [127]. But in our complex, we found H, Cl and $SiCl_3$ to be in the trigonal plane, as discussed in Chapter 4. The complex [RhCl-(*R*-amphos)(PPh_3)] reacts with $HSiCl_3$ to form a six-coordinate [RhHCl(*R*-amphos)$(PPh_3)(SiCl_3)$] complex, in which H and Cl occupy the axial positions and *R*-amphos, PPh_3 and $SiCl_3$ the equatorial ones. We call this model the H....Cl model (Chapter 4). As the $HSiCl_3$ substrate approaches the parent complex, the Rh-Cl bond bends such that complex + substrate form a trigonal bipyramid in the transition state [85]. The bending ligand, the Cl atom, and the $HSiCl_3$ substrate occupy the equatorial sites of the trigonal bipyramid. Although the molecule is a by-product in the catalytic cycle, the crystal structure of the complex $[Rh(III)HCl(SiCl_3)(PPh_3)_2]$ is not inconsistent with the H.....Cl model we proposed in Chapter 4.

The formation of the complex $[RhHCl(SiCl_3)(PPh_3)_2]$,

crystallized by acc'dent, helps us to understand that this by-product, produced in the catalytic cycle, may affect the chemical yields, but not the optical yields in the hydrosilylation of prochiral ketones catalyzed by [RhCl(*R*-amphos)(PPh_3)] (Chapter 6).

CHAPTER 6

Hydrosilylation of Prochiral Ketones with α-Naphthylphenyl dihydrosilane Catalyzed by [Rh(*R*-amphos)NBD]ClO_4 and [RhCl(*R*- or *S*-amphos)(PPh_3)] Complexes

6.1 Introduction

Rhodium metal complexes with chiral amphos ligands have proved effective for the catalytic asymmetric hydrosilylation of prochiral ketones [31]. However, the optical yields of chiral alcohols showed a large dependence on the type of silane used [31,32,102]. The need for a match between the chiral catalyst and a chiral substrate has been noted [42], in that the extent of the asymmetric induction as well as the configuration of the predominant alcohol produced are dependent not only on the structure of the prochiral ketone but also on the particular silane used [27,103]. A different silane may affect the asymmetric reduction process due to differences in stability of the two diastereomeric α-silyloxyalkyl (α-silyloxyaryl) rhodium intermediates. Reductive elimination by transfer of a hydrogen from the rhodium to the carbon in this intermediate yields the products. We decided therefore to study hydrosilylation of prochiral ketones with α-naphthylphenyldihydrosilane catalyzed by a rhodium metal complex containing a chiral amphos ligand. Acetophenone, propiophenone and butanone were chosen. Such catalytic asymmetric hydrosilylation reactions have

been carried out with chiral rhodium complexes prepared from (-)- or (+)-2,3-O-isopropylidene-2,3-dihydroxy--1,4-bis(diphenylphosphino)butane, (-)- or (+)-DIOP by Corriu et al [27,104]. The use of a silane of formula H_2SiRR' can lead to asymmetric induction at both carbon and silicon. For example, hydrosilylation of methyl ethyl ketone with α-naphthylphenylsilane catalyzed by a (-)-diop rhodium complex leads to a chiral silyl ether. Reaction of this silyl ether with a methyl Grignard and subsequent hydrolysis yield both optically active (-)-α-naphthylphenyl-methylsilane (40% e.e.) and (-)-2-butanol (42% e.e.).

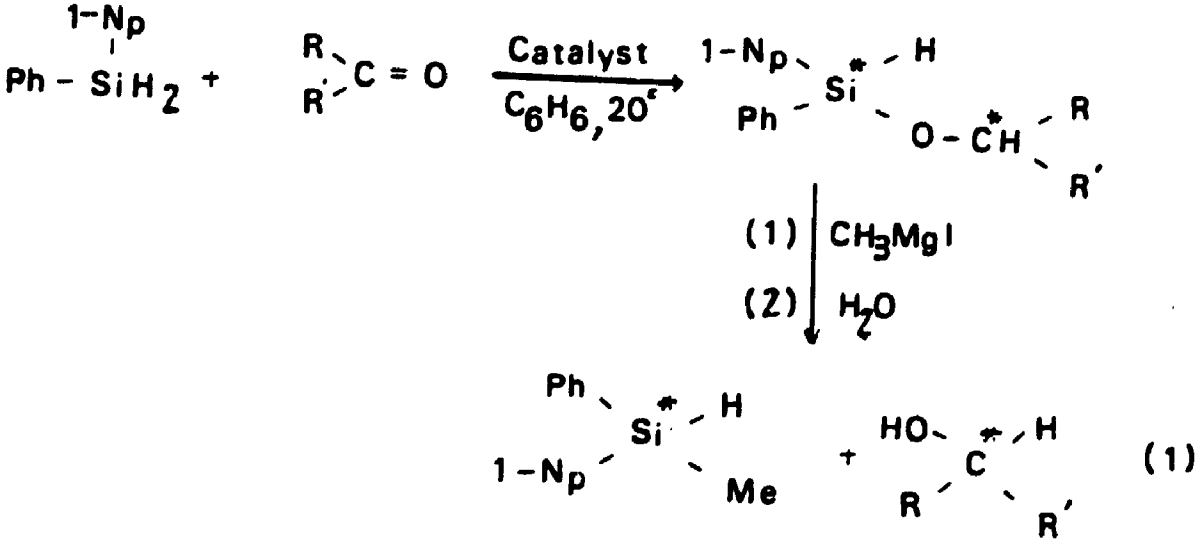

Catalyst: $[(C_8H_{14})_2RhCl]_2$ + (-)-or (+)-DIOP.

The silyl ethers obtained in these reactions can also be quantitatively solvolyzed by such reagents as KOH in aqueous methanol, methanolic p-toluene sulfonic acid, and

1M hydrochloric acid to give the corresponding alcohol [105,106]. The ready hydrolysis of the resulting silyl ethers gives asymmetric hydrosilylation great importance as a preparative method.

The resolution of α-NpPhMeSi*H (α-Np=α-naphthyl) by Sommer and coworkers [115] has been accomplished. Hence, any α-NpPhSi*H group of a silyl ether [α-NpPh(H)Si*OC*HRR'] can be converted to a trisubstituted silane α-NpPhMeSi*H of known maximum specific rotation by reaction with a methyl Grignard reagent. The maximum specific rotation of (+)-α-NpPhHSi*Me is +36.0°, $[\alpha]_D^{20}$, in pentane. This conversion is accompanied by retention of configuration at the silicon atom [27]. With this knowledge, it is possible to calculate the optical yield from a hydrosilylation reaction.

6.2 Experimental

1. Preparation of α-naphthylphenyldihydrosilane

(a) Preparation of phenyltrimethoxysilane [108].

106g (0.50 mole) of phenyltrichlorosilane in 300 mL of anhydrous ether was mixed slowly with 48g (1.5 mole) of methanol and 149g (1.5 mole) of cyclohexylamine in 800 mL anhydrous ether with cooling in an ice bath. After addition, the reaction solution was refluxed for two hours and then filtered. The filtrate was washed with aqueous HCl (0.1 M) and dried with anhydrous sodium sulfate. The solvent was removed by distillation. The product was

characterized by ^1H NMR which showed the signal of MeO-group at 3.50 ppm and the signal of the phenyl group at 7.26-7.62 ppm. As expected, the intensity ratio was 9 to 5 (the signal of MeO-group to the signal of the phenyl group). The yield was 72.5g (73%).

(b) Preparation of α-naphthylphenyldimethoxysilane [108].

A Grignard reagent was prepared by reacting 54g (0.26 mole) of α-bromonaphthalene and 6.35g (0.26 mole) of magnesium turnings in anhydrous ether (0.5 L). After refluxing for one hour, 42.5g (0.21 mole) of phenyltrimethoxysilane in 200 mL of anhydrous ether was added dropwise into the Grignard reagent, followed by refluxing for four hours. The product was hydrolyzed by cautious addition of dilute hydrochloric acid (0.1 M). The organic phase was separated and dried with anhydrous sodium sulfate. The product was collected by vacuum distillation at 150-152°C/0.1 mmHg. The ^1H NMR spectrum of the product showed signals at 7.29-8.24 ppm for α-naphthyl and phenyl and at 3.50 ppm for the methoxy group. The yield was 70.8g (66%).

(c) Preparation of α-naphthylphenyldihydrosilane [108].

90.0g (0.305 mole) of α-naphthylphenyldimethoxysilane in 100 mL anhydrous ether was reacted with 24.4g $LiAlH_4$ (0.610 mole) in 500 mL anhydrous ether under nitrogen. After addition, the reaction mixture was refluxed overnight under nitrogen. Excess $LiAlH_4$ was destroyed by addition of 67 mL acetone (0.915 mole) followed by washing with 900

mL 1 M HCl. The solution was filtered under nitrogen. The filtrate was washed again with 500 mL 1 M HCl. The organic phase was extracted and dried over anhydrous sodium sulfate. The residue was purified by column chromatography (120g SiO_2 Kieselgel 60), eluted with benzene/hexane 4/6. 59.2g (83% yield) of α-naphthylphenyldihydrosilane was obtained. The ^1H NMR spectrum showed signals at 5.32 ppm (Si-H) and at 6.95-8.06 ppm (α-naphthyl and phenyl groups).

2. Asymmetric hydrosilylation of prochiral ketones [27].

All hydrosilylation reactions were carried out in Schlenk tubes at 20° under a nitrogen atmosphere. The asymmetric catalyst was prepared "in situ" by dissolving $[(C_2H_4)_2RhCl]_2$ or $[Rh(NBD)_2]ClO_4$ (2.5×10^{-5}, 1.34×10^{-4} mole) with 5.0×10^{-5}, 2.68×10^{-4} mole of (+)- or (-)-amphos ligand in 5 mL of anhydrous degassed benzene respectively. A further 5.0×10^{-5}, 2.68×10^{-4} mole of PPh_3 ligand was added to the $[(C_2H_4)_2RhCl]_2$ and amphos ligand combination. The mixture was stirred for 10 min. and 2.42×10^{-2} mole of the ketone mixed with 5 mL of benzene was introduced by syringe. The silane (2.42×10^{-2} mole) dissolved in 5 mL of benzene was then added. The progress of the reaction was monitored by TLC. Thin layer silica plates (plastic sheet, UV-sensitized) were developed with 10% EtOAc - 90% pet. ether. Reactants and products containing the naphthylsilyl group were both UV-positive and iodine staining. Ketones, for example, acetophenone, were seen

only under UV. The positions of these spots are calculated as Rf values, for example, Rf values for $PhNpSiH_2$, $PhCOCH_3$ and their product silylether were 0.64, 0.28, and 0.51 respectively. Reactions were judged complete when only product and a small amount of dihydrosilane could be seen on the plates. When all the starting silane and ketone had disappeared, the solvent was removed under vacuum. The silyl ether products were characterized by ^1H NMR (see Table 6.3.1). The residue was dissolved in 5 mL of anhydrous ether and added to a solution of the appropriate Grignard reagent (MeMgI). After reaction, the mixture was hydrolyzed (1 M HCl). The organic phase was extracted with ether, washed with water, and dried over anhydrous sodium sulphate. After removal of the solvent, the alcohol was distilled out at the appropriate temperature; the residue of silane α-NpPhMeSi*H was purified by column chromatography (60g SiO_2, eluant benzene/hexane 1/9). The alcohol and silane were characterized by ^1H NMR. The ^1H NMR spectra in C_6D_6 (TMS) of α-NpPhMeSi*H showed signals at 5.64 ppm (q) (Si-H), at 0.71 ppm (d) (methyl group) and at 7.17-8.30 ppm (m) (α-naphthyl and phenyl groups).

3. Measurement of the optical yields of alcohols and the silane

The optical rotations (degree) of both alcohols and the α-NpPhSiHMe silane were measured on an automatic polarimeter (AUTOPOL ^{R} III, Rudolph Research) at the sodium

line, 589.3 nm, 20°C. The sample diluted in an appropriate solvent was placed in a 2 dm cell. The concentration of the samples in % was reported in Table 6.3.2. The pure solvent used to dilute the sample filled another 2 dm cell for background reference.

The specific rotations $[\alpha]_D^{20}$ and optical yields (%) were calculated with the following equations [114],

$$[\alpha]_D^{20} = \alpha/(\ell d)$$

Here α = observed rotation (degrees), ℓ = cell length, d = concentration (g/cc);

the optical yield = $[\alpha]_D^{20}/[\alpha]_{max} \times 100\%$

Where $[\alpha]_{max}$ = the known maximum specific rotation.

The optical yields of both alcohols and the α-NpPhHSi*Me silane are summarized in Table 6.3.2. The known maximum specific rotations were obtained from the references (see Table 6.3.2) [116].

6.3 Results.

We studied the reactions of ketones and prochiral ketones with the silane (α-NpPhSiH$_2$) catalyzed by the asymmetric rhodium complex containing the chiral amphos ligand.

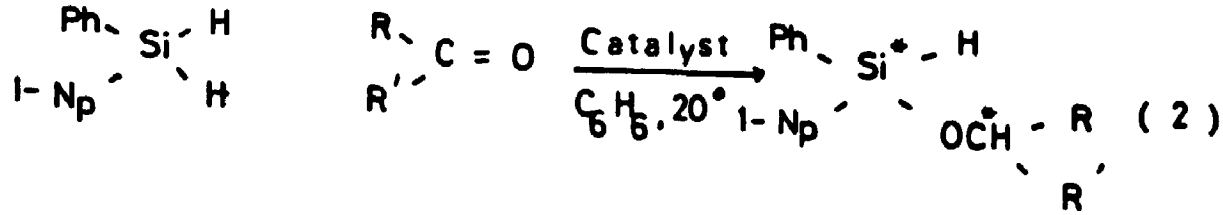

(2)

where R or R' are methyl, ethyl, phenyl groups.

If R = R', the ketone is achiral, and no optical activity is observed at carbon, but optical activity appears at silicon. If R ≠ R', the substrate is a prochiral ketone, and optical activity can be observed at both silicon and carbon atoms in the products. $[Rh(NBD)_2]ClO_4$ containing either (+)- or (-)-amphos ligand, and $[Rh(C_2H_4)_2Cl]_2$, with (+)- or (-)-amphos + PPh_3 ligand were employed as catalysts.

The preferential addition of one of the two Si-H groups to the metal lead to optically active silyl ether products, which were characterized by ^1H NMR. We found that two diastereomers appeared in the ^1H NMR spectrum. The data obtained are presented in Table 6.3.1.

The silyl ether (R ≠ R') can have two chiral centers, one at the silicon atom, another at the carbon atom. In this case, four diastereomeric silyl ethers can be formed,

R^C-R^{Si}, S^C-S^{Si}, R^C-S^{Si} and S^C-R^{Si}. In a pair of R^C-R^{Si} and S^C-S^{Si} enantiomeric silyl ethers, the same signals appear in the ^1H NMR spectra. Another enantiomeric pair of R^C-S^{Si} and S^C-R^{Si} silyl ethers should also give equivalent signals. But the two pairs of diastereomeric silyl ethers are expected to have different chemical shifts and intensities. In practice we could observe two different diastereomeric silyl ethers. Given the relative intensities for these two pairs of silyl ethers, the enantiomeric purity of the alcohol may be used to determine the optical yield at the the silicon atom by NMR spectroscopy [109]. The silyl ethers formed by achiral ketones, i.e. R = R', have only one chiral centre at the silicon atom. Therefore only one signal for each chemically equivalent proton is expected. However, we found two signals with the same intensity for the methyl α- to the CHOSi carbon in the case of isopropyloxysilanes and two signals each for CH_2 and CH_3 α- and β- to the CHOSi carbon in the case of 3-pentyloxysilanes. The non-equivalence of the chemical shifts of the two CH_2 and CH_3 groups is due to the presence of the chiral Si centre.

The addition product, the silyl ether, was formed quantitatively. Treatment of the reaction mixture with a Grignard reagent allowed recovery of an organosilane and an alcohol of varying optical purity.

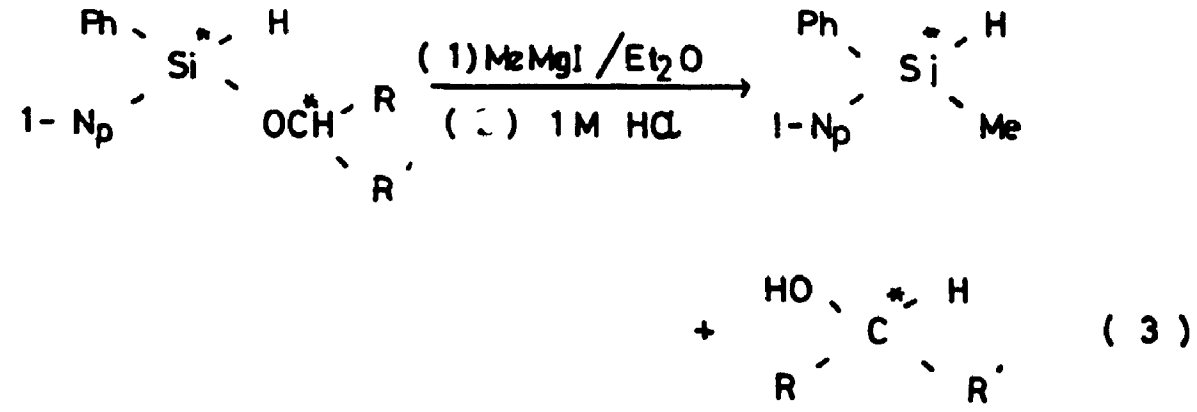

The results obtained are given in Table 6.3.2. The optical yield of the silane measured was poor, but the chemical yield of the silane was as high as 85% for achiral ketones (the optical yield of the silane for achiral ketones is not shown in Table 6.3.2). For chiral ketones, the chemical yields of both alcohols and the silane are from 80% to 95%; the optical yield for alcohols is from 3% to 57% depending on the ratio of catalyst to substrate, (if the ratio of catalyst to substrate is 1 to 100, the optical yield of alcohol can reach as high as 57%); but the optical yield for the silane is only from 0.86% to 8.78%, which is relatively low.

On the other hand it is very interesting to note that addition, in the presence of [(*R*- or *S*-amphos)RhCl] and

[(*R*-amphos)(NBD)Rh]ClO_4, of α-NpPhSiH_2 leads to silanes with only the *S*(-)-α-NpPhMeSi*H configuration. One can explain this by considering the relative stabilities of the two diastereomeric complexes I and II (see Figures 6.4.1 and 6.4.3). The one asymmetric carbon atom of the amphos ligand imposes a conformation in which one of the phenyl groups is quasi-axial and the other quasi-equatorial. In the equilibrium between the two diastereomers I and II, the more abundant is that for which the steric interactions are minimum. The preferred configuration of the silicon atom is that in which the biggest α-naphthyl group is on the side of the chelate ring (Figure 6.3.1).

The reaction of this preferred diastereomer with the ketone, followed by reaction of the Grignard reagent (MeMgI) with the silyl ether obtained, retains the configuration of *S*(-) at

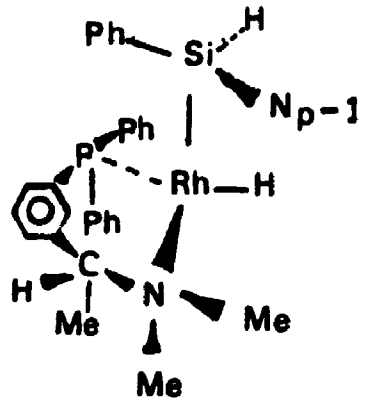

Figure 6.3.1 The configuration of silyl hydrido rhodium amphos complex.

the silicon atom. The α-NpPhMeSi*H will therefore lead preferentially to an organosilane of configuration shown below in agreement with the observed results (Figure 6.3.2).

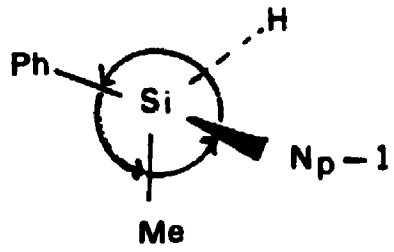

Figure 6.3.2 An organosilane of *S*(−) configuration.

The results in Table 6.3.2 indicate that the optical yield of the alcohol depends on the ratio of the catalyst to the substrate used, in that a 1 to 100 ratio produced much higher optical yield than a 1 to 500 ratio did. It is possible that the rhodium catalyst dissociated in solution to form an optically inactive species. Both can catalyze the hydrosilylation reaction [110], leading to a low optical yield, thus this phenomenon can be responsible for the variation in optical yield with catalyst concentration. Having an asymmetric environment presented by a catalyst to the substrate molecule appears to be very

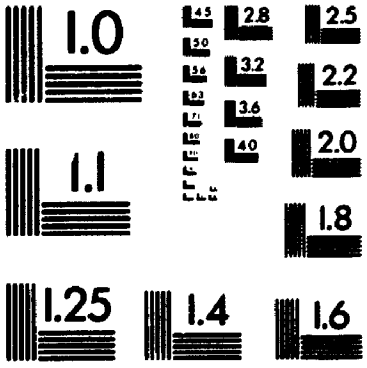

important. In order to overcome this shortage, one can increase the ratio of the catalyst to the substrate molecule or use an excess of the chiral ligand [112] to produce a higher optical yield.

The results (Table 6.3.2) also indicated that the neutral [RhCl(*R*- or *S*-amphos)(PPh_3)] catalyst produced only slightly higher optical yields of both alcohol and silane than the cationic [(*R*-amphos)(NBD)Rh]ClO_4 catalyst did. The neutral [RhCl(*R*- or *S*-amphos)(PPh_3)] catalyst can form a six- coordinate complex with addition of the silane and the ketone, while the cationic [(*R*-amphos)(NBD)Rh]ClO_4 only forms a five-coordinate complex with addition of the silane and the ketone. The six-coordinate rhodium complex might be sterically favourable for the asymmetric hydrosilylation.

6.4 Discussion

The results obtained may be explained as follows. The oxidative addition of the silane α-NpPhSi$^*H_2$ to the rhodium amphos complex will lead to the formation of two diastereomeric complexes (I) and (II) (Figure 6.4.1). These two complexes in equilibrium will not occur in the same abundance in the reaction medium. They will react with the ketone with different rate constants, k_1 and k_2. If we suppose that complexes I and II are in a rapid equilibrium, greater than the rate of reaction of the ketone, the silyl ether enantiomers will be formed in a ratio equal to $k_1[I]/k_2[II]$.

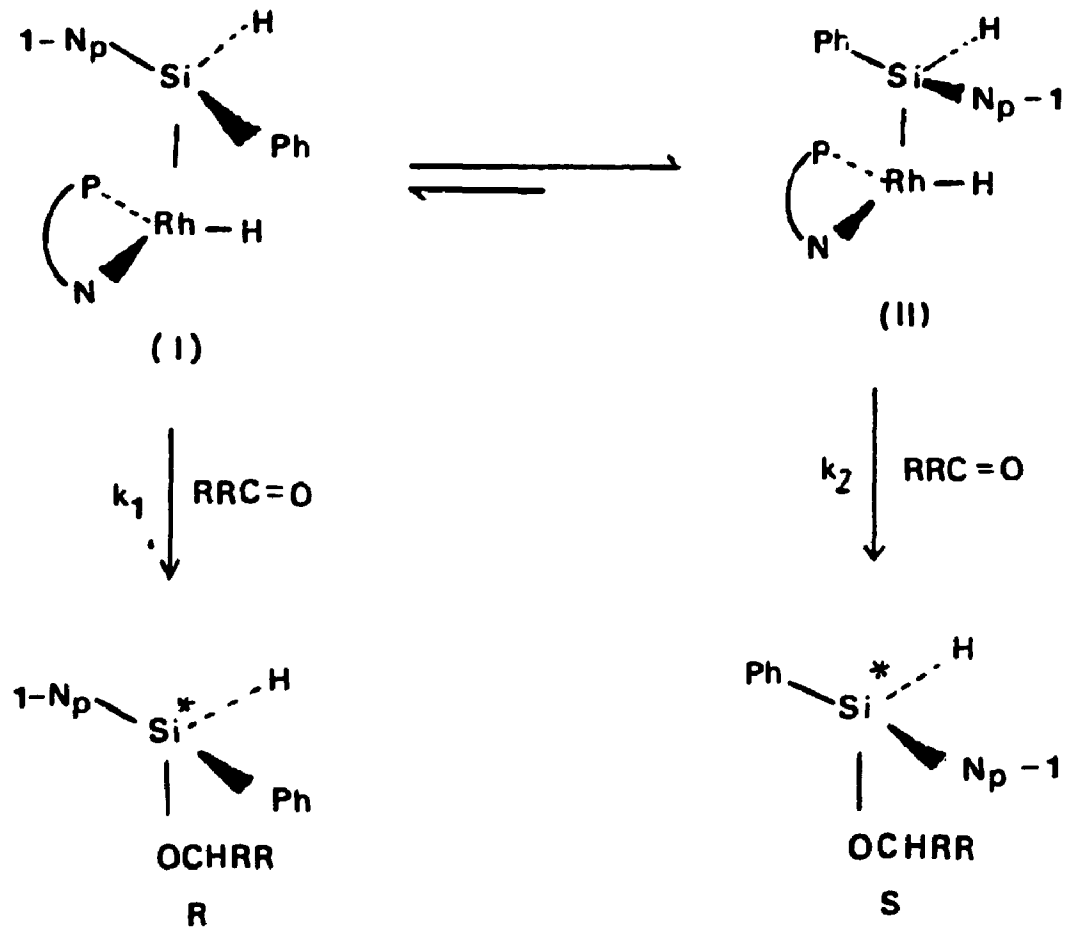

Figure 6.4.1 A kinetics scheme for the formation of the opposite configuration silyl ether products (R=R).

For hydrosilylation of a prochiral ketone, a kinetic scheme of the same type as that in Figure 6.4.1 is shown in Figure 6.4.3 It is necessary, however, to distinguish between the two faces (α and β) of the ketone (Figure 6.4.2).

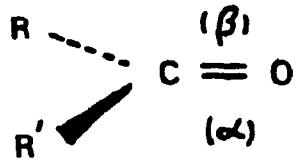

Figure 6.4.2 The two faces of prochiral ketone.

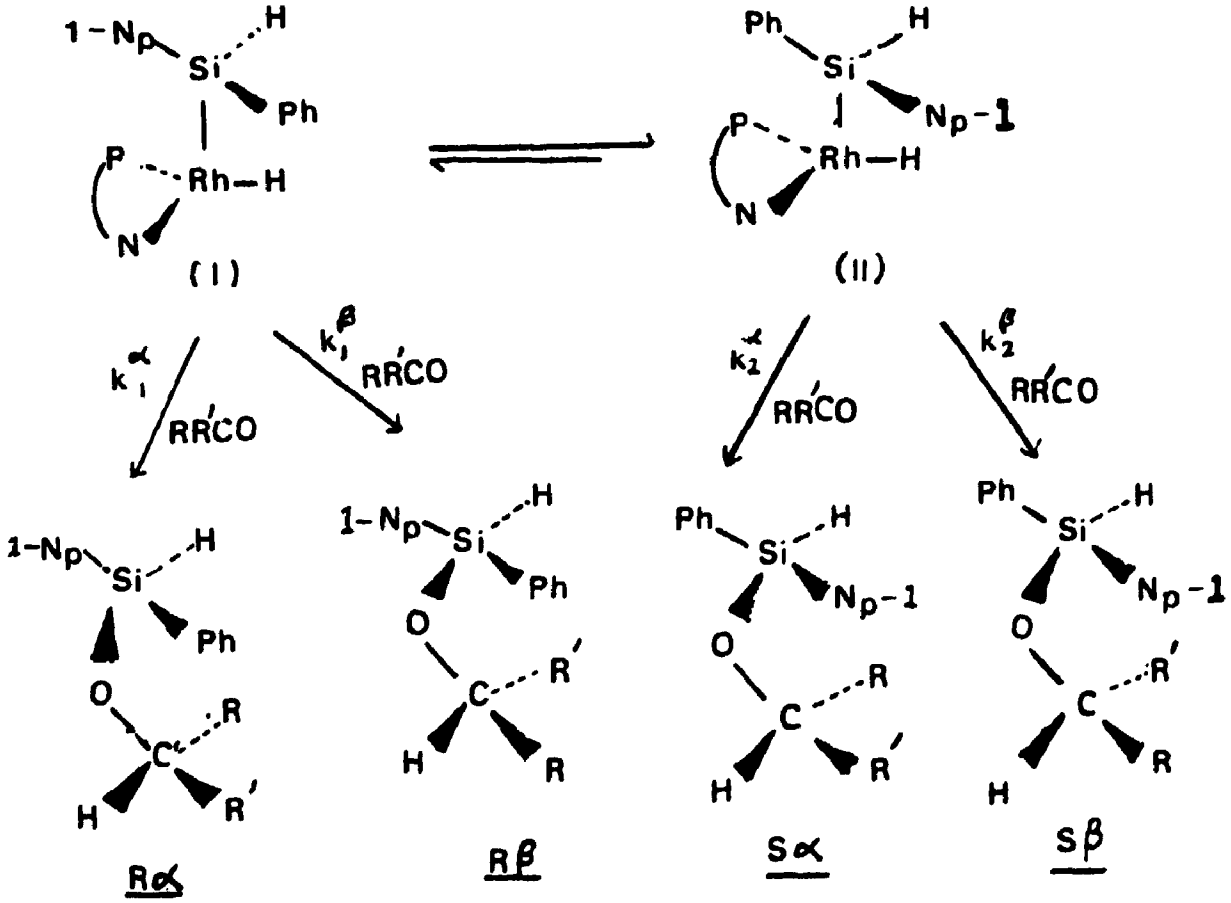

Figure 6.4.3 A kinetics scheme for the formation of the four diastereomeric silyl ethers.

The diastereomeric complexes I and II react at the two faces of the prochiral ketone with rate constants k_1^{α}, k_1^{β} for complex I and k_2^{α}, k_2^{β} for II. The optical purity at the silicon centre (P_{Si}) depends on the relative rates of reaction of the complexes I and II:

$$P_{Si} = (k_1^{\alpha} + k_1^{\beta})[I]/(k_2^{\alpha} + k_2^{\beta})[II].$$

The optical purity at the carbon atom centre P(C) will be different. It depends on the attack on the faces (α) and (β):

$$P_C = k_1^{\alpha}\,[I] + k_2^{\alpha}\,[II]/\ k_1^{\beta}\,[I] + k_2^{\beta}\,[II].$$

This explains why there is no relationship between the optical purity of the asymmetric silane and that of the alcohol [27].

6.5 Conclusions

Hydrosilylation of the prochiral ketone with α-naphthylphenyldihydrosilane catalyzed by [(*R*-amphos)(NBD)Rh]ClO_4 and [RhCl(*R*- or *S*-amphos)(PPh_3)] complexes gave very high chemical yields from 80% to 95%, fairly high optical yields of the alcohol, up to 57%, and relatively low optical yields of silane, up to 8%, for a ratio of catalyst to substrate of 1 to 100. The results we obtained with α-NpPhSiH_2 silane are much better than those previously achieved with the Ph_2SiH_2 and $PhMe_2SiH$ silanes [32]. The contribution from the relative bulkiness of the silane, which can influence the free rotation of the prochiral ketone in the α-silyloxyalkyl or α-silyloxyaryl hydrido

rhodium metal intermediates, is apparently of maximum importance in this system. From our results, we can confirm that the extent of the asymmetric induction, as well as the configuration of the predominant alcohol produced, are dependent not only the structure of the chiral catalyst but also on the particular silane used.

Table 6.3.1 ^1H NMR data of silyl ether products

Compound		Catalyst	^1H NMR data		Δδ(ppm)
		The ratio of catalyst to substrate			
R	R'		δ(ppm), , J(Hz), ratio.		
CH_3	CH_3'	[(R-amphos)(NBD) Rh]ClO_4 1:490	δ_{CH_3}=1.14(d)	1:1	0.06
			$\delta_{CH_3'}$=1.20(d)	CH_3-CH_3'	
			J(OCH-CH_3)=6		
			δ_{OCH}=4.14(S)	0:0	
				OCH-OCH'	
			δ_{Si-H}=6.02;6.17; 6.26.	3:2:3 H-H'	0.15,0.09
CH_2-CH_3	$CH_2'-CH_3'$	[(R-amphos)(NBD) Rh]ClO_4 1:490	δ_{CH_3}=0.78(t)	1:1	0.1
			δ_{CH_3}=0.89(t)	CH_3-CH_3'	
			J(CH_2-CH_3)=8		
			δ_{CH_2}=1.58(q of d)	1:1	0.01
				CH_2-CH_2'	
			δ_{OCH}=3.78(m)	0:0	
			J(OCH-CH_2)=6	OCH-OCH'	0.0
			δ_{Si-H}=6.06;6.20; 6.30(S).	1:0.13:0.06	0.14,0.10

Table 6.3.1 continued

compound		Catalyst	^{1}H NMR data		
R	R'	The ratio of catalyst to substrate	δ(ppm), J(Hz)	ratio	Δδ(ppm)
CH_2-CH_3 (A)	CH_3 (B)	[(*R*-amphos)(NBD)Rh]$C\ell O_4$ 1:490 or 1:100	δ_{CH_3}(B)=1.12(d)	1:0.8	0.08
			δ_{CH_3}'(B)=1.20(d)		
			J(OCH-CH_3)=6		
			δ_{CH_3}(A)=0.82(t)	1:0.85	0.09
			δ_{CH_3}'(A)=0.91(t)		
			J(CH_2-CH_3)=8		
			δ_{CH_2}=1.53(q of d)	1:0.9	0.01
			δ_{OCH}=3.94(q of t)	0:0	0.0
			δ_{Si-H}=5.827;5.833(S)	1:0.95	0.006
CH_3	C_6H_5	[(*R*-amphos)(NBD)Rh]$C\ell O_4$ [RhCℓ(*S*-amphos)(PPh_3)] 1:490	δ_{CH_3}=1.42(d)	1:0.55	0.08
			δ_{CH_3}'=1.50(d)		
			J(OCH-CH_3)=6		
			δ_{OCH}=5.04(q)	0:0	0.0
			J(CH_3-OCH)=6		
			δ_{Si-H}=5.95;6.07; 6.32(S)	0.4:0.2:1	0.12; 0.25

Table 6.3.1 continued

Compound		Catalyst	^{1}H NMR data		
R	R'	The ratio of catalyst	δ(ppm) , J(Hz)	ratio	Δδ(ppm)
CH_2CH_3	C_6H_5	[(*R*-amphos)(NBD)Rh]ClO_4 1:490 [RhCl(*R*-amphos)(PPh_3)] 1:100	δ_{CH_3}=0.80(t)	1:0.95	0.07
			δ_{CH_3}'=0.87(t) $J(CH_2-CH_3)$=8		
			δ_{CH_2}=1.92(q of d)	1:0.75	0.01
			δ_{OCH}=4.80(q)	0:0	0.0
			δ_{Si-H}=5.65; 5.73(S)	1:0.95	0.08

δ is the chemical shift (C_6D_6, TMS); J is the coupling constant; Δδ is the difference of the chemical shifts.

Table 6.3.2 The optical yields of α-NpPhMeSi*H silane and RC*HOHR' alcohols

Catalyst	RR'=O	Rh/substrate	RC*HOHR' Alcohol	%yield	$[\alpha]D^{20}$ (C %)	e.e.%	Config.
[(*R*-amphos)(NBD)Rh]ClO_4	$CH_3COC_6H_5$	1:490	$C_6H_5CHOHCH_3$	95%	-1.64° (3.62)	3.13%	*S*
[(*R*-amphos)(NBD)Rh]ClO_4	$C_2H_5COC_6H_5$	1:490	$C_6H_5CHOHC_2H_5$	90%	-1.88° (5.62)	5.70%	*S*
[(*R*-amphos)(NBD)Rh]ClO_4	$CH_3COC_2H_5$	1:490	$CH_3CHOHC_2H_5$	80%	-1.12° (3.81)	8.66%	*R*
[(*S*-amphos)$RhCl(PPh_3)$]	$CH_3COC_6H_5$	1:490	$CH_3CHOHC_6H_5$	90%	-2.33° (3.22)	4.44%	*S*
[(*R*-amphos)$RhCl(PPh_3)$]	$C_2H_5COC_6H_5$	1:490	$C_2H_5CHOHC_6H_5$	90%	+2.35° (8.22)	7.11%	*R*
[(*R*-amphos)$RhCl(PPh_3)$]	$CH_3COC_2H_5$	1:100	$CH_3CHOHC_2H_5$	80%	-7.43° (1.38)	57.62%	*R*
[(*S*-amphos)$RhCl(PPh_3)$]	$C_2H_5COC_6H_5$	1:100	$C_2H_5CHOHC_6H_5$	85%	-14.85° (2.45)	41.50%	*S*

Table 6.3.2 continuned

Catalyst	RR'C=O	Rh/substrate	α-NpPhSi*MeH %yield	$[\alpha]_D^{20}$ (C %)	e.e.%	Config.
[(*R*-amphos)(NBD)Rh]$C\ell O_4$	$CH_3COC_6H_5$	1:490	90%	-1.14° (10.06)	3.16%	*S*
[(*R*-amphos)(NBD)Rh]$C\ell O_4$	$C_2H_5COC_6H_5$	1:490	90%	-0.48° (10.64)	1.33%	*S*
[(*R*-amphos)(NBD)Rh]$C\ell O_4$	$CH_3COC_2H_5$	1:490	95%	-0.31° (26.15)	0.86%	*S*
[Rh$C\ell$(*S*-amphos)(PPh_3)]	$CH_3COC_6H_5$	1:490	90%	-2.40° (8.42)	6.67%	*S*
[Rh$C\ell$(*R*-amphos)(PPh_3)]	$C_2H_5COC_6H_5$	1:490	95%	-1.28° (16.96)	3.57%	*S*
[(*R*-amphos)(NBD)Rh]$C\ell O_4$	$CH_3COC_2H_5$	1:100	90%	-3.16° (13.53)	8.78%	*S*
[Rh$C\ell$(*S*-amphos)(PPh_3)]	$C_2H_5COC_6H_5$	1:100	90%	-2.87° (10.16)	7.96%	*S*

R(+)-α-NpPhMeSiH: $[\alpha]_D^{20}$=+36° (pentane) [27]; *S*(-)-PhCHOHMe: $[\alpha]_D^{20}$=-52.5° ($CH_2C\ell_2$) [27]; *S*(-)-PhCHOHEt: $[\alpha]_D^{20}$=-33° (c=5%, C_2H_5OH) [111]; *R*(-)EtCHOHMe: $[\alpha]_D^{24}$=-12.9° (c=10%, CH_3OH) [111]; C is concentration of sample in %.

CHAPTER 7

CONCLUSIONS

7.1 Introduction.

Three research objectives were expressed in this thesis, which has described our studies of homogeneous, asymmetric hydrosilylation using Rh catalysts of chiral P-N and P-N-N ligands. The first goal was to obtain an understanding of the catalyst's features that give rise to the asymmetric environment presented to an incoming substrate molecule. Solid state X-ray studies have provided the basis for an explanation of the observed catalytic results in terms of the shape of the chiral ligand (Chapter 2 and Chapter 3).

The second objective focussed on the stability of the [Rh(I)Cl(*R*-amphos)(PPh_3)] catalyst in solution and the formation of its oxidative addition products, as well as the labilities of species actually present in the solution during a hydrosilylation reaction. Spectroscopic techniques, including ^{1}H & ^{31}P NMR, Visible, Infra Red, and mass spectroscopies have resulted in the elucidation of a mechanistic scheme for homogeneous, asymmetric hydrosilylation (Chapter 2 and Chapter 4). In a certain favourable case, one of the oxidative addition products was isolated and characterized by X-ray diffraction techniques (Chapter 5).

The third objective was to synthesize a new and bulky α-naphthylphenyldihydrosilane and to test the optical

yields generated by the Rh-amphos catalyst and this silane. The results obtained have helped us to understand that the α-silyloxyalkyl or α-silyloxyaryl hydrido rhodium metal intermediates can be apparently of maximum importance in this system (Chapter 6).

7.2 Discussion and Conclusions.

All successful asymmetric catalysts display one specific feature, which is the ability to present a stable asymmetric environment to an incoming substrate molecule. For the phosphine complexes (Chapter 1), the chiral centres can either be the phosphorus atom itself, or incorporated into the backbone of a chelating ligand. The chiralities of the catalysts [Rh(I)Cl(*R*-amphos)(PPh_3)], (A), and [Rh(I)-Cl(diamphos)], (B), are both on the backbone of the chelating ligands. In these cases chirality is transferred to the substrate through the medium of the phenyl rings attached to the phosphorus atom. In the case of complex (A), *R*-amphos is a bidentate ligand with the only chiral centre being a C atom, whereas in complex (B), diamphos is a tridentate ligand with chiral centres at a C atom and at an adjacent N atom. Both centres are distant from the substrate molecule, and transmission of chirality does not occur effectively through the phosphorus atom.

The tests for the hydrosilylation of prochiral ketones catalyzed by (A) and (B) showed that (A) gave fairly high optical yields, while (B) had very low optical yields.

Solid state X-ray structural analyses indicated that (A) adopts a single conformation, one in which the methyl group bound to the chiral C atom is axially situated relative to the plane of the chelate ring, in order to minimize non-bonded interactions between H atoms on the methyl group and the nearest H atom on the neighbouring phenylene ring. The N-methyl substituents then adopt staggered dispositions; one of the phenyl rings on the triphenylphosphine ligand is roughly parallel to the edge-exposed phenyl ring on amphos in order to reduce steric hindrance, the six phenyl rings being constrained with little free rotation for each phenyl ring; a reversal of the phenyl ring orientation is probably strongly hindered. The complex, as a result of these interactions, is a fairly rigid molecule.

The structure of the [Rh(III)Cl_3(diamphos)] complex, (C), displays two conformations. The two independent molecules in the unit cell differ in several ways: (1) Two diastereomers exist in both solid and solution: *RS* and *RR*; the unchanging *R* conformation represents chirality at the C atom, while the other describes the chirality at the N atom. (2) The different conformations in the six-membered chelate ring are λ in molecule I and δ in molecule II. (3) Of the methyl groups at the chiral C atoms, C7 is neither axial nor equatorial in molecule I, but C20 is axially situated in molecule II. (4) Of the methyl groups at the chiral N atoms, C5 is hanging down

toward the chelate ring in molecule I and C18 is axial on the chelate ring (up) in molecule II. (5) The orientations of the phenyl rings at the P atoms are face-edge in molecule I and edge-face in molecule II. When the silane oxidatively adds to (B) in the absence of a substrate, the actual species to which the substrate is bound can well be the Rh(III)-hydridosilyl complex. So addition of the silane could produce a ratio of conformers similar to that observed in (C). As a consequence, the function of inducing chirality can be lost in this complex.

Comparing the two structures of (A) and (C), we can conclude that the ligand must not form a rather flexible chelate ring, and that a tightly-bonded, rigid arrangement is required for successful chiral induction.

For the Rh-amphos complex, i.e. [Rh(*R*-amphos)(NBD)]ClO_4, (D), [32] and [RhCl(*R*- or *S*-amphos)(PPh_3)], (A), these species have a common feature in that both have an amphos ligand and a single conformation in the solid state. The orientation that the methyl group bound to the chiral C atom in the amphos ligand adopts is one that is axial to the chelate ring, and as a result the edge-exposed phenyl ring is roughly parallel to this methyl group, in which the non-bonded interactions between H atoms on the methyl group and the H atoms on the edge-exposed phenyl ring are minimal. In these cases, the orientations of the phenyl rings are probably restricted to a certain range, and a complete reversion of orientations, i.e. face-edge to

edge-face, may not occur in solution. Furthermore, the orientations of the phenyl rings in complex (A) and in complex (D) are both more constrained by the neighbouring PPh_3 and NBD groups respectively.

Although solid state X-ray structure analyses gave us help in understanding the catalytic process, the real homogeneous, asymmetric, hydrosilylation catalysis occurs in solution. Therefore the second objective concentrated on studying the mechanism of hydrosilylation in solution, specifically, on examining the oxidative addition step of silane to complex (A).

Before addition of silane, dissociations (up to 30%) of Rh-PPh_3 and Rh-N bonds in solution for [Rh(I)Cl(*R*-amphos)-(PPh_3)] were observed. The breakage of the Rh-PPh_3 bond makes a vacancy for the incoming substrate, but loses some constraint for the orientations of the phenyl rings. The breakage of the Rh-N bond in complex (A), which is due to the greater trans influence of the P atom in the PPh_3 group, leads to the loss of a rigid chiral centre and consequent low optical yields. The hydrosilylation experiment (Chapter 6) found that to obtain higher optical yields, a higher ratio of catalyst to substrate (1 to 100) was required.

With addition of $HSiCl_3$ to the Rh(I)-amphos complex, (A), we observed much of the catalytic cycle with ^{31}P, ^1H NMR and visible spectroscopy. Initial oxidative addition of $HSiCl_3$ silane to a neutral [Rh(I)Cl(*S*-amphos)(PPh_3)]

complex, with cleavage of the Si-H bond, forms a kinetically favoured six-coordination complex, [Rh(III)Cl-H(*S*-amphos)(PPh_3)($SiCl_3$)]. Then breakage of the Rh-PPh_3 bond to form a five-coordinate complex, [Rh(III)Cl-H(*S*-amphos)($SiCl_3$)], is followed by prochiral ketone or solvent addition to form a six-coordinate complex, [Rh(III)ClH(*S*-amphos)($SiCl_3$)(solv.)]. The final steps involve insertion and reductive elimination reactions, which are apparently fast, and were not directly observed.

A side product in the catalytic cycle, [Rh(III)ClH(PPh_3)$_2$-($SiCl_3$)], was isolated and characterized by a single crystal X-ray structure determination. Such complexes are extremely difficult to isolate and only one other related example exists in the literature [65]. This complex can catalyze the hydrosilylation reaction and contribute to the chemical yield, but it will produce 0% optical yield. If present, it will contribute to a low optical yield for reaction catalyzed by the Rh(I)Cl(*S*-amphos)(PPh_3) complex. In order to overcome this problem, extra amphos ligand needs to be added, which provides more of an asymmetric environment, reducing the relative amount of inactive side products.

The extent of the asymmetric induction, as well as the configuration of the predominant alcohol produced, are dependent not only on the chiral catalyst and the structure of the prochiral ketone, but also on the particular silane used. Hydrosilylation of prochiral ketones with a more

bulky α-naphthylphenyldihydrosilane catalyzed by [Rh(I)-(*R*-amphos)(NBD)]ClO_4 and [Rh(I)Cl(*R*- or *S*-amphos)(PPh_3)] complexes gave very high chemical yields, from 80% to 95%, fairly high optical yields of the alcohol, up to 57%, and relatively low optical yields of (-)-α-NpPhMeSi*H for a ratio of catalyst to substrate of 1 to 100. However, this reaction is specific, in that only (*S*)-configuration of this silane can be observed.

The results obtained in this thesis have improved upon the optical yields previously achieved for the hydrosilylation of prochiral ketones with Ph_2SiH_2 and $PhMe_2SiH$. The configuration of the α-silyloxyalkyl (or aryl) rhodium complex intermediate can play an important role. With a silyloxy group bulkier than either of the substituents of the ketone, the silyloxy group should occupy the quasi-apical position, and the largest species of the silyloxy group, i.e. α-naphthyl, lies at the opposite side of the chelate ring to the amphos ligand, which is the least hindered site for the silyloxy group. In this case, the rotation of the prochiral ketone in the α-silyloxyalkyl (or aryl) hydridorhodium intermediates is constrained.

In summary, our purpose was to improve the optical yields for the hydrosilylation of prochiral ketones catalyzed by Rh(I)Cl(*R*- or *S*-amphos)(PPh_3) complexes. As a result of this study some improvements have been made, and we are now in a position to make the following suggestions to future

workers:

(1) The chiral catalyst must not have a rather flexible chelate ring, but instead must have a tightly-bounded, rigid arrangement.

(2) Higher optical yields can be obtained with a higher ratio of catalyst to substrate (up to 1 to 100), and with extra chiral amphos ligand.

(3) A more bulky silane, at least as bulky as α-NpPhSiH_2, needs to be used.

APPENDIX

OBSERVED AND CALCULATED STRUCTURE FACTORS

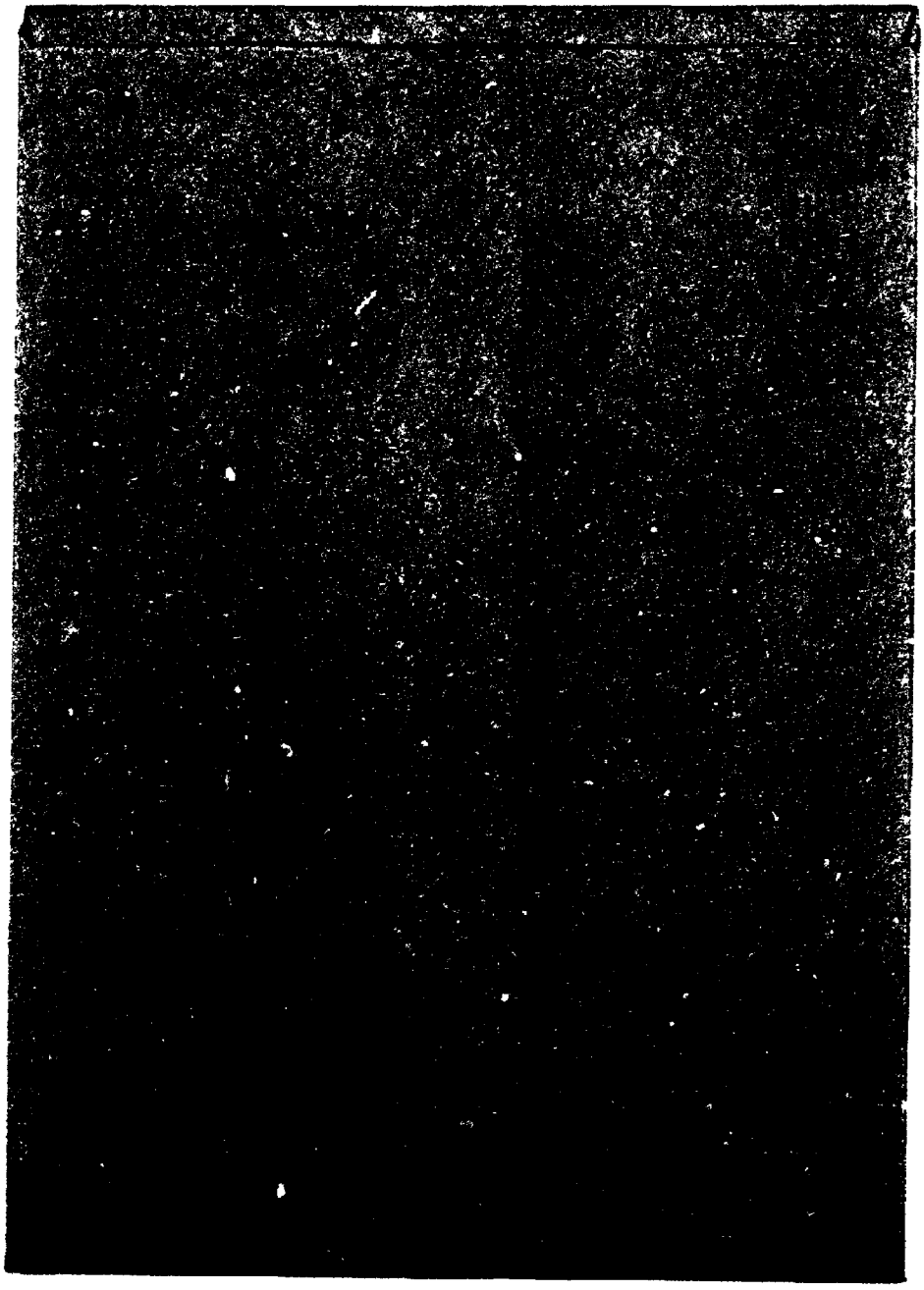

References

1. Morrison, J. D.; Mosher, H. S. Asymmetric Organic Reactions, Prentice Hall Inc., New York, 1971, pp. 4-6.

2. Mislow, K.; Raban, M. Topics in Stereochemistry, E. L. Eliel and N. L. Allinger Editors, Interscience Pub. Inc., New York, 1966, 1, pp. 1.

3. Goldberg, S. I.; Bailey, W. D. J. Am. Chem. Soc., 1969, 91, 5685.

4. Weller, S. W.; Mills, G. A. Adv. in Catalysis, 1956, 8, 163.

5. Klabunovskii, E. I. Absolute Asymmetric Synthesis and Asymmetric Catalysis in Origins of Life on Earth, Rept. Int'l Symp., Moscow, Pergamon Press, New York, 1959, pp. 158-168.

6. Brunner, H. J. of Organometallic Chem., 1986, 300, 39-56.

7. Horner, L.; Siegel, H.; Buthe, H. Angew. Chem., 1968, 80, 1034.; Angew. Chem. Int. Ed. Engl., 1968, 7, 942.

8. Knowles, W. S.; Sabacky, M. J. J. Chem. Soc., Chem. Commun., 1968, 1445.

9. Dang, T. P.; Kagan, H. B. J. Chem. Soc., Chem. Commun., 1971, 481.

10. Kagan, H. B.; Dang, T. P. J. Am. Chem. Soc., 1972, 94, 6429.

11. Brunner, H. Angew. Chem., 1983, 95, 921.; Angew. Chem. Int. Ed. Engl., 1983, 22, 897.

12. Dang, T. P.; Poulin, J. C.; Kagan, H. B. J. Organomet. Chem., 1975, 91, 105.

13. Kagan, H. B. Pure Appl. Chem., 1975, 43, 401.

14. Merrill, R. E. Chem. Technol., 1981, 118.

15. Caplar, V.; Comisso, G.; Sunjic, V. Synthesis, 1981, 85.

16. Marko, L; Bakos, J. Aspects of Homogeneous Catalysis, R. Vgo Editor, Reidel Publishing Company, Dordrecht, 1981, pp. 145

17. Kagan, H. B. Comprehensive Organometallic Chemistry, G. Wilkinson; F. G. A. Stone; E. W. Abel Editors, Pergamon Press. Oxford, 1982, 8, pp. 46^

18. Morrison, J. D. Asymmetric Synthesis, J. W. Scott Editor, Academic Press Inc., 1984, 4, pp. 263.

19. Knowles, W. S.; Sabacky, M. J.; Vineyard, B. D.; Weinkauff, D. J. J. Am. Chem. Soc., 1975, 97, 2567.

20. Fryzuk, M. D.; Bosnich, B. J. Am. Chem. Soc., 1978, 100, 5491.

21. Fryzuk, M. D.; Bosnich, B. J. Am. Chem. Soc., 1977, 99, 6262.

22. Achiwa, K. J. Am. Chem. Soc., 1976, 98, 8265.

23. Hayashi, T.; Yamamoto, K.; Kumada, M. Tetrahedron Lett., 1974, 4405.

24. Yamamoto, K.; Hayashi, T.; Kumada, M. J. Organometal. Chem., 1972, 46, C65.

25. Hayashi, T.; Yamamoto, K.; Kumada, M. J. Organometal. Chem., 1976, 112, 253.

26. Yamamoto, K.; Hayashi, T.; Kumada, M. J. Organometal. Chem., 1973, 54, C45.

27. Corriu, R. J. P.; Moreau, J. J. E. J. of Organometal. Chem., 1975, 85, 19-33.

28. Poulin, J.C.; Dumont, W.; Dang T. P.; Kagan, H. B. Compt. Rend. Acad. Sci., Paris, 1973, 277, C41.

29. Corriu, R. J. P.; Moreau, J. J. E. Noun. J. de Chim. 1977, 1, 71.

30. Brunner, H.; Riepl, G.; Weitzer, H. Angew. Chem. Int. Ed. Engl., 1983, 22, 331.

31. Payne, N. C.; Stephan, D. W. Inorg. Chem., 1982, 21, 182.

32. Mckay, I. D. Ph.D. Thesis, Univ. of Western Ont., London, Ont., 1985.

33. Yamamoto, A. Organotransition Metal Chemistry Fundamental Concepts and Applications, John Wiley & Sons Inc., 1986, pp. 177-182, pp. 364-383.

34. Chan, A. S. C.; Pluth, J. J.; Halpern, J. Inorganica Chimica Acta, 1979, 37, L477-L479; Chan, A. S. C.; Halpern, J. J. Am. Chem. Soc., 1980, 102, 838.

35. Chan, A. S. C.; Pluth, J. J.; Halpern, J. J. Am. Chem. Soc., 1980, 102, 5952.

36. Jardine, F. H. Progress in Inorganic Chemistry, S. J. Lippard Editor, John Wiley & Sons Inc., 1981, 28, pp. 122-166.

37. Meakin, P.; Jesson, J. P.; Tolman, C. A. J. Am. Chem. Soc., 1972, 94, 3240.

38. Tolman, C. A.; Meakin, P. Z.; Lindner, D. I.; Jesson, J. P. J. Am. Chem. Soc., 1974, 96, 2762.

39. Halpern, J. Organotransition- Metal Chemistry Y. Ishil and M. Tsutsui Editors, Plenum Press, New York, 1975, pp. 109-117.

40. De Croon, M. H. J. M.; Van Nisselrooij, P. F. M. T.; Kuipers, H. J. A. M.; Coenen, J. W. E. J. Mol. Catal, 1978, 4, 325.

41. Ohtani, Y.; Yamagishi, A.; Fujimoto, M. Bull. Chem. Soc. Japan, 1979, 52, 69.

42. Osborn, J. A.; Jardine, F. H.; Wilkinson, G.; Young, J. F. J. Chem. Soc. A, 1966, 1711.

43. Halpern, H.; Okamoto, T.; Zakhariev, A. J. Mol. Catal, 1976, 2, 65.

44. De Charentenay, F.; Osborn, J. A.; Wilkinson, G. J. Chem. Soc. A., 1968, 787.

45. Muir, K. W.; Ibers, J. A. Inorg. Chem., 1970, 9, 440.

46. Weber, W. P. Silicon Reagents for Organic Synthesis, Springer - Verlag, Berlin Heidelberg, 1983, pp. 292.

47. Ojima, I.; Hirai, K. Asymmetric Synthesis, Academic Press Inc., 1985, 5, pp.111.

48. Ojima, I.; Kogure, T.; Kumagai, M.; Horiuchi, S.; Sato, T. J. of Organomet. Chem.,1976, 122, 83-97.

49. Cahn, R. S.; Ingold, C. K.; Prelog, V. Angrew. Chemie. Int. Ed. Engl., 1966, 5, 385.

50. Brown, J. M.; Chaloner, P. A. Tet. Lett., 1978, 21, 1877.

51. Hayashi, T.; Yamamoto, K.; Kasuga, K.; Omizu, H.; Kumada, M. J. of Organomet. Chem., 1976, 113, 127.

52. Yamamoto, K.; Tomita, A.; Tsuji, J. Chem. Lett., 1978, 3.

53. Takenaka, A.; Sasada, Y.; Yamamoto, K.; Tsuji, J. Bull. Chem. Soc. Japan, 1977, 50, 3177.

54. Stephan, D. W. Ph.D. Thesis, University of Western Ontario, 1980.

55. Cramer, R. Inorg. Chem., 1962, 1, 722.

56. (a) McKay, I. D.; Payne, N. C. Acta. Cryst., 1986, C42, 304.
(b) McKay, I. D.; Payne, N. C. Acta. Cryst., 1986, C42, 307.

57. Ozawa, F.; Ito, T.; Nakamura, Y.; Yamamoto, A. Bull. Chem. Soc. Japan, 1981, 54, 1868.

58. Paonessa, R. S.; Trogler, W. C. J. Am. Chem. Soc., 1982, 104, 3529.

59. Goldwhite H. Introduction to Phosphorus Chemistry, Cambridge University Press, 1981, pp.20.

60. Brown J. M.; Chaloner, P. A.; Descotes, G.; Glaser, R.; Lafont, D.; Sinod, D. J. C. S. Chem. Comm., 1979, 611.

61. Stout, G. H.; Jensen, L. H. X-ray Structure Determination A Practical Guide, Collier-MacMillan Limited, London, 1968.

62. Fleet, M. E.; J. of Solid State Chem., 1986, 62, 75.

63. "Enraf-Nonius Structure Determination Package, SDP-PLUS", Version 3.0, 1986.

64. "International Tables for X-ray Crystallography"; Kynoch Press: Birmingham, England (a) 1969, Vol. I; (b) 1974, Vol. IV.

65. Ibers, J. A.; Snyder, R. G. Acta. Cryst., 1962, 15, 923.

66. Mason, R.; Scollary, G. R. Aust. J. Chem., 1978, 31, 781.

67. Ball, R. G.; Payne, N. C. Inorg. Chem., 1977, 16, 1187.

68. Knowles, W. S.; Vineyard, B. D.; Sabcky, M. J.; Stults, B. R. Fundamental Research in Homogeneous Catalysis, Plenum Press, New York, 1979, Vol.3, pp. 537.

69. Bosnich, B. Paper presented at The CIC-ACS Biannual Inorg. Chem. Symposium, University of Guelph, Guelph, Ontario, 1980.

70. Brunner, H. J. of Organomet. Chem., 1986, 300, 39.

71. Hazeldine, R. N.; Parish, R. V.; Parry, D. J. J. Chem. Soc. (A), 1969, 683.

72. Egglestone, D. L.; Baird, M. C. J. Organomet. Chem., 1976, 113, C25.

73. Egglestone, D. L.; Baird, M. C.; Lock, C. J. L.; Turner, G., J. Chem. Soc., Dalton Trans., 1977, 1576.

74. Egglestone, D. L.; Slack, D. A.; Baird, M. C. J. Organomet. Chem., 1978, 146, 71.

75. Slack, D. A.; Greveling, I.; Baird, M. C. Inorg. Chem., 1979, 18, 3125.

76. Brown, T. H.; Green, P. J. J. Am. Chem. Soc., 1970, 92, 2359.

77. Mann, B. E.; Masters, C.; Shaw, B. L. J. Chem. Soc. A, 1971, 1104.

78. Sanger, A. R. J. Chem. Soc., Dalton Trans., 1977, 120.

79. Mann, B. E.; Masters, C.; Shaw, B. L. J. Chem. Soc., Dalton Trans., 1972, 704.

80. Grim, S. O.; Satek, L. C. J. Coord Chem., 1974, 3, 307.

81. Garrou, P. E. Inorg. Chem., 1975, 14, 1435.

82. Brown J. M.; Canning, L. R. J. of Organomet. Chem., 1984, 267, 179-190.

83. Brown, J. M.; Murrer, B. A. Tet. Lett., 1979, 50, 4859.

84. Wegman, R. W.; Abatjoglou, A. G.; Harrison, A. M. J. Chem. Soc., Chem. Commun., 1987, 24, 1891.

85. Johnson, C. E.; Eisenberg, R. J. Am. Chem. Soc., 1985, 107, 6351.

86. (a) Cotton, F. A.; Wilkinson, G. Advanced Inorganic Chemistry, 4th. Edn., J. Wiley and Sons, New York, 1980, PP. 1201-1290.
(b) Huheey, J. E. Inorganic Chemistry, 2nd. Edn., Harper and Row Publishers, New York, 1978, pp. 496.

87. Master, C.; McDonald, W. S.; Raper, G.; Shaw, B. L. J Chem. Soc., Chem. Commun., 1971, 210.

88. Slack, D. A.; Egglestone, D. L.; Baird, M. C. J. Organomet. Chem., 1978, 71, 146.

89. Vineyard, B. D.; Knowles, W. S.; Sabacky, M. J.; Backman G. L.; Weinkauff, D. J. J. Am. Chem. Soc., 1977, 99, 5946.

90. Marder, T. B.; Chan, D. M. T.; Fultz, W. C.; Calabrese, J. C.; Milstein, D. J. Chem. Soc., Chem. Commun., 1987, 1885.

91. Alcock, N. W.; Brown, J. M.; Derome, A. E.; Lucy, A. R. J. Chem. Soc., Chem. Commun., 1985, 575.

92. Bezman, S. A.; Shapley, J. R.; White, R.; Osborn, J. A.; Fraser, A. R.; Bird, P. H. J. Chem. Soc., Chem. Commun., 1973, 597.

93. Bezman, S. A.; Bird, P. H.; Fraser, A. R.; Osborn, J. A. Inorg. Chem., 1980, 19, 3755.

94. Halpern, J. Inorganica Chimica Acta., 1981, 50, 11.

95. Harrod, J. F.; Smith, C. A.; Than, K. A. J. Am. Chem. Soc., 1972, 94, 8321.

96. Halpern, J.; Riley, D. P.; Chan, A. S. C.; Pluth, J. J. J. Am. Chem. Soc., 1977, 99, 8055.

97. Chalk, A. J. SPEX Industries Inc., March,1983.

98. Halpern, J. Science, 1982, 217, 406.

99. "Enraf-Nonius CAD4F Users Manual", Enraf-Nonius Delft, Delft, The Netherlands. 1982.

100. Busing, W. R.; Levy, H. A.; J. Chem. Phys., 1957, 26, 563.

101. Brunner, H.; Rahman, A. F. M. M. Inorg. Chem. 1970, 9, 1.

102. Ojima, I.; Nihonyanagi, M.; Nagai, Y. Bull. Chem. Soc. Japan. 1972, 45, 3722.

103. Corriu, R. J. P.; Moreau, J.J.E. J. Organomet. Chem., 1975, 91, C27.

104. Corriu, R. J. P.; Moreau, J. J. E. J. Organomet. Chem., 1974, 64, C51.

105. Ojima, I.; Nihonyanagi, M.; Kogure, T.; Kumagai, M.; Horiuchi, S; Nakatsugawa, K. J. Organomet. Chem., 1975, 94,449.

106. Ojima, I.; Nihonyanagi, M.; Nagai, Y. J. Chem. Soc., Chem. Commun., 1972, 938.

107. Sommer, L.H.; Frye,C.L. J. Am. Chem. Soc. 1959, 81, 1959.

108. Corriu, R. J. P.; Lanneau, G. F.; Royo, G. L. J. Organomet. Chem. 1972, 35.

109. Chan, T.H.; Peng, Q. J.; Wang, D.; Guo, J. A. J. Chem. Soc. Chem. Commun., 1987, 325.

110. Sommer, L. H. Stereochemistry, Mechanism and Silicon McGraw-Hill, New York, 1965, pp144.

111. Aldrich. Catalog Handbook of Fine Chemicals, Aldrich Chemical Company Inc.

112. Brunner, H; Riepl, G. Angew. Chem. Int. Ed. Engl.,1982 21, No.5, 377.

113. Alderman, P. R. H.; Owston, P. G.; Rowe, J. M., Acta Crystallogr. ,1960, 13, 149.

114. Morrison, R. T. and Boyd, R. N. Organic Chemistry, Allyn and Bacon, Inc. 3nd Ed.,1976, pp.120, pp.469.

115. Sommer, L. H. and Fujimoto, H. J. Am. Chem. Soc., 1968, 90, 982.

116. International Critical Tables, vol. VII, W. W. Washburn Editor, McGraw-Hill Book Company, Inc., New York.

117. Sheldrick, G. M. SHELX-76: A Program for Crystal Structure Determination, Cambridge Univ. Press: Cambridge, England, 1976.

118. Bennett, M. A.; Jeffery, J. C.; Robertson, G. B. Inorg. Chem., 1981, 20, 330.

119. Bennett, M. A.; Jeffery, J. C.; Robertson, G. B. Inorg. Chem., 1981, 20, 323.

120. Farr, J. P.; Olmstead, M. M.; Hunt, C. H.; Balch, A. C. Inorg. Chem., 1981, 20, 1182.

121. Kelly, B. A.; Welch, A. J.; Woodward, W. P. J. Chem. Soc., Dalton, 1977, 2237.

122. Rigby, W.; Bailey, P. M.; McCleverty, J. A.; Maitlis, P. M., J. Chem. Soc., Dalton, 1979, 371.

123. Varira, M. DI; Peruzzini, M.; Zanobini, F.; Stoppioni, P., Inorg. Chim. Acta, 1983, 69, 37.

124. Robinson, W. T.; Ibers, J. A., Inorg. Chem., 1967, 6 1208.

125. Sutton, L. E., Special publication No.18. The Chemical

Society London, 1965.

126. Manojlovic-Muir, L.; Muir, K. W.; Ibers, J. A., Inorg. Chem., 1970, 9, 447.

127. La Placa, S.J.; Ibers, J. A., Acta. Cryst., 1965, 18, 511.

128. La Placa, S.J.; Ibers, J.A., Inorg. Chem., 1965, 4, 778

129. Skapski, A.C.; Troughton, P.G.H., Chem. Commun., 1968, 1230.